unclassified

SECURITY CLASSIFICATION OF THIS PAGE (When Data Entered)

(9)

REPORT DOCUMENTATION PAGE	READ INSTRUCTIONS BEFORE COMPLETING FORM
1. REPORT NUMBER	2. GOVT ACCESSION NO. AD-A108822	3. RECIPIENT'S CATALOG NUMBER
4. TITLE (and Subtitle) Dynamical nonlinear material response and failure	5. TYPE OF REPORT & PERIOD COVERED Interim technical Oct '79 - June '81
	6. PERFORMING ORG. REPORT NUMBER CUA/VSL - 010781
7. AUTHOR(s) C.J. Montrose, T.A. Litovitz, D.M. Heyes J.H. Simmons, R.K. Mohr, J.J. Kim, S.D. Grant and S.M. Rekhson	8. CONTRACT OR GRANT NUMBER(s) N00014-75-C-0856 N00014-81-K-0296
9. PERFORMING ORGANIZATION NAME AND ADDRESS Vitreous State Laboratory Catholic University of America Washington, DC 20064	10. PROGRAM ELEMENT, PROJECT, TASK AREA & WORK UNIT NUMBERS
11. CONTROLLING OFFICE NAME AND ADDRESS Office of Naval Research 800 N. Quincy Street Arlington, VA 22217	12. REPORT DATE July 1, 1981
	13. NUMBER OF PAGES 129
14. MONITORING AGENCY NAME & ADDRESS(if different from Controlling Office)	15. SECURITY CLASS. (of this report) unclassified
	15a. DECLASSIFICATION/DOWNGRADING SCHEDULE

16. DISTRIBUTION STATEMENT (of this Report)

unlimited

(12) 136

DTIC ELECTE DEC 2 3 1981 S D A

17. DISTRIBUTION STATEMENT (of the abstract entered in Block 20, if different from Report)

---

18. SUPPLEMENTARY NOTES

---

19. KEY WORDS (Continue on reverse side if necessary and identify by block number)

Nonlinear response, viscoelasticity, molecular dynamics shear thinning, ductile failure, strain-induced crystallization

20. ABSTRACT (Continue on reverse side if necessary and identify by block number)

Molecular dynamics (MD) studies of the nonlinear viscoelastic response of Lennard-Jones model liquid and glassy systems have shown that strain-induced structural changes occur at elevated strain rates and are the microscopic origin of such phenomena as shear (viscosity) thinning and stress overshoot. The structural changes result in a limit to the

DD FORM 1 JAN 73 1473 EDITION OF 1 NOV 65 IS OBSOLETE S/N 0102-014-6601

404951

unclassified

SECURITY CLASSIFICATION OF THIS PAGE (When Data Entered)

81 12 22

AD A108822

DTIC FILE COPY

20. ABSTRACT (cont)

steady state stress that the material can sustain. In terms of them it was possible to develop a framework for describing ductile failure and the ductile-to-brittle transition. The semi-quantitative agreement of the MD results and primary laboratory studies in organic liquids, polymers and inorganic glasses suggests that the microscopic processes observed in the former are occuring in, and can be used to interpret phenomen in, the latter three.

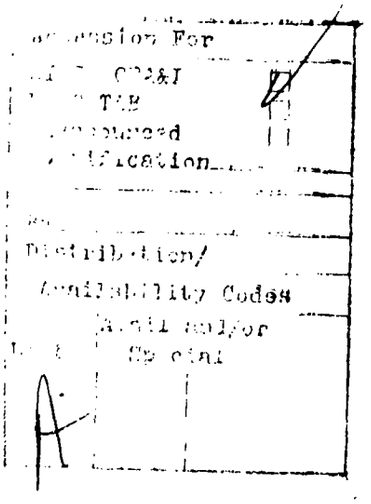

TECHNICAL REPORT: CUA/VSL - 010781

DYNAMICAL NONLINEAR MATERIAL RESPONSE AND FAILURE

by

C. J. Montrose, T.A. Litovitz, D. M. Heyes,
Joseph H. Simmons, R. K. Mohr, J.J. Kim,
S.D. Grant and S. M. Rekhson

Vitreous State Laboratory
Catholic University of America
Washington, D.C. 20064

submitted to

Office of Naval Research
Arlington, Va. 22217

ONR Contract: "High Pressure Liquid Theory"
N00014-75-C-0856
N00014-81-K-0296

July 1, 1981

Approved for public release; distribution unlimited.

TABLE OF CONTENTS

DIGEST

The past decade has witnessed the rapid assembly of rather large body of data relating to the mechanical behavior and failure of materials under extreme pressure, temperature and shear loading conditions. Although this has led to a number of important phenomenological insights, the molecular engineering of new materials with improved response and strength characteristics in impeded by the absence of a fundamental understanding of the failure modes of substances subjected to these conditions.

For the past several years a group at the Vitreous State Laboratory of Catholic University of America has been engaged in the investigation of the response of liquids and amorphous solids to large, rapidly imposed disturbances. Initially our approach was to make use of Molecular Dynamics (MD) experiment simulations to probe the microscopic origins and mechanisms of certain anomalous macroscopic response features of liquids under such conditions.

In its initial stages the work was focused on such non-linear viscoelastic phenomena as shear viscosity thinning and stress overshoot under conditions of large shearing rates. In carrying out this work it became apparent that the behavior that was observed in the simple MD model system (of point particles interacting via a Lennard-Jones 6-12 potential) were quite general--having been seen in such diverse systems as organic lubricants, polymers, metals, glasses and composites. In each of these cases, the extant explanations of the behavior involved mechanisms specific to the particular structural, configurational, or bonding properties of the individual systems; the MD data suggest that the origin of many of these observations can be understood in a more general fundamental way.

In particular, our studies showed that it is possible to rationalize much of the behavior as a consequence of the strain-induced (or stress-induced) structural changes that were observed to occur in the MD experiments. In the liquid and high temperature glass systems, for example, it was found that large shear rates cause the development of locally organized anisotropic structures in terms of which the dynamical pseudo-plastic behavior of these materials can be understood. These structural changes result in a limit to the steady-state stress that the material can support and offer a framework for understanding the ductile failure process in these substances.

To complement the MD work a supporting experimental program was established with in-house university funds. This joint experimental/MD effort has proven to be unusually valuable both in assisting in the interpretation of the data that is obtained, and in providing guidance for continuing studies. It was found, for instance that effective viscosity data from both the MD and laboratory experiments exhibited essentially the same dependence on im-

posed strain rate and could be interpreted in terms of the same nonlinear viscoelastic response hypothesis. The analysis of the MD results showed that the crucial material property in the data reduction can be represented by a parameter that can be interpreted as the maximum steady-state stress that can be developed in the material under the application of a uniform strain note. In the experimental work it was found that when a material is subjected to a stress exceeding this value, it initially deforms plastically; however, as the stress is continued, this ductile response is arrested and the material fails in sudden fracture.

This transition of ductile flow to fracture occurs as the material attempts to rearrange its structure to reduce the stress accompanying the applied strain rate. When these structural changes cannot occur rapidly enough to compensate for the development of stress levels in excess of the limiting stress (initially conceived as the parameter used in fitting the MD and experimental data), the material fractures spontaneously. The limiting steady-state stress value is therefore the actual cohesive strength of the material.

In the MD studies of low-temperature glasses the imposition of large strain rates causes initially a pseudo-plastic material response leading to ductile failure; under confinement conditions the material then restructures itself in a crystalline form with improved modulus and strength properties. Some preliminary studies in a crystalline system suggest that qualitatively similar behavior (the development of transient dislocations followed by recrystallization) occurs at elevated shear stress levels in crystals.

INTRODUCTION

This technical report presents the results of research in the dynamical response of materials to large, suddenly applied disturbances. The work reported herein was carried out under the sponsorship of the Office of Naval Research Research (Contract Numbers N00014-75-C-0856 and N00014-81-K-0296) and covers the time period October 1, 1979 through May 31, 1981.

The body of the report consists of six sections. In the first is presented a molecular dynamics (MD) investigation of the non-linear shear response of a Lennard-Jones model system at elevated pressures. Among the key results reported here are the observations of "shear thinning" and "shear overshoot" effects at high shear rates. These are accompanied by, and indeed are, a consequence of dynamical strain-induced organization of the liquid structure. In the second section, these data are compared with results obtained in both inorganiz glass and polymeric systems. While there are quantitative differences among the various materials, several important features are qualitiatively quite similar, indicating that the molecular dynamics studies (where one is able to extract detailed microscopic information) can be quite useful in the interpretation of phenomena observed in "real materials." The third section continues this comparison of the molecular dynamics "experimental results" with primary laboratory data. In this work it is shown that the concept of shear induced structural organization derived from the MD work can be applied in characterizing and understanding the mechanical and thermal responses of organic traction lubricants at high shearing

rates.

To interpret these results a model proposed by Bair and Winer [S. Bair and W.O. Winer, ASME J. Lub. Tech. 100, 40, (1979)] was generalized to provide a mathematical framework in which to consider dynamical nonlinear viscoelasticity. This constitutes the fourth section of the report. One of the key features in this work is the identification of the dimensionless quantity

$$x = \dot{\epsilon}\tau_o(G_\infty/\sigma^*)$$

(here $\dot{\epsilon}$ = strain rate, τ_o = shear relaxation time, G_∞ = shear rigidity modulus, and σ^* = maximum steady-state stress) as the parameter governing the type of behavior, i.e., linear viscoelastic, pseudoplastic, etc., that is observed. It was hypothesized that for large x values ductile failure of the material will be the result. In sections five and six, MD and primary laboratory results obtained in such circumstances are given, respectively. In these experiments low temperature glassy materials for which τ_o (and therefore x) is large were studied and the predicted failure was indeed observed. In the MD work the initial pseudoplastic response of the material gave way to ductile failure in which the stress that was developed dropped precipitously to zero. Under confinement conditions the continued application of shear led to strain-induced crystallization as the material restructured itself in a higher strength form.

Section I. Time dependent non-linear shear stress effects in simple liquids: A molecular dynamics study.

by D. M. Heyes, J. J. Kim, C. J. Montrose
and T. A. Litovitz

Time dependent nonlinear shear stress effects in simple liquids: A molecular dynamics study[a)]

D. M. Heyes, J. J. Kim,[b)] C. J. Montrose, and T. A. Litovitz

Vitreous State Laboratory, Catholic University of America, Washington D.C. 20064
(Received 17 December 1979; accepted 11 July 1980)

The effects of large amplitude shearing rates on 108 particle amorphous Lennard-Jones systems have been examined. A resolution of the structural and dynamical properties reveals that there is a tendency for shear to reorganize the liquid into layers to facilitate flow and hence reduce shear viscosity. The first steps have been made to determine those physical phenomena that are necessary to develop a theory of time dependent nonlinear shear viscoelastic effects. The form of the distortion giving rise to nonlinear shear stresses is well understood although its magnitude is intimately linked with parallel structural changes in an, at present, intractable way.

I. INTRODUCTION

In a rather wide variety of technological applications, e.g., elastohydrodynamic lubrication, shock loading, fatigue, liquids and amorphous solids are subjected to large shearing forces. The microscopic mechanisms that are of importance in such nonlinear situations are not well understood. To attempt to gain some insights into this phenomenon, a molecular dynamics (MD) investigation of the viscoelastic response of liquids subjected to large shear strain rates was undertaken.

We have used a modification of the normal MD procedure in order to follow the response of the system to an applied perturbation. In the past, nonequilibrium MD has been used to produce steady shear flow[1] in a number of ways. Ashurst and Hoover[2] sheared a molecular system through the action of "fluid walls" on two opposite faces of the MD cell. Their technique produces surface effects which lead to an inhomogeneous material being sheared. This problem is largely eliminated by the homogeneous shear method[3] (HSM), which uses periodic boundary conditions in all directions. A modification of the HSM, similar to one proposed by Evans,[4] was used in these calculations. It enables a particular strain rate to be established instantaneously. The unperturbed velocity of the real or image molecule i, i.e., $\mathbf{v}_i$, is altered to $\mathbf{V}_i$ by applying a shear rate $\dot{\epsilon}_{xz}$ so that it only alters the x component of velocity

$$\mathbf{V}_i = \mathbf{v}_i + \begin{pmatrix} \dot{\epsilon}_{xz} z_i \\ 0 \\ 0 \end{pmatrix} , \tag{1}$$

where z_i is the z coordinate of particle i measured from the center of the cubic MD cell of side length L. A molecule that leaves the MD cell in the z direction is reintroduced through the opposite face with the (x, y) coordinates and velocity of its nearest displaced image. All the calculations were conducted isothermally by scaling the $\mathbf{v}_i$ to maintain the desired temperature.

Calculations were performed under steady state shear conditions. In addition, the response of the system to a time dependent strain rate was studied. These latter calculations consisted of segments lasting for 898 time steps. In each segment the same "large" strain rate $\dot{\epsilon}_{xz}$ was applied during the first time step and was maintained for the next 450 steps, at which time it was suddenly switched off and then held at zero for the remainder of the segment. The time dependent system properties were averaged over approximately 20 such segments in order to reduce the statistical noise.

The segmented MD procedure was modified to allow the response of the system to small shear strain rates $\delta\dot{\epsilon}_{xz}$ to be followed.[5] The system was allowed to evolve from the same starting configuration with and without the perturbation. A great deal of the statistical noise was eliminated by subtracting at each time step the value for the property under examination of the undisturbed system from that of the perturbed medium.

The MD cell contained 108 particles interacting through the Lennard-Jones (LJ) potential

$$\phi(r) = 4\epsilon[(\sigma/r)^{12} - (\sigma/r)^{6}] . \tag{2}$$

The units of energy, length, and time used throughout this paper are ϵ, σ, and $(m\sigma^2/\epsilon)^{1/2}$, respectively; m is the particle's mass. All other quantities are expressed in terms of these fundamental units. The equations of motion were integrated using the Verlet algorithm[6] with a time step having a typical duration of 0.005. The interactions were truncated beyond $r = 2.5\sigma$. The system was investigated at an average temperature T of 0.722 (ϵ/k_B) and number densities ρ of 0.8442, 0.92862, 1.01304, and 1.2663. Had each of the latter three states been achieved slowly, the system would have crystallized[7]; however, these states were in fact achieved by suddenly (in one time step) reducing the volume of the $\rho = 0.8442$ system by 10%, 30%, and 50%, respectively. This rapid densification prohibited those structural rearrangements that are necessary for crystallization to occur so that a "superdensified" liquid system was produced. Accumulation of the configurational averages followed an initial equilibration period of several thousand time steps. The calculations were performed on a PDP 11/40 computer.

a)Research supported in part by the office of Naval Research Contract No. N00014-75-C-0856.
b)On leave from Korea Advanced Institute of Science, P. O. Box 150 Chonguangni, Seoul, Korea.

 0021-9606/80/203987-10$01.00

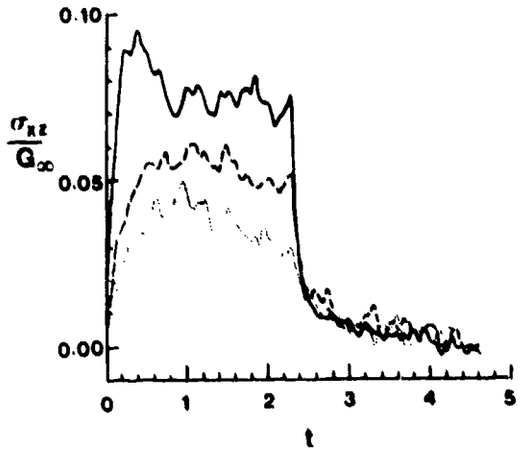

FIG. 1. The time dependence of the reduced shear stress $\sigma_{xz}(t)/G_\infty$ for the $\rho = 1.01304$ systems subjected to the following strain rate history: $\dot{\epsilon}_{xz}(t) = \dot{\epsilon}$, $0 \le t \le 2.3$. $\dot{\epsilon}_{xz}(t) = 0$, $2.3 < t \le 4.6$; ····, $\dot{\epsilon} = 0.1792$; ----, $\dot{\epsilon} = 0.3584$; and —, $\dot{\epsilon} = 0.7168$.

II. RESULTS AND DISCUSSION

We first discuss the nature of the relaxational processes that accompany a time varying large strain rate. The segmented technique was used. Each segment consisted of continuous shear for $0 \le t \le 2.3$. The system was then allowed to evolve in the absence of shear from $t \approx 2.3$ to $t \approx 4.5$, when the shear rate was again applied.

The development of the stress tensor σ is of particular interest; the $\alpha\beta$ component of this was computed using the formula[8]

$$\sigma_{\alpha\beta} = -(1/V)\left[\sum_{i=1}^{N} m v_i^\alpha v_i^\beta - \frac{1}{2}\sum_{i=1}^{N}\sum_{j}^{N}(\alpha_{ij}\beta_{ij}/r_{ij})\frac{\partial\phi}{\partial r_{ij}}\right], \quad (3)$$

where V is the volume of the MD cell which contains N molecules; v_i^α is the α component of the velocity of the ith particle relative to the imposed velocity; α_{ij} and β_{ij} are the α and β components, respectively, of the vector $\mathbf{r}_{ij} = \mathbf{r}_i - \mathbf{r}_j$, where $\mathbf{r}_i$ defines the position of molecule i.

Immediately after a strain rate $\dot{\epsilon}_{xz}$ is applied at time $t = 0$, a liquid takes time to respond structurally. As a result, at first the shear stress rises linearly with time as in an elastic material

$$\sigma_{xz}(t) = G_\infty \dot{\epsilon}_{xz} t, \quad (4)$$

where G_∞ is the shear rigidity modulus. Since a liquid will not support a static stress (it will flow), the rate of ascent of shear stress decreases until it reaches a limiting value governed by the shear viscosity η, i.e., $\sigma_{xz}(t \to \infty) = \eta \dot{\epsilon}_{xz}$. This is illustrated in Fig. 1, which shows the shear rate dependence of $\sigma_{xz}(t)/G_\infty$ for the $\rho = 1.01304$ state. Observe that the steady state stress does not increase in proportion to the shear rate, i.e., the shear viscosity decreases with increasing shear rate—so-called shear thinning. Table I reveals that this trend is manifest at all densities. This is strong evidence that, on shearing, structural changes are induced in a liquid which alters its physical properties.

A second experiment was carried out to probe the viscosity behavior at high shear rates. For a given $\dot{\epsilon}_{xz}$,

TABLE I. The density ρ and steady state shear rate $\dot{\epsilon}_{xz}$ dependence of the shear viscosity η, normal pressure components $P_{\alpha\alpha}$, configurational energy U_ϕ, shear rigidity modulus G_∞, and stress-optical coefficient C_ϕ. Values of G_∞ obtained from Eq. (3) are given in parentheses. The estimated maximum standard error is ≈ 10% at the lowest shear rate of each density.

ρ	$\dot{\epsilon}_{xz}$	η	P_{xx}	P_{yy}	P_{zz}	U_ϕ	G_∞	$C_\phi G_\infty n_0$
0.8442	0.0	~2.70	0.8	0.8	0.8	−5.65	22.5 (23.7)	
0.8442	0.0422	2.64	0.8	0.9	0.9	−5.64		
0.8442	0.1686	2.56	1.0	0.9	1.0	−5.62		
0.8442	0.3373	2.44	1.2	1.0	1.3	−5.58		
0.8442	0.6745	2.12	1.6	1.4	1.7	−5.51		3.5
0.92862	0.0	~10	3.0	3.0	3.0	−6.05	33.4 (37.3)	
0.92862	0.0435	7.4	3.0	2.9	3.0	−6.05		
0.92862	0.1741	4.6	3.3	3.2	3.3	−5.99		
0.92862	0.3482	4.0	3.7	3.5	3.9	−5.91		
0.92862	0.6963	3.3	4.4	4.2	4.7	−5.77		4.0
1.01304	0.0	~20	<7.0	<7.0	<7.0	<−6.36	46.9 (49.4)	
1.01304	0.0896	12.5	7.0	6.4	7.0	−6.22		4.0
1.01304	0.1792	9.0	7.5	7.4	7.3	−6.14		4.0
1.01304	0.3584	5.7	8.3	7.9	8.4	−5.96		4.5
1.01304	0.7168	4.6	9.5	8.8	9.9	−5.75		5.0
1.2663	0.0	~200	<37	<37	<37	<−4.5	123.8 (108.6)	
1.2663	0.0483	104	40	36	36	−4.49		
1.2663	0.1930	25	42	39	41	−3.94		
1.2663	0.3861	16	45	43	45	−3.29		
1.2663	0.7721	11	49	47	48	−2.68		8.5

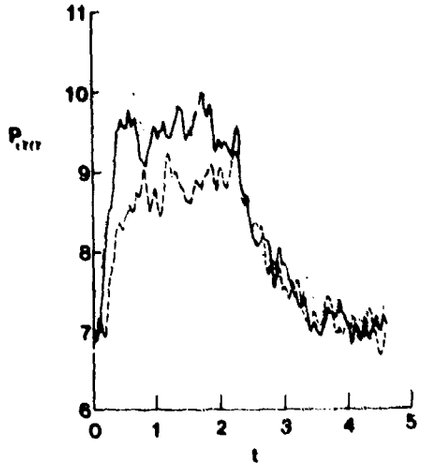

FIG. 2. The time dependent normal pressure components for the strain rate history of Fig. 1 and $\dot{\epsilon}=0.7168$, $\rho=1.01304$. —, $P_{xx}(t)$; ---- $P_{yy}(t)$; and ····, $P_{zz}(t)$.

the system was allowed to reach its steady state stress value σ_{xz}, at which time, say t', a small increment in shear rate $\delta\dot{\epsilon}_{xz}$ was applied. The stress $\delta\sigma_{xz}(t)$ resulting from the application of $\delta\dot{\epsilon}_{xz}$ continuously from t' is given by linear response theory as

$$\delta\sigma_{xz}(t)=G_\infty\int_{t'}^{t}dt''\,\delta\epsilon_{xz}(t'')C(t-t'')\,, \tag{5}$$

where the relaxation function to be used in Eq. (5) is that characteristic of the sheared state (see below). This leads directly to an alternate measurement of the shear viscosity at high shear rates:

$$\eta=\lim_{t-t'\to\infty}\delta\sigma_{xz}(t)/\delta\dot{\epsilon}_{xz}\,. \tag{6}$$

The values obtained in this manner, although less precise, agree reasonably well with and follow qualitatively the same trends as those shown in Table I derived from $\eta=\sigma_{xz}(t-\infty)/\dot{\epsilon}_{xz}$.

The time evolution of the shear stress is also affected rather dramatically at the higher shear rates. In Fig. 1 it can be seen that the shear stress rises to a peak before descending to its steady-state value. This behavior is observed for shear rates such that $\dot{\epsilon}_{xz}\eta/G_\infty \gtrsim 0.05$; at lower shear rates no local maxima in the σ_{xz} versus t curves were discernible. One also finds that upon cessation of the applied shear rate, the immediate stress relaxation is faster for the more highly sheared media. The rate of stress decay slows with time as the equilibrium state is approached. We shall later consider the possible microscopic origin of the shear thinning and shear stress overshoot phenomena; before doing so, however, we examine some of the other changes that occur in the system in response to the large and suddenly applied shear disturbances.

Each normal pressure component $P_{\alpha\alpha}=-\sigma_{\alpha\alpha}$ rises when the liquid is sheared. They reflect the structural changes that the shear forces introduce into the liquid. The $P_{\alpha\alpha}(t)$ of the $\rho=1.01304$, $\dot{\epsilon}_{xz}=0.7168$ state are given in Fig. 2. The time scale of the development of the normal pressure components is longer than that of the shear stress. No normal pressure overshoot is present and a P_{xz} overshoot is observed only when $\rho=1.2663$. Table I reveals that the configurational energy per particle

$$U_c=(1/2N)\sum_{i}^{N}\sum_{j\neq i}^{N}\phi(r_{ij})$$

increases with shear rate. This is additional evidence of structural alteration of the fluid to states which are only energetically favorable in the presence of steady shear flow.

The shear stress viscoelastic behavior is usefully cast in relaxation function formalism. The normalized shear stress relaxation function $C(t)$ has been evaluated from both the sheared and unsheared media using the aforementioned small perturbation technique. The change in shear stress $\delta\sigma_{xz}(t)$ following the application of a small strain rate $\delta\dot{\epsilon}_{xz}$ for the duration of one time step Δt at t' is given by $C(t-t')$ as follows:

$$\delta\sigma_{xz}(t-t')=G_\infty\delta\dot{\epsilon}_{xz}\Delta t C(t-t')\,, \tag{7}$$

where $C(0)=1$ and $C(\infty)=0$. The $C(t-t')$ derived for the $\rho=1.01304$ state with $\dot{\epsilon}_{xz}=0.7168$, taking time origins at $t'=0.16$, 1.2, and 3.6, are shown in Fig. 3. At short times ($t-t'\leq 0.2$), all the $C(t-t')$ coincide, presumably because this portion of stress decay is inertial and results from small motions of molecules within the free space of the random network structure. After this, the remaining portion of the stress decays more slowly because it involves the structural rearrangement of the medium, requiring the participation of the cooperative motions of larger molecular groups. Figure 3 reveals that as shear stress increases, the more slowly decaying process progressively disappears. This has been observed experimentally[9] and is further evidence of the structural changes that take place in the liquid at high shear stresses to make shear flow easier. For the $\rho=0.8442$ state, the form of $C(t)$ with $\epsilon_{xz}=0$ is, within statistical uncertainty, the same as that given by Levesque, Verlet, and Kürkijarvi.[10] The variation for nonzero values of $\dot{\epsilon}_{xz}$ is qualitatively the same as for the $\rho=1.01304$ state, although the changes in the long-time behavior are somewhat less pronounced.

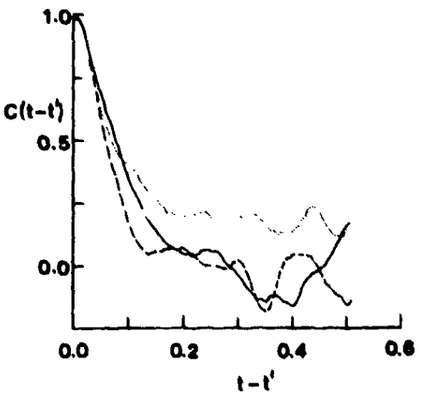

FIG. 3. The shear stress relaxation function $C(t-t')$ for the state of Fig. 2 and time origins t' at ----, $t'=0.16$; —, $t'=1.2$; and ···· $t'=3.6$.

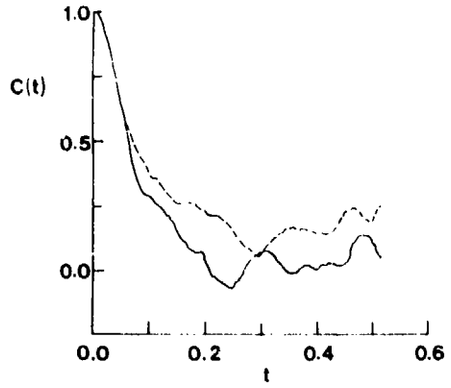

FIG. 4. The shear stress relaxation functions $C(t)$ for the sheared (—) and unsheared (----) portions of the segment for the state $\rho = 0.92862$, $\dot{\epsilon}_{xz} = 0.6963$.

A selection of the $C(t)$ obtained at the other densities in the steady state shear and zero shear portions of the segment are presented in Figs. 4 and 5. Their forms are consistent with the above interpretation. It is certainly not surprising that the characteristic response functions are different for the highly stressed steady state system as compared with the equilibrium system. On fairly general grounds, one expects that the existence of large shear stresses in the liquid reflects the fact that local structural distortions are present. That these should impact on the response characteristics of the liquid seems quite apparent.

The values obtained for the shear rigidity modulus G_∞ are presented in Table I, where they are compared with the values derived using the expression of Zwanzig and Mountain[11]:

$$G_\infty = \rho k_B T + \frac{2\pi}{15}\rho^2 \int_0^\infty dr\, g_0(r) \frac{d}{dr}(r^4 d\phi/dr) \,. \tag{8}$$

In this equation $g_0(r)$ is the radial distribution function, which was computed as a part of the MD runs at each density. Within the statistical uncertainties, G_∞ was found to be independent of the shear stress at a particular density.

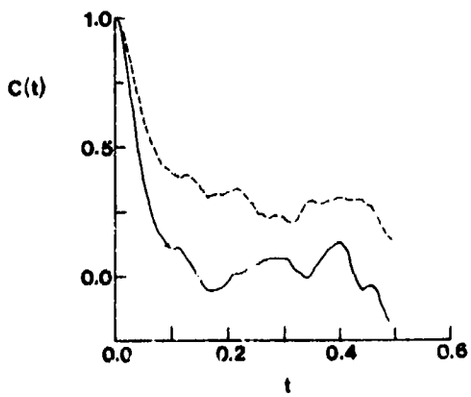

FIG. 5. The shear stress relaxation functions $C(t)$ for the sheared (—) and the unsheared (----) portions of the segment for the state $\rho = 1.2663$, $\dot{\epsilon}_{xz} = 0.7721$.

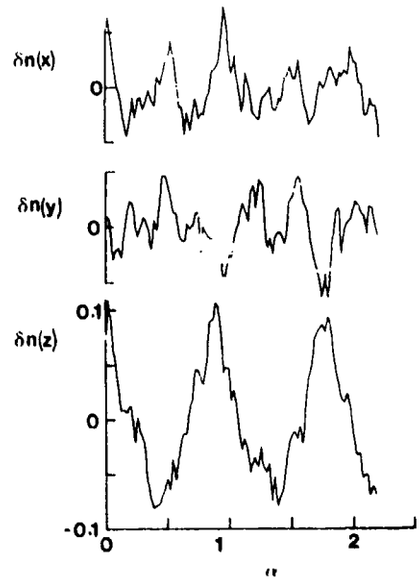

FIG. 6. The excess directional number density functions $\delta n(\alpha)$ for the $\rho = 1.2663$ and $\dot{\epsilon}_{xz} = 0.7721$ state.

We now turn to consider the nature of the structural and dynamical changes that these large shear rates produce in the LJ liquids. For the purpose of investigating shear-induced structural anisotropy, a directional probability density function $n(\alpha)$ was defined: $\rho L^2 n(\alpha) d\alpha \equiv$ the probability of locating a particle in the plane lamina (of thickness $d\alpha$ and dimensions $L \times L$) oriented normal to the α axis and located a perpendicular distance α from a given particle. Structural anisotropy is then revealed by examining $\delta n(\alpha)$, the difference between $n_s(\alpha)$ characterizing the sheared system and $n_0(\alpha)$ of the equilibrium system. In terms of the pair distribution function this can be written as (for the $\alpha = z$ case, for example)

$$\delta n(z) = (1/L^2) \int_0^L dx \int_0^L dy\, [g_s(\mathbf{r}) - g_0(r)] \,, \tag{9}$$

where $g_s(\mathbf{r})$ is the pair distribution function for the sheared system and $g_0(r)$ is the equilibrium radial distribution function. We have obtained the $\delta n(\alpha)$ by computing the average number of particles from a reference particle in the distance range $|x|$ to $|x| + \Delta x$ (where Δx was taken as $L/200$) selected from the $N-1$ particles in the reorientated MD cell. Figure 6 shows the $\delta n(\alpha)$ under the conditions $\rho = 1.2663$ and $\dot{\epsilon}_{xz} = 0.7721$. Although the maximum displacement is 10% at most, there is evidence of a tendency of the molecules to reorder themselves into xy layers (layers normal to the velocity gradient). The xz shearing increases the probability of the molecules in an xz plane being found at multiples of the intermolecular diameter from each other in the z direction. It is energetically favorable for these layers to be staggered in the y direction. Although not so well defined, these trends are present at the lower densities. The (grossly simplified) picture that emerges is one of corrugated sheets of atoms sliding past one another. A pictorial representation of this suggested structure is given in Fig. 7.

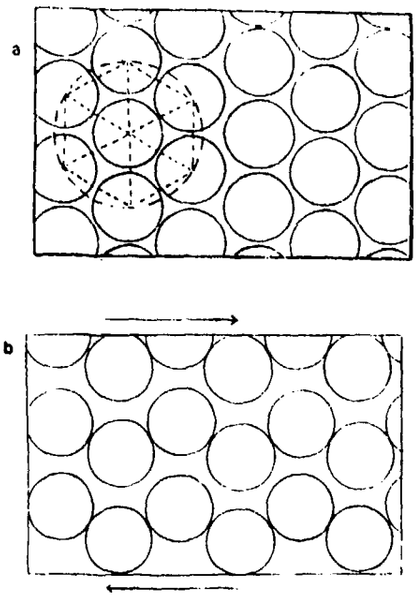

FIG. 7. A pictorial representation of the structural changes that take place on going from an unsheared (a) to a sheared (b) state. The arrows denote the line and plane of shear.

The structural reorganization results from the action of the imposed velocity profile which, at the shear rates considered, dominates the molecular motion. This is well demonstrated by the trajectory plots of Fig. 8, which show time-elapsed positions in the xz plane of a selection of the particles from the $\rho = 1.01304$ and $\dot{\epsilon}_{xz} = 0.7168$ state. Major movements are confined to the line of shear.

It is to be expected that the effect of the shear should not be confined to structural changes but must also alter the self-diffusional dynamics of the molecules. To assess this, the x, y, and z components of the mean square displacements $\langle r_\alpha^2(t)\rangle$, which exclude the imposed flow, have been calculated, i.e.,

$$\langle r_\alpha^2(t)\rangle = \sum_i^N \left\langle \left[\int_0^t v_i^\alpha(t')dt' - \alpha_i(0) \right]^2 \right\rangle / N \,. \tag{10}$$

The directional diffusion coefficients

TABLE II. The density and shear rate dependence of the directional diffusion coefficients D_α obtained from the MD experiments using Eq. (10). The results are taken from the unsheared and sheared portions of the segments.

ρ	$\dot{\epsilon}_{xz}$	D_x	D_y	D_z
0.8442	0.0	0.032	0.032	0.032
0.8442	0.6745	0.052	0.045	0.052
0.92862	0.0	0.018	0.018	0.018
0.92862	0.6963	0.043	0.037	0.046
1.01304	0.0	0.008	0.008	0.008
1.01304	0.1792	0.02	0.014	0.02
1.01304	0.3584	0.03	0.025	0.03
1.2663	0.0	0.0045	0.0045	0.0045
1.2663	0.7721	0.045	0.03	0.03

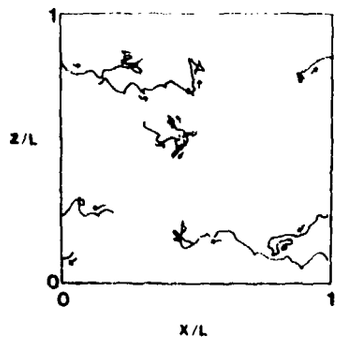

FIG. 8. The trajectories of five molecules in the xz plane during the $\rho = 1.01304$ and $\dot{\epsilon}_{xz} = 0.7168$ segment. The molecules originated from within a xz slice of thickness $\sim L/10$ taken through the center of the cell.

$$D_\alpha = \frac{1}{2}\left(\frac{d\langle r_\alpha^2(t \to \infty)\rangle}{dt}\right)$$

for a selection of the states are presented in Table II. The value of $D_\alpha = 0.032$ for the unsheared liquid near the triple point compares favorably with the value of 0.033 previously obtained.[10] The D_α of the unsheared liquid decrease by approximately an order of magnitude on increasing the density from $\rho = 0.8442$ to 1.2663. However, at larger shear rates the density has a diminishing influence on the diffusion coefficients. The high shear stresses enhance the fluidity and create a "liquid" which has directionality. All the diffusion coefficient components rise with shear rate at a particular density because the structural reorganization that takes place on shearing apparently creates paths along which particles can more readily move. The D_y are typically two thirds of the D_x and D_z, indicating that the self-diffusion is favored in the shearing plane. Thus, paradoxically, although structural aspects of the liquids under shear present a more solid-like appearance, other more dynamically related properties such as self-diffusion and shear viscosity manifest changes which are associated with enhanced fluidity.

Another aspect of the shear induced structural distortion is presented by the time dependent pair radial distribution function $g(\mathbf{r}, t)$, which is conveniently decomposed into the following component configurational averages:

$$g(\mathbf{r}, t) = g_0(r) + (x^2/r^2)u_{xx}(r, t) + (y^2/r^2)u_{yy}(r, t) + (z^2/r^2)u_{zz}(r, t) + (xz/r^2)u_{xz}(r, t) + \cdots \,. \tag{11}$$

If $f_{\alpha\beta}(r, t)$ is the average of $\langle \alpha_{ij}\beta_{ij}/r_{ij}^2\rangle$ in the radial element $r \to r + dr$ about a molecule i at time t, then

$$g_{\alpha\alpha}(r, t) = 15 f_{\alpha\alpha}(r, t)/(4\pi\rho r^2 dr) \,, = 3u_{\alpha\alpha}(r, t) + u_{\beta\beta}(r, t) + u_{\gamma\gamma}(r, t) \,, \tag{12}$$

where $\alpha \neq \beta \neq \gamma$, and

$$g_{\alpha\beta}(r, t) = 15 f_{\alpha\beta}(r, t)/(4\pi\rho r^2 dr) \,, = u_{\alpha\beta}(r, t) \,, \tag{13}$$

where $\alpha \neq \beta$.

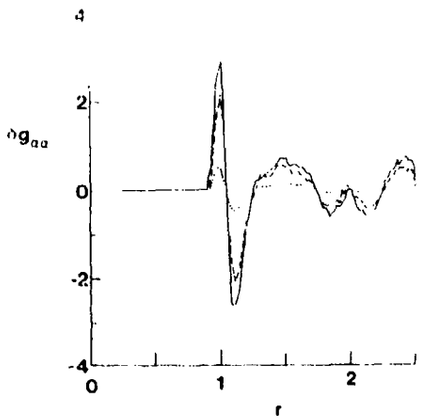

FIG. 9. The $g(r)$ (····), $g_{xx}(r)$ (—), and $g_{yy}(r)$ (----) of the sheared minus the unsheared portions of the $\rho = 1.01301$ and $\dot{\epsilon}_{xz} = 0.7168$ segmented calculation.

The $f_{\alpha\beta}(r, t)$ have been calculated at various times during the segment. The difference between the $g_{\alpha\alpha}(r, t)$ of the steady state sheared ($\rho = 1.01304$ and $\dot{\epsilon}_{xz} = 0.7168$) system and the unsheared system at the same density $\delta g_{\alpha\alpha}(r, t)$ is shown in Fig. 9. It reveals that shearing produces a net movement of particles in each coordination shell towards the origin molecule. This is also illustrated by the difference between the pair distribution functions of the sheared and unsheared liquids shown in Fig. 10.

The shear rate dependent $g_{xz}(r, t)$ at steady state of the $\rho = 0.8442$ system are compared with the spherically averaged $g(r, t)$ from these samples in Fig. 10. They give convincing evidence of angular distortion in each coordination shell such that in the positive xz quadrants the inside of each shell is on average depleted of particles when compared with the unsheared liquid. In contrast, the outside of each shell has an excess of molecules in the positive xz quadrants, when compared with the unsheared medium. The opposite changes take place in the negative quadrants.

The time dependence of $g_{\alpha\alpha}(r, t)$ and $g_{\alpha\beta}(r, t)$, shown in Fig. 11, reveal that structural reorganization having the symmetry of shear $\langle xz/r^2 \rangle$ is much faster than that of $\langle \alpha^2/r^2 \rangle$ symmetry. Within the latter series, $\langle x^2/r^2 \rangle$ and $\langle z^2/r^2 \rangle$ evolve more rapidly to their steady state values than $\langle y^2/r^2 \rangle$. For example, when $\rho = 1.01304$ and $\dot{\epsilon}_{xz} = 0.7168$, the former three averages have nearly reached their steady state values by $t = 0.25$ whereas that of the $\langle y^2/r^2 \rangle$ summation hardly differs from zero by that time.

These observations suggest a possible mechanism for the origin of the stress overshoot. When a liquid is sheared, the shearing forces alter its structure so that the steady state stress attained corresponds to a new lower viscosity, not that characterizing the starting liquid. At high rates of shear the structural evolution necessary to attain this new viscosity is significantly slower than the viscoelastic shear relaxation. Viewed simply this means that the original viscosity can remain for a sufficiently long time to enable the shear stress to exceed its steady state value. The situation is more complicated than this simple explanation presents, however, because the overshoot takes place at times when a purely viscous model for shear stress is not an entirely acceptable approximation.

Another probe into the time dependent structural changes associated with shear stress viscoelasticity is provided by the angular rotation function $\dot{\theta}(r)$ defined below:

$$\dot{\theta}(r) = \left\langle \sum_{i}^{N} \sum_{j \neq i}^{N} (\mathbf{v}_j \times \mathbf{r}_{ij})/r_{ij}^2 \right\rangle / N \,, \tag{14}$$

where the cross product is confined to the xz plane. When a material is sheared, molecules observe their neighbors rotate around them with an angular velocity such that on average $\dot{\theta}(r) = \dot{\epsilon}_{xz}/3$. The time and radial dependence of th · function gives information about hindered rotation and hence the nature of structural disruption associated with shear stress relaxation. Large departures in $\dot{\theta}(r)$ from its continuum value of $\dot{\epsilon}_{xz}/3$ indicate major structural rearrangement at that intermolecular separation. Figure 12 shows $\dot{\theta}(r)$ averaged over three time zones after the start of steady shear in the $\rho = 1.01304$, $\dot{\epsilon}_{xz} = 0.7168$ calculation. This and similar plots for the calculation involving a step in strain only exhibit a spike in $\dot{\theta}(r)$ at $r \approx 0.9$ at times when the strain rate has been turned off and which is clearly above the noise. This shows that the slowly decaying part of the stress, after a change in applied strain rate, results from further rearrangements in the inside of the first coordination shell, which presumably require reorganization of the liquid structure before they can occur.

The following discussion uses the MD results to evaluate models for nonlinear shear behavior.

Previous MD studies of this subject have used the Ree–Eyring hyperbolic sine model[2] to fit the shear rate dependence of η. From simple activation energy considerations the following relationship can be derived:

$$\eta/\eta_0 = \sinh^{-1}(\dot{\epsilon}_{xz}\tau)/(\dot{\epsilon}_{xz}\tau) \,, \tag{15}$$

where η_0 is the shear viscosity in the limit of zero shear rate. The relaxation time τ characterizes the

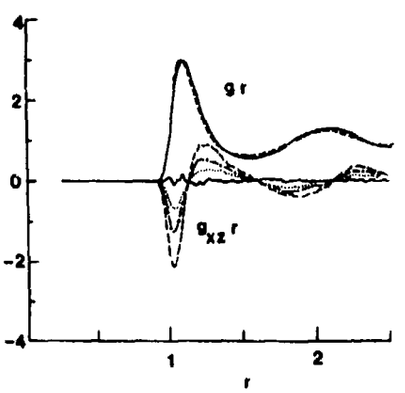

FIG. 10. The shear rate dependence of $g(r)$ and $g_{xz}(r)$ for the $\rho = 0.8442$ states. $\dot{\epsilon}_{xz} = 0$ (—); $\dot{\epsilon}_{xz} = 0.1686$ (····); $\dot{\epsilon}_{xz} = 0.3373$ (-·-·-·); $\dot{\epsilon}_{xz} = 0.6745$ (----).

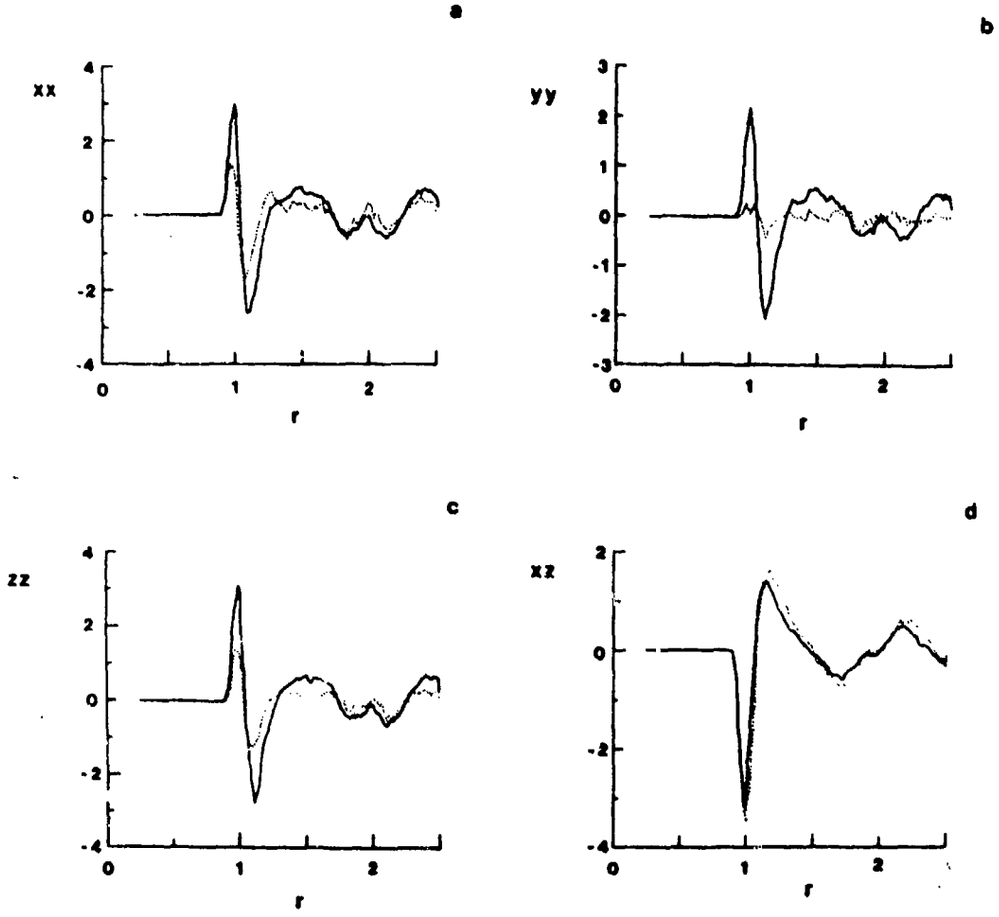

FIG. 11. The functions $g_{\alpha\alpha}(r,t)$ and $g_{\alpha\beta}(r,t)$ for the calculation of Fig. 10: (a) xx, (b) yy, (c) zz, (d) xz for the $t=0.25$ (····) and $t=1.8$ (—) states.

medium's unsheared state and is roughly an order of magnitude larger than the average shear relaxation time $[=\int_0^\infty C(t)dt=\eta_0/G_\infty]$. Although the model relates τ to a flow volume V_f through the relationship

$$\tau=\eta_0 V_f/2k_BT\ , \tag{16}$$

τ is usually taken as an adjustable parameter. Reasonable fits to the MD results can be achieved by taking $V_f=1.1$ independent of density. For example, for the $\rho=1.01304$ state, this provides better than 15% agreement with the data; at the other densities the agreement ranges from 13% to 18%. The general trends in the plots of η/η_0 versus $\dot{\epsilon}_{xz}$ at all densities suggest that the disagreement is not totally statistical; the shear thinning effect is systematically more pronounced (i.e., η/η_0 falls more rapidly) than Eq. (15) would predict. We also note that the parameter τ increases more rapidly with density than does the shear relaxation time τ_s. At the lowest density $\tau/\tau_s\approx 20$ whereas for the highest density state $\tau/\tau_s\approx 100$.

A perhaps more satisfying model has its basis in a trend in the shear rate dependence of $g_{xz}(r,t)$, shown in Fig. 10. The magnitude of the angular distortion roughly increases in proportion to the shear rate, as does the shear stress. This suggests that some of the properties of a sheared liquid can be characterized by a quasielastic solid model in which the only nonequilibrium property is a time dependent recoverable shear

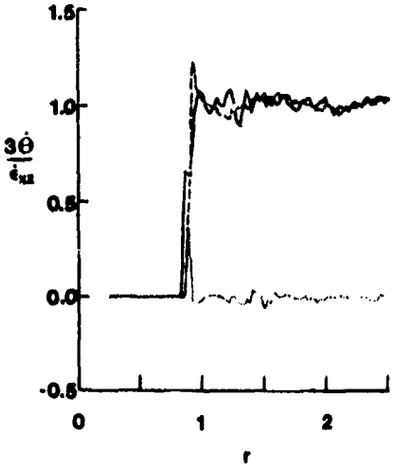

FIG. 12. The normalized angular rotation function $3\dot{\theta}(r)/\dot{\epsilon}_{xz}$ averaged over the time regions 0.17 to 0.33 (—), 1.54 to 2.05 (----), and 3.85 to 4.46 (····) for the segmented $\rho=1.01304$ and $\dot{\epsilon}_{xz}=0.7165$ calculation.

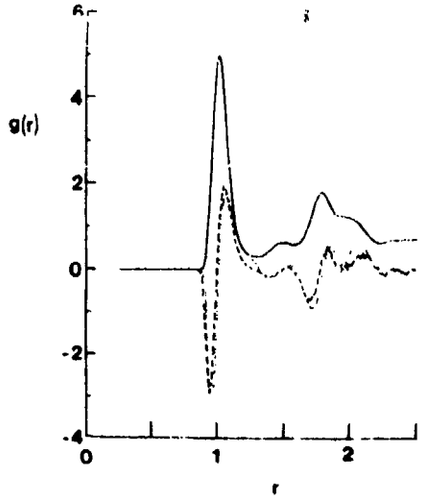

FIG. 13. A comparison between the spherically averaged pair correlation function $g(r)$ (—), $g_{xz}(r)$ (· · · ·), and $-\Delta\epsilon_{xz}r(\partial g/\partial r)$ (----) for the $\rho = 1.2663$ and $\dot{\epsilon}_{xz} = 0.0483$ state.

strain $\Delta\epsilon_{xz}(t)$. Such an approach[2] is obtained from a Taylor expansion of $g(\mathbf{r}, t)$:

$$g(\mathbf{r}, t) = g_0(r) + z\,\Delta\epsilon_{xz}(t)\frac{\partial g_0(r)}{\partial x} + \frac{z^2}{2}\Delta\epsilon_{xz}^2(t)\frac{\partial^2 g_0(r)}{\partial x^2} + \cdots . \tag{17}$$

Hence,

$$g(\mathbf{r}, t) = g_0(r) + xz\,\Delta\epsilon_{xz}(t)g_0'/r + x^2z^2\,\Delta\epsilon_{xz}^2(t)(g_0''/r^2 - g_0'/r^3)/2 + z^2\,\Delta\epsilon_{xz}^2(t)g_0'/(2r) + \cdots , \tag{18}$$

where g_0' and g_0'' denote dg_0/dr and d^2g_0/dr^2, respectively. A comparison between Eqs. (11) and (18) reveals that

$$r\Delta\epsilon_{xz}(t)g_0' = u_{xz}(r, t) . \tag{19}$$

For most of the density/shear rate combinations studied, a $\Delta\epsilon_{xz}(t)$ can always be chosen so that Eq. (19) is an excellent approximation. Good agreement for the $\rho = 1.2663$ and $\dot{\epsilon}_{xz} = 0.048$ calculation is illustrated in Fig. 13. The $g_0(r)$ was approximated with little error by the spherically symmetrical $g(r)$ of that calculation. The recoverable strain necessary to satisfy Eq. (19) was found to be the Hooke's law strain ($= \sigma_{xz}/G_\infty$) to a good approximation. Similar calculations were performed for the other states. The $g_0(r)$ were taken from the lowest shear rate at each density or where possible from the unsheared portion of the segment in non-steady state calculations. This latter method was adopted in order to explore a larger region of phase space than would be possible with a single simulation at equilibrium, especially at these high densities. The best fits for $\Delta\epsilon_{xz}$ are again given with few exceptions by σ_{xz}/G_∞, as Table III reveals.

Equations (17)–(19) also predict changes in the configurational parts of the total energy and normal pressure components that take the form

$$\delta U_c(t) = \rho^2\pi\Delta\epsilon_{xz}^2(t)\int_0^\infty r^4\,dr\,\phi(r)(g_0'' - g_0'/r)/15 + \rho^2\pi\Delta\epsilon_{xz}^2(t)\int_0^\infty r^3\,dr\,\phi'(r)g_0'/3 + \cdots \tag{20}$$

and

$$\delta P_{\alpha\alpha}(t) = -\rho^2\pi A_{\alpha\alpha}\Delta\epsilon_{xz}^2(t)\int_0^\infty r^3\,dr\,\frac{\partial\phi(r)}{\partial r}(g_0'' - g_0'/r) - \rho^2\pi B_{\alpha\alpha}\Delta\epsilon_{xz}^2(t)\int_0^\infty r^4\,dr\,\frac{\partial\phi(r)}{\partial r}g_0' + \cdots , \tag{21}$$

where $A_{xx} = A_{zz} = 3/105$, $A_{yy} = 1/105$; and $B_{xx} = B_{yy} = 1/15$, $B_{zz} = 1/5$.

The predictions for $\delta U_c(t)$ and $\delta P_{xz}(t)$, using this model and taking strains from Eq. (19), are several orders of magnitude less than those obtained by MD. It is thought that this is because the model only takes into account those changes in "bulk" properties (e.g., U_c and $P_{\alpha\alpha}$) which arise directly from distortion of the liquid having g_{xz} symmetry. Clear evidence of other induced strains, having $g_{\alpha\alpha}$ symmetry, has already been presented. Although these are derived from the shearing action, they are not, at present, related to it in a well defined way. It is apparent that in the MD results the major source of the δU_c and $\delta P_{\alpha\alpha}$ originates from this latter structural alteration of the liquid which is not incorporated in the above model. The success of this theory for predicting shear stress follows from the relatively small change in $g(r)$ that occurs on shearing the fluids—even in the nonlinear region. In addition, the recoverable shear strain (which can be considered to be an expansion argument) induced is small ($\lesssim 0.07$). It suggests that models characterizing the nonlinear shear stress can be constructed using a recoverable shear strain as the only nonequilibrium parameter.

The analysis in the preceding paragraph should be regarded as a tentative hypothesis to be explored, rather than as a firm conclusion. It is not unreasonable to expect that the shear induced changes δU_c and $\delta P_{\alpha\alpha}$ will

TABLE III. A comparison between the fitted recoverable strain of Eq. (19) and the equivalent elastic medium strain σ_{xz}/G_∞.

ρ	$\dot{\epsilon}_{xz}$	$\Delta\epsilon_{xz}$	σ_{xz}/G_∞
0.8442	0.0422	0.005	0.005
0.8442	0.1686	0.027	0.019
0.8442	0.3373	0.037	0.037
0.8442	0.6745	0.064	0.064
0.92862	0.0435	0.01	0.01
0.92862	0.1741	0.026	0.024
0.92862	0.3482	0.042	0.042
0.92862	0.6963	0.069	0.069
1.01304	0.0896	0.024	0.024
1.01304	0.1792	0.034	0.034
1.01304	0.3584	0.044	0.044
1.01304	0.7168	0.070	0.070
1.2663	0.0483	0.041	0.041
1.2663	0.1930	0.039	0.039
1.2663	0.3861	0.046	0.050
1.2663	0.7721	0.051	0.069

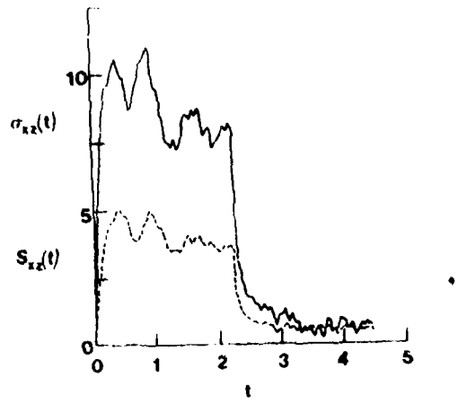

FIG. 14. The time dependence of the xz components of the stress (—) and susceptibility (----) tensors for the $\rho = 1.2663$ system subjected to the strain rate history: $\dot{\epsilon}_{xz} = 0.7721$, $0 \le t < 2.2$; $\dot{\epsilon}_{xz}(t) = 0$, $2.2 < t < 4.4$.

depend (perhaps rather strongly) on system size. If this is indeed the case, one might find that the discrepancies between the measured changes and those calculated from Eqs. (20) and (21) are artifacts resulting from the small size of the MD system.

Experimentally, the stress produced by large amplitude strains can be measured using the optical technique of birefringence.[12] A fundamental assumption of the analysis requires that the stress and susceptibility tensor $\mathbf{S}$ respond in a fixed ratio to the shear strains. In order to test this assumption the components of $\mathbf{S}$, i.e.,

$$S_{\alpha\alpha} = -\frac{4\pi\alpha^2}{V}\sum_{i\neq j}^{N}\sum^{N}\frac{3\alpha_{ij}^2 - r_{ij}^2}{r_{ij}^5} \tag{22}$$

and

$$S_{\alpha\beta} = -\frac{4\pi\alpha^2}{V}\sum_{i\neq j}^{N}\sum^{N}\frac{\alpha_{ij}\beta_{ij}}{r_{ij}^5}\,, \tag{23}$$

have been calculated. In Eqs. (22) and (23), α is the molecular polarizability, which is assumed to be equal to σ^3 here. A stress-optical coefficient C_0 is defined to be

$$C_0 = S_{xz}/2\sigma_{xz}n_0\,, \tag{24}$$

where n_0 is the refractive index of the medium. The stress-optical coefficient is found to be $\propto 1/G_\infty$ for many materials.[13,14] In order to test this assumption, $\sigma_{xz}(t)$ and $S_{xz}(t)$, taken from the $\rho = 1.2663$ and $\dot{\epsilon}_{xz} = 0.7721$ segmented calculation, are shown in Fig. 14. Even under these highly nonlinear conditions this proportionality is obeyed quite well. This is perhaps not surprising when the similarity of the configurational average for each is considered. Table I reveals that C_0 is relatively insensitive to shear rate when compared with η, in agreement with experimental evidence,[11] and to a lesser extent density.

The susceptibility is a probe which weights longer range interactions to a greater extent than the stress. This is evident in comparable $\sigma_{\alpha\alpha}(t)$ and $S_{\alpha\alpha}(t)$ profiles. The $S_{\alpha\alpha}(t)$ do not exhibit the same definite time dependence as does the $\sigma_{\alpha\alpha}(t)$. The latter is dependent on the interaction potential and is thus more sensitive to the short range structural distortions accompanying shear. Nevertheless, these calculations give support for the use of this technique in studying stresses in the nonlinear regime.

For each normal tensorial property $T_{\alpha\alpha}$ (e.g., stress, recoverable strain, and susceptibility) the direction and its perpendicular along which the minimum and maximum value of that property occur define the minor and major axes of the tensorial distortion ellipsoid. The smallest angle χ between either of these two directions and the x direction is to a first approximation the same for stress, recoverable strain, and susceptibility. The expressions

$$\chi = \tan^{-1}[2T_{xz}/(T_{xx} - T_{zz})] \tag{25}$$

and

$$\chi = \tan^{-1}(2/\Delta\epsilon_{xz})/2 \tag{26}$$

are readily derived and predict that for the states studied χ differs little from 45°.

III. CONCLUSIONS

We have performed nonequilibrium molecular dynamics calculations on LJ fluids with the aim of gaining insights into the mechanism of liquid failure at high levels of shear stress. The shearing action has been found to change the liquid structure so that there is a tendency to stratify along the lines of shear, enabling flow to take place more easily. The resulting increase in fluidity is evident in the enhanced self-diffusion coefficients and the rate of decay of the relaxation functions relative to the unsheared parent system. In other words, the fluid has a shorter memory of its past behavior.

The structural distortions giving rise to the shear stress changes are relatively small and are to a large extent decoupled from other structural changes. They can be characterized using a first order perturbation expansion from the equilibrium structure. The only nonequilibrium parameter needed is a recoverable shear strain which is given to a good approximation by the shear stress divided by the shear rigidity modulus. Unfortunately, we do not understand how to formulate the mechanism by which the shearing changes the other aspects of the liquid's structure, which undoubtedly has a strong influence in determining the recoverable shear strain. Model predictions of "bulk" property changes, e.g., in configurational and normal pressure components, are similarly only at an elementary stage of development.

ACKNOWLEDGMENT

The authors would like to express their gratitude to Mr. S. F. Shirron for his computational assistance.

[1] A. S. Lodge, *Elastic Liquids* (Academic, London, 1964), p. 42.
[2] W. T. Ashurst and W. G. Hoover, Phys. Rev. A 11, 658

(1975).
[3]T. Naitoh and S. Ono, J. Chem. Phys. 70, 4515 (1979).
[4]D. J. Evans, Mol. Phys. 37, 1745 (1979).
[5]G. Ciccotti, G. Jacucci, and I. R. McDonald, J. Stat. Phys. 21, 1 (1979).
[6]L. Verlet, Phys. Rev. 159, 98 (1967).
[7]J. J. Nicolas, K. E. Gubbins, W. B. Street, and D. J. Tildesley, Mol. Phys. 37, 1429 (1979).
[8]J. Hansen and I. R. McDonald, *Theory of Simple Liquids* (Academic, London, 1976).
[9]Yu G. Yanovski, in *Relaksatsionnye Yavleniya v Polimerakh* (*Relaxation Phenomena in Polymers*), edited by G. Bartenev and Yu V. Zelenev (Khimiya, Leningrad, 1972) p. 113.
[10]D. Levesque, L. Verlet, and J. Kurkijarvi, Phys. Rev. A 7, 1690 (1973).
[11]R. Zwanzig and R. D. Mountain, J. Chem. Phys. 43, 4464 (1965).
[12]H. Janeschitz-Kriegl and J. L. S. Wales, in *The Photoelastic Effect and Its Applications*, edited by J. Kestens (Springer, Berlin, 1975), p. 271.
[13]K. Osaki, N. Reasho, T. Koitmoto, and M. Kurata, J. Rheol. 23, 617 (1979).
[14]J. W. Dally, in *The Photoelastic Effect and Its Applications*, edited by J. Kestens (Springer, Berlin, 1975), p. 17.

Section II. Comparison of viscoelastic behavior of glass with a Lennard-Jones model system.

by S. M. Rekhson, D. M. Heyes, C. J. Montrose
and T. A. Litovitz

Journal of Non-Crystalline Solids 38 & 39 (1980) 403-408

COMPARISON OF VISCOELASTIC BEHAVIOR OF GLASS WITH A LENNARD-JONES MODEL SYSTEM

by

S. M. Rekhson*, D. M. Heyes, C. J. Montrose, and T. A. Litovitz

Vitreous State Laboratory
The Catholic University of America
Washington, DC 20064
U.S.A.

Viscoelastic properties of a Lennard-Jones (LJ) model system studied in a previous work were compared with the behavior of inorganic and organic glass-forming liquids and solid glasses. In the region of small stresses and strains both the LJ model system and "real materials" demonstrate linear behavior. After adjustment of time scales the stress relaxation curves for LJ model and fused silica were found to be similar despite the 16 orders of magnitude difference in viscosities of the liquids.

At high stresses the viscosity of the LJ model system drops, stress relaxation occurs faster, and a peak appears in the stress versus time plots for shearing with a constant rate. This phenomenon, well-known for high polymers, has also been observed for inorganic glasses. The curves, $\Delta \log \eta$ vs. $\log \sigma$, that show a drop of viscosity of $Rb_2O - SiO_2$ glass and LJ model at stresses higher than 10^8 Pa, are in remarkable agreement. The LJ model is shown to provide a semi-quantitative representation of a variety of glass-forming liquids.

INTRODUCTION

Inorganic glass-forming liquids are often subjected to severe manufacturing and operating conditions. For example, during forming operations glass melts experience shear strains and rates about 10^5 cm/cm and 10^6 sec^{-1}, respectively -- enormous values. Calculations of melt behavior, however, are normally made using experimental data obtained at strains and rates 10 orders of magnitude lower. On looking for methods to study the behavior glass-forming liquids subjected to high amplitude disturbances we came to a molecular dynamics (MD) investigation of a model liquid system.

*Now with General Electric Co., Lighting Business Group, Nela Park, Cleveland, Ohio 44112.

MD is a computer simulation technique for probing the microscopic behavior of a system that allows one to account for the many-body nature of the molecular interactions. It involves following some representative number of molecules, N, by solving the classical equations of motion on a high speed computer to obtain their trajectories in time steps $\Delta t \sim 10^{-14}$. From the results of an MD experiment -- essentially a record of the system's path through phase space -- one can determine any measurable property of the system, as well as many that are experimentally inaccessible.

Heyes, Kim, Montrose and Litovitz [1] studied by this method the model system of 108 Lennard-Jones (LJ) particles. These "molecules" interact through pairwise additive forces described by the LJ 6-12 potential

$$\phi(r) = -4u\,[(a/r)^6 - (a/r)^{12}], \qquad (1)$$

where r is the separation of an interacting pair and u and a are constants with dimensions of energy and distance respectively. The method of computer simulation was shown [1] to be a very effective technique for studying the behavior of an LJ model. In this paper we compare the results obtained for the LJ system with the behavior of inorganic and organic glass-forming liquids to assess the extent to which it can be considered representative of real materials. Although no real glass-forming liquid can be characterized by a potential of the LJ form (only the noble gas fluids Ar, Kr, etc., are quantitatively represented in this way) there may be some important common features in dynamical behavior of liquids which are essentially independent on the chemical composition and the extent of supercooling relative to the melting point.

SHEAR STRESS RELAXATION, LINEAR BEHAVIOR

Consider first the linear (small stress and strain) behavior. Figure 1 shows the stress response when a shear strain is switched on at the instant t = 0 and is kept constant.

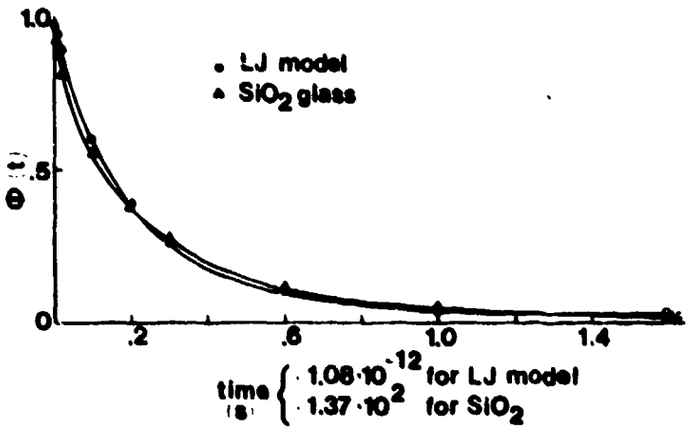

Figure 1
A Comparison of the Normalized Stress Relaxation Functions for the LJ Model System and SiO_2 Glass

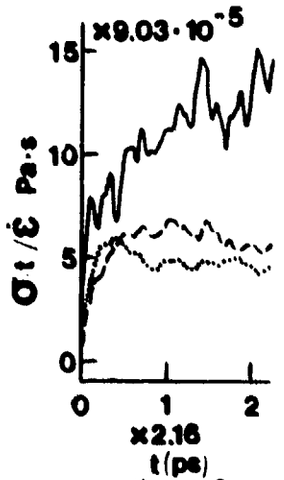

Figure 2

The Time Dependence of the Reduced Stress, $\sigma(t)/\dot{\epsilon}$, for the LJ model: —— $\dot{\epsilon} = 4.4 \times 10^{10}\ s^{-1}$, ---- $\dot{\epsilon} = 1.66 \times 10^{11}\ s^{-1}$, ···· $\dot{\epsilon} = 3.32 \times 10^{11}\ s^{-1}$.

VISCOSITY: NON-LINEAR BEHAVIOR

Figure 3 shows experimental data for 4 systems with viscosities ranging from 10^{-4} to 10^{14} Pa·s. Despite an enormous difference in structures for all systems we have similar behavior; that is, a decrease of viscosity beginning at a certain range of values of the stress. The stresses at which deviations begin are different and clearly dependent on the details of structure. In this connection it is interesting to note the coincidence of the curves for inorganic glass and the LJ model.

STRESSES IN A LIQUID SHEARED WITH A CONSTANT RATE $\dot{\epsilon}$

Typical curves obtained for the LJ model at small and large $\dot{\epsilon}$ are shown in Fig. 2. The fact that at high $\dot{\epsilon}$ the stress versus time curve rises to a maximum value and then decays to its long time limiting value is well known for real materials. The curves, quite similar to ones shown in Fig. 2, were reported for poly(vinyl acetate) [9], and other glass-forming liquids.

STRESS RELAXATION: NON-LINEAR BEHAVIOR

Experiments on stress relaxation for constant strain ϵ_0 imposed at $t = 0$ were carried out as a function of ϵ_0. There is little change in the instantaneous shear rigidity as a function of ϵ_0; however, there is a marked difference in the relaxation function, $\phi(t)$. The relaxation function in the high initial strain case decays more rapidly to zero at long times. Precisely the same conclusions were drawn by the authors [6] who studied extensively the stress relaxation in polyisobutylene. Their data demonstrate the dependence of the storage modulus G' on radian frequency ω for different maximum amplitudes of deformation rate $\dot{\epsilon}_{max} = \epsilon_0 \nu$ (where ν is the frequency). Increase of $\dot{\epsilon}_{max}$ (or ϵ_0 for any given ν) cuts off the long time tail of $G'(\omega)$ function similarly to that observed in this work for $\phi(t)$.

DISCUSSION

1. Experimental evidence is provided to support the assumption that there are important basic features in viscoelastic behavior which are common to materials with enormous differences in structure. These are: a) transition from elastic behavior at $t \to 0$ to viscous flow at larger times. The transition itself can be characterized by fairly similar distributions of relaxation times for LJ model compared to that of real materials: inorganic glasses, inorganic and organic monomeric liquids. b) In all systems studied similar

Adjusting time scales we compare relaxation of stresses (in portions of initial stress) in fused silica glass and the LJ model. For SiO_2 we used the data of Leko and Mescheryakova [2]. Taking into account the 16 orders of magnitude difference in viscosities the similarity in behavior seems to be remarkable. The LJ curve indicates that the stress relaxation in the LJ model is characterized by the distribution of relaxation times. The LJ curve in Fig. 1 is well approximated by a function of the double exponential form

$$G(t) = G_\infty [(1 - a) \exp(-t/\tau_1) + a \exp(-t/\tau_2)], \qquad (2)$$

where G_∞ is the instantaneous shear rigidity and a the constant. The ratio τ_2/τ_1, which is usually considered as a characteristic of the distribution width, is equal to 10. This ratio ir very close to that found in most inorganic and organic monomeric liquids [3,4]. For example, for B_2O_3, $\tau_2/\tau_1 = 9$, and for borosilicate glass, $\tau_2/\tau_1 = 8$.

Coincidence of the parameters describing macroscopic behavior does not mean the identity of microscopic mechanisms. It means, however, that the varieties of mechanisms are similar in the sense that much faster mechanisms coexist with slower ones.

VISCOSITY: LINEAR BEHAVIOR

The next step is to apply to the LJ model some of the equations of the linear theory of viscoelasticity which were proven to be valid for inorganic glasses. The equation relating the normalized shear stress relaxation function, $\phi(t)$, the shear rigidity modulus, G_∞, to the viscosity of the material, is

$$\eta = G_\infty \int_0^\infty dt\, \phi(t). \qquad (3)$$

In Ref. [1] η was computed for the LJ system in this fashion, i.e., using G_∞ and $\phi(t)$ obtained in the stress relaxation experiment at constant strain ϵ. Then the experiment on LJ model was carried out to determine the stress response of the system when a constant shear rate $\dot{\epsilon}$ is initiated at $t = 0$.

The stress was found to behave as shown in Fig. 2 (see the upper curve). Again using the linear theory, this response is described by the form

$$\sigma(t) = \dot{\epsilon}\, G_\infty \int_0^t dt'\, \phi(t'), \qquad (4)$$

which gives Eq. (3) at $t = \infty$: $\sigma(t\to\infty)/\dot{\epsilon} = \eta = G_\infty \int_0^\infty dt\, \phi(t)$. The initial slope is $G_\infty \dot{\epsilon}$ and the long-time value is $\eta \cdot \dot{\epsilon}$. The shear rigidity and viscosity determined in this second type of experiment agreed to within statistical uncertainty with that found in the first type of experiment. This procedure or similar ones were carried out for many commercial silicate glasses [5] to show that they behave as linear viscoelastic bodies at low stress and strain. Thus the LJ model is quite representative of many real materials, the behavior of which at low amplitudes, is described by linear theory.

25

non-linear effects were observed at higher amplitudes of shearing strain or stress.

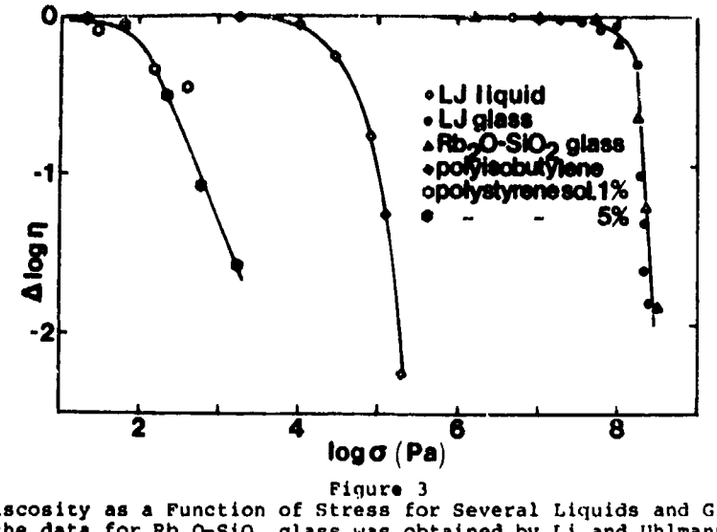

Figure 3
Viscosity as a Function of Stress for Several Liquids and Glasses (the data for Rb_2O-SiO_2 glass was obtained by Li and Uhlmann [7] the data for polymer solutions are given by Ferry in [8]).

2. The drop of liquid viscosity with increasing stress or strain rate seems to be a general phenomenon; it occurs in all liquids studied under shear, uniaxial extension and compression, and in some liquids even under hydrostatic pressure.

All viscoelastic functions and parameters as defined refer to isothermal changes of state. At the same time the energy, dissipated during viscous flow may heat the sample. The work of viscous shearing heating is $W = \sigma\varepsilon = \sigma\dot{\varepsilon}t = \sigma^2 t/\eta$, which indicates that the dissipated energy increases as σ^2. Therefore, the control of constant temperature of the sample is an important feature of the measurements of viscosity as a function of stress. While it is a difficult problem in some "real" experiments is was fairly easy to keep constant the temperature of the "sample" during MD experiments. Thus, the factor which might be considered as a reason for the drop in viscosity has been excluded. Large deformations are likely to produce distortion or reorganization of the system's structure. Evidence supporting this hypothesis was obtained in Ref. [1] by defining and measuring a set of planar distribution functions for the LJ model system. The representation of the modified structure is sketched in Fig. 4 (neglect at first the line connecting the center of the molecules).

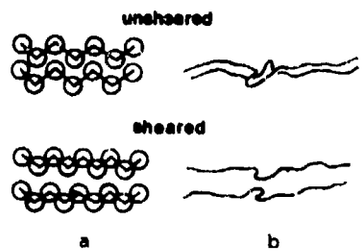

Figure 4
A Pictorial Representation of the Structural Changes Under Influence of Large Deformations in Simple Liquids (a) and Polymers with Entanglement Coupling (b).

From this one can see the nature of the structural reorganization that has occurred; the system has arranged itself into layers aligned with the flow direction. The connection of the center of the molecules by the line gives an impression of the analogy in the behavior of simple liquids and polymers of high molecular weight. Figure 4b shows the influence of shearing upon the two polymer chains with entanglement coupling. The nature of stress or strain induced structural rearrangements is still quite speculative. Figure 4 gives one of the possible pictorial interpretations of the similarity in behavior which has been found in this work for the materials with different structures.

References

[1] Heyes, D.M., Kim, J.J., Montrose, C.J., and Litovitz, T.A., (to be submitted to the J. Chem. Phys.).

[2] Leko, V.K., and Mescheryakova, E.V., Stress relaxation in fused silica, The Soviet Jrnl. of Glass Physics and Chemistry, (Translation of Fizika i Khimiya Stekla, Consultants Bureau, New York) 2 (1976) 311-316.

[3] Litovitz, T.A. and Davis, C.M., Structural and shear relaxation in liquids, in: W.P. Mason (ed.), Physical Acoustics, Vol. II A, 281 (Academic Press, New York, 1965).

[4] Macedo, P.B. and Napolitano, A., Effects of a distribution of volume relaxation times in the annealing of BSC glass, J. of Res. of the NBS, A. Phys. and Chem. 71A (1967) 231-238.

[5] Rekhson, S.M. and Ginzburg, V.A., Relaxation of stress and deformation in stabilized silicate glasses, The Soviet Jrnl. of Glass Physics and Chemistry, (Translation of Fizika i Khimiya Stekla, Consultants Bureau, New York) 2 (1976) 422-428.

[6] Yanovski, Yu.G., Non-linear relaxation during flow of polymer systems, in: Bartenev, G.M. and Zelenev Yu.G. (eds.), Relaksatzionnye Yavleniya v Polymerakh (Relaxation Phenomena in Polymers) 113 (Khimiya, Leningrad, 1972).

[7] Li, J.H. and Uhlmann, D.R., The flow of glass at high stress levels, J. Non-Cryst. Solids 3(1970) 127-147.

[8] Ferry, J.D., Viscoelastic Properties of Polymers (John Wiley and Sons, Inc., New York, 1970).

[9] Joseph, S.H. and Duckett, R.A., Effects of pressure on the non-linear viscoelastic behavior of polymers: 2. Poly(vinyl acetate), Polymer, 19 (1978) 844-849.

Section III. The viscoelastic behavior and rheology of liquids under shear at high pressures: A molecular dynamic study.

by D. M. Heyes, T. A. Litovitz
and C. J. Montrose

The viscoelastic behavior and rheology of liquids under shear at high pressures: A molecular dynamics study

by

D.M. Heyes, T.A. Litovitz and C.J. Montrose
Vitreous State Laboratory
Catholic University of America
Washington, D.C. 20064

ABSTRACT

A molecular dynamics investigation of the microscopic behavior of simple liquids subjected to shearing conditions similar to those found in elastohydrodynamic rolling contacts is outlined. The behavior of a model liquid and more complicated traction fluids at high levels of stress are strikingly similar. The calculations give insights into the structural origin of shear failure and reveal a restructuring of the compacted material into layers, which significantly reduces its shear viscosity. This change is also manifest in an increase of bulk pressure and decrease in high frequency shear rigidity modulus and thermal conductivity. Thermal effects in the nonlinear region of viscosity are consistent with standard macroscopic theory.

can be done by appending the idea of a limiting shear stress to the low amplitude, i.e. linear, shear response. In order to test this hypothesis and, more generally, to provide a framework on which to base analytical representations of lubricant viscoelastic behavior, we have undertaken a Molecular Dynamics (MD) investigation of a model liquid system under conditions approximating those found in an EHD contact. Even though the model system is particularly simple, one can expect to reproduce the major features of shear characteristics of real lubricants. Then, because an MD experiment provides one with a complete microscopic record of the system's evolution in time, one can "measure" aspects of its behavior that are not accessible in conventional experiments, but which provide useful insights into the origin of the properties of liquids under the above extreme conditions.

The MD calculation procedure follows rather closely that pursued in certain model calculations of the contact [3] in that we observe a portion of liquid as it is sheared. This is equivalent to concentrating on a "slice" of lubricant as it traverses the region of contact. Although a simultaneously applied time dependent pressure and shear rate could have been studied, we have confined our attention at this stage to considering the response of a model fluid to a time varying shear rate at a series of densities (pressures).

INTRODUCTION

In several recent papers Bair and Winer [1,2] have examined the problem of understanding the shear stress response of liquids in concentrated contacts with particular attention to the possibility of predicting elastohydrodynamic (EHD) traction data. They point out that, under the severe conditions to which the lubricant is subjected -- large shearing rates and large, rapidly varing normal pressures, there is a dearth of primary laboratory data on which to base a physical model of the lubricant's behavior. In a series of well conceived experiments, they have attempted to remedy, at least partially, this situation. Using their data, they were then able to develop a physically appealing phenomenological model of the non-linear shear response of liquids that is reasonably successful in predicting EHD traction results.

In order to predict traction, one must be able to compute the average shear stress in the contact, which is equivalent to knowing the time evolution of the stress in a fluid element as it moves through the contact zone, where it encounters a simultaneously applied steady shear rate and a time varying pressure. The response of the system under these conditions can, for low shearing rates, be parameterized in terms of the shear viscosity, η, a shear rigidity modulus, G_∞, and a distribution of relaxation times. At the rather large shearing rates generally encountered, this relatively simple description must be modified to incorporate the non-linear character of the dynamical stress response. Bair and Winer [2] suppose that this

THE MODEL

MD is a computer simulation technique for probing the microscopic behavior of a system that allows one to account for the many-body nature of the molecular interactions. It involves following some representative number of molecules, N, by solving the classical equations of motion on a high speed computer to obtain their trajectories in time steps of typically 0.01 ps [4]. Since only a rather a limited number of molecules is treated (generally less than a thousand), the molecules are confined to remain in a cubic box which is surrounded by images of itself to avoid severe boundary effects. In many circumstances the artificialities introduced by this procedure are rather insignificant. From the results of an MD "experiment" -- essentially a record of the system's path through phase space -- one can determine any measurable property of the system, as well as many that are experimentally inaccessible.

The model system under investigation is an assembly of 108 Lennard-Jones (LJ) particles; these molecules interact through pairwise additive forces described by the LJ 6-12 potential,

$$\phi(r) = -4u\left[(a/r)^6 - (a/r)^{12}\right], \qquad (1)$$

where r is the separation of an interacting pair, and u and a are constants with dimensions of energy and distance, respectively. All the computed quantities are in so-called LJ reduced units which are given in terms of u, a, and m, the mass

of an individual particle. Although no real lubricant can be characterized by a potential of the LJ form (only the noble gas fluids Ar, Kr, etc., are quantatively represented in this way) their structural and dynamical behavior can be expected to be qualitatively similar to that of the model fluid. As a result one can expect that the microscopic insights derived from MD experiments will serve as useful guidelines for understanding and modeling the behavior of real lubricants and perhaps for the "molecular engineering" of improved liquid traction fluids and lubricants. For the purpose of comparison with experiment frequent conversion from reduced to "real" units will be made, using the parameters for Ar which are given in Table 1.

Two methods of shearing the box of molecules were adopted. The results of each method agree within statistical error; however, each method is well suited to examine a particular aspect of the investigated phenomenon.

The first method attempts to mimic the enviroment a lubricant experiences in EHD rolling contacts, in which the fluid forms a thin, almost parallel film of length 400μm and thickness 1μm, typically under fully flooded conditions. This thin film is achieved in the model system by employing periodicity in the x and y directions only, so that an infinitely thin film is simulated [5]. The moving rollers are replaced by two fluid layers translating with the desired velocities, U_1 and U_2. Molecules from the three regions are not allowed to mix and are kept from doing so by reflection boundary conditions in the z direction, which are discussed in detail

elsewhere [5]. The fluid walls (FW) are maintained at a preset temperature by adjusting their velocities at each time step of the integration scheme. The main features of the model are pictorially represented in Fig. 1.

The second method is a modification of the Homogeneous Shear technique [4] (MHS), which is better suited to study the viscoelastic behavior of the fluid because it employs periodicity in all directions so that a bulk material is sheared. It also enables a desired strain rate to be instantaneously achieved throughout the liquid. The molecular trajectories are disturbed from those governed by equilibrium fluctuations by imposing a shear strain rate, $\dot{\epsilon}$, on the system. This is accomplished by displacing the x-coordinate of the i'th molecule in the MD cell by an amount $\delta x_i = \dot{\epsilon} z_i \Delta t$, where z_i is the z coordinate of particle i and Δt is the length of the time step, for as long as the shearing is required. The results of this technique, in particular those relating to viscoelasticity (derived using a time dependent strain rate), complement those of the FW method.

We have used non-equilibrium MD experiments to investigate the linear and non-linear shear response of the LJ system under a variety of thermodynamic conditions. The temperature, T, and number density, ρ, initially studied were close to the normal freezing temperature, T_0, of the LJ liquid, that is, 0.722 $k_B T/u$ and 0.8442 Na^3/V, respectively. Densifications of 10%, 20%, and 50% relative to the starting density were achieved by suddenly (within one time step) compressing the system at constant

temperature. The densifications were achieved so rapidly that the systems were kinetically prevented from crystallizing. The reduced number densities of the other states considered are thus 0.92862, 1.01304 and 1.2663.

Each calculation was undertaken for a duration of at least 30 reduced time units (65 ps). The computations were carried out on a PDP 11/40 computer.

RESULTS AND DISCUSSION

We first consider the $\dot{\epsilon}$ dependence of shear viscosity on shear rate in the non-linear region.

In the MHS method a uniform x velocity profile was set up instantaneously whereas a period of several time units was required for the fluid walls to drive the central region into this state. An x velocity gradient was achieved by maintaining the upper and lower walls at velocities of U and -U, respectively. It is relevant here to mention that at all densities and shear rates considered, the fluid film sheared uniformly in the z direction without slip at the walls, and not concentrated in the center as has been speculated before [6]. An example of a $v_x(z)$ so derived from the $\rho = 0.8442$ and $\dot{\epsilon} = 0.3373$ calculation is shown in Fig. 2. The value of $\dot{\epsilon}$ corresponds to an extremely large shear rate -- on the order of $10^{10} s^{-1}$ depending somewhat upon the particular values of u, a, and m that are chosen. Such large values of $\dot{\epsilon}$ were chosen since it is desirable to explore the system's behavior at shear rates on the order of the reciprocal of the viscoelastic relaxation times. For the LJ fluids these are approximately unity (about 10^{-12} s). The shear stress needed to define a shear viscosity is readily derived from the velocities and positions of the molecules. The $\alpha\beta$ component of the stress tensor is defined below,

$$\sigma_{\alpha\beta} = - (1/V) \left[\sum_{i=1}^{N} m v_i^{\alpha} v_i^{\beta} - \frac{1}{2} \sum_{i \neq j}^{N} \sum_{j}^{N} (\alpha_{ij} \beta_{ij} / r_{ij}) \frac{\partial \phi}{\partial r_{ij}} \right], \quad (2)$$

where V is the volume of the MD cell, v_i^α is the α velocity component of molecule i relative to the average velocity and α_{ij} is the α component of the separation between molecules i and j. The subscripts for the shear stress component, σ_{xz}, are dropped in further discussion.

At low shear rates ($\Delta U/h$) plots of traction versus slip are linear, however at high stress levels ($\sim G_\infty/100$) the traction increases less rapidly than slip speed. In other words the shear viscosity ($= \sigma/\dot{\varepsilon}$) decreases from the equilibrium value of η_0 with inreasing shear rate. The MHS method was used to obtain η versus $\dot{\varepsilon}$ for a variety of densities. The forms of η/η_0 versus stress in Fig. 3 resemble closely those obtained from twin-disk experiments for the fluids 5P4E [7], L63/1271 [8] and Oxilube 85/140 [9] after making the appropriate conversions to real units. The ratio η/η_0 descends markedly from unity in the region ~ 50MPa. The decrease in η with $\dot{\varepsilon}$ is not due to thermal heating because the calculations were conducted isothermally. Another method of presenting the behavior, $\log[\eta/\eta_0]$ vs. $\log[\dot{\varepsilon}\tau]$, where τ is a characteristic shear relaxation time ($= \eta_0/G_\infty$), again shows marked quantitative similarity between the model fluid and a real fluid, which is in this case 5P4E [2]. These results suggest that the model and real liquids might share a common mechanism of failure at high levels of shear stress. With the support of the previous results we now discuss associated changes in the fluids which until now have only been speculated upon.

These high stresses cause extreme distortions of the system's structure. The intermolecular forces are not sufficiently strong to support the enormous stress levels that develop; consequently there is a rupturing and reorganization of the structure resulting in enhanced flow behavior. Evidence supporting this hypothesis was obtained by measuring the number density in the z direction between the fluid walls. The density profile of Fig. 5, derived for ρ = 1.01304 and $\dot{\epsilon}$ = 0.3584 suggests the form of this structural reordering. The molecules align themselves into "glide" planes along the line of shear. A pictorial representation of the structure suggested is given in Fig. 6. This layering was not observed when the walls were stationary or moving in the same direction with equal velocity. In this context it is relevant to note that IR studies of flow under EHD conditions have also been interpreted in terms of molecular alignment along the line of shear [10].

These structural rearrangements are also manifest in changes in the so-called normal pressure components , $P_{\alpha\alpha}$ ($= -\sigma_{\alpha\alpha}$). Typically, $P_{zz} > P_{xx} > P_{yy}$ although their differences are small when compared with each component's change on shearing. The zz pressure component increases are shown in Fig. 7 and predict an improvement in the load carrying capacity equivalent to ~0.5GPa at most.

It is now widely accepted that knowledge of the viscoelastic response of lubricants is necessary to interpret EHD results over the range of possible operating conditions [9].

In order to better understand non-linear viscoelasticity the MD calculations were conducted with a time varying strain rate.

We consider the dynamical response of the LJ material to an imposed shear that is "switched on" suddenly using the MHS method. Two types of MD experiments are of interest: (a) the response of the system to a steady shearing rate (uniform velocity gradient) $\dot{\epsilon} = \partial v_x/\partial z$ that is initiated at time $t = 0$; and (b) the response of the system to a constant shear strain (a pulse of shearing rate) imposed at time $t = t'$. Linear response theory provides us with relations between the two types of responses: the shear stress response to a step of shear strain can be written as

$$\sigma(t)/\epsilon = G_\infty \phi(t), \tag{3}$$

where $\phi(t)$ is the normalized ($\phi(0) = 1$) shear stress relaxation function. In terms of these parameters the shear stress response to a "small" steady shear rate imposed at $t = 0$ is,

$$\sigma(t)/\dot{\epsilon} = G_\infty \int_0^t dt' \, \phi(t'). \tag{4}$$

Since the steady state ($t \to \infty$) value of this is just the viscosity of the material, η_0, we have,

$$\eta_0 = G_\infty \int_0^\infty dt' \, \phi(t') = G_\infty \tau. \tag{5}$$

The last equality serves to define the shear relaxation time τ.

Experiments of the type described as (a) above were then carried out as a function of $\dot{\varepsilon}$ for values of $\dot{\varepsilon}$ well beyond the range for which linear behavior can be expected. A representative selection of the results is displayed in Figs. 8 and 9 in which the density (constant $\dot{\varepsilon}$) and shear rate (constant density) dependence of η are shown, respectively.

Several features of these figures are worthy of comment. At short times the system behaves largely as an elastic solid in that the stress increases linearly with time,

$$\sigma(t) = G_\infty \dot{\varepsilon} t. \qquad (6)$$

The shear rigidity modulus rises linearly with pressure at roughly the same rate as more complicated fluids, as is revealed in Fig. 10. Liquids cannot permanently support a shear strain and consequently the stress levels off to a value determined by the shear viscosity of the sheared state. There is evident "shear thinning," or a decrease of viscosity with increasing shear rate. The predicted value of the stress build-up for the $\rho = 0.92862$, $\dot{\varepsilon} = 0.6963$ state using equation (4), shown in Fig. 8, clearly overestimates the actual stress obtained.

Also, a maximum in the stress versus time curve for those simulations in the high density/shear rate regime is observed. This indicates that the large shear deformations are producing structural distortions which lag in time somewhat behind the growth of the shear stress but follow rather closely the observed time variation of the normal pressure components in the

material (see Fig. 11). This relatively slower development of what can be thought of as transient stress-induced glide planes is consistent with the observed shear thinning and stress "overshoot" behavior presented. It is also consistent with the observation that the stress relaxation function decays more rapidly in a highly sheared system than in an equilibrium system. A comparison of the two types of behavior is presented in Fig. 12. The form of these $\phi(t)$ consists of a rapidly ($t < 0.2$) decaying portion which is presumably inertial in origin and due to small motions of the molecules within the random network structure. Further stress relaxation requires the cooperative rearrangement of larger molecular groups and is consequently slower. The attenuation of $\phi(t)$ with increasing shear rate is indicative of the enhanced stress relieving properties of the structurally reorganized system. The stress overshoot observed in non-linear viscoelastic experiments on polymers [11] has a form that is quite similar to the curves obtained for the LJ system. While the microscopic mechanisms for the two systems are obviously quite different, the general principle that associates the stress overshoot phenomena (as well as shear thinning) with a time dependent structural reorganization process remains quite valid.

In this context it is perhaps relevant to note that a more rapid decay of the stress relaxation function can be thought of as both a suppression of the long relaxation times associated with stress relaxation and also a reduction in the shear rigidity modulus, at low frequencies, G, (a rather well known

phenomenon in polymeric systems [12]). It is found experimentally that the extracted shear rigidity modulus of the liquids confined in concentrated contacts is up to an order of magnitude smaller than those observed obtained from independent laboratory (ultrasonic) measurements at the same temperature and pressure. The large shear rates ($\sim 10^4 s^{-1}$) that exist in the inlet zone, even under "pure rolling" conditions, could be sufficient to reorder the liquid preferentially along the line of shear. The observed increase in shear modulus with rolling speed [13] for a wide range of fluids is particularly significant evidence for this interpretation because if molecular orientation of the molecule along the line of flow is the cause of this phenomenon then it would be expected that the modulus would increase with rolling speed because there is less time for molecular rearrangement to take place.

Thermal effects are a major factor in limiting the ability of a fluid to sustain a shear stress at high strain rates [6]. The FW technique is well suited to determine the validity of using standard macroscopic theory on thin films. From conservation of energy considerations the temperature profile under conditions of steady shear flow as given by [14],

$$K \frac{\partial^2 T(z)}{\partial z^2} = - \eta \dot{\varepsilon}^2/(\rho C), \qquad (7)$$

where $K = \lambda/(\rho C)$, and λ and C are the thermal conductivity and specific heat, respectively. Assuming a temperature independent shear viscosity then the solution to equation (7) is

$$T(z) = T(0) - \eta\, \dot{\varepsilon}^2\, z^2/(2\lambda). \qquad (8)$$

A typical temperature profile, taken from the $\rho = 1.01304$ and $\dot{\varepsilon} = 0.3584$ state, is shown in Fig. 13. All the temperature profiles can be fitted rather well to the above form which is parabolic in z and hence can be used to estimate λ. Note that these macroscopic equations only apply to a steady state viscous material and do not apply under viscoelastic conditions where some energy is stored as potential energy and is not dissipated. The density and shear rate dependence of λ is given in Fig. 14. The trends are consistent with the general behavior that thermal conductivity decreases as a material becomes more fluid-like.

CONCLUSIONS

We have performed non-equilibrium molecular dynamics calculations on LJ fluids with the aim of gaining insights into the mechanisms of liquid failure at high levels of stress such as is found in EHD contacts.

The model liquids "rupture" at similar stresses to those of more complicated real fluids due to marked structural reordering into layers. Paradoxically, although structural aspects of the liquids present a more solid-like appearance, other more dynamically related properties such as shear viscosity and thermal conductivity manifest changes which are associated with enhanced fluidity.

ACKNOWLEDGEMENTS: The authors would like to thank Mr. S.F. Shirron for his computational assistance.

REFERENCES

1. Bair, S., and Winer, W.O., "Shear Strength Measurements of Lubricants at High Pressure," ASME JOURNAL OF LUBRICATION TECHNOLOGY, Vol. 101, 1979, pp. 251-257.

2. Bair, S., and Winer, W.O., "A Rheological Model for Elastohydrodynamic Contacts Based on Primary Laboratory Data," ASME JOURNAL OF LUBRICATION TECHNOLOGY, Vol. 101, 1979, pp. 258-265.

3. Heyes, D.M., and Montrose, C.J., "A Viscoelastic Free Volume Theory of Traction in Elastohydrodynamic Lubrication," in "Proceedings of the International Conference on Fundamentals of Tribology," June 19-22, 1978, Massachusetts Institute of Technology (to be published).

4. Naitoh, T., and Ono, S., "The Shear Viscosity of a Hard-Sphere Fluid via Nonequilibrium Molecular Dynamics," Journal of Chemical Physics, Vol. 70, 1979, pp. 4515-4523.

5. Ashurst, W.T., and Hoover, W.G., "Dense-Fluid Shear Viscosity via Nonequilibrium Molecular Dynamics," Physical Review, Series A, Vol. 11, 1975, pp. 658-678.

6. Johnson, K.L., and Cameron, R., "Shear Behaviour of Elastohydrodynamic Oil Films at High Rolling Contact Pressures," Proceedings of the Institution of Mechanical Engineers, Vol. 182 (pt. 1), pp. 307-330.

7. Hirst, W., and Moore, A.J., "The Elastohydrodynamic Behavior of Polyphenyl Ether," Proceedings of the Royal Society of London, Series A, Vol. 344, 1975, pp. 403-426.

8. Hirst, W., and Moore, A.J., "Non-Newtonian Behaviour in Elastohydrodynamic Lubrication," Proceedings of the Royal Society of London, Series A, Vol. 337, 1974, pp. 101-121.

9. Hirst, W., and Moore, A.J., "Elastohydrodynamic Lubrication at High Pressures II. Non-Newtonian Behaviour," Proceedings of the Royal Society of London, Series A, Vol. 365, 1979, pp. 537-565.

10. Lauer, J.L., "Study of Polyphenyl Ether Fluid (5P4E) in Operating Elastohydrodynamic Contacts by Infrared Emission Spectroscopy," ASME JOURNAL OF LUBRICATION TECHNOLOGY, Vol. 101, 1979, pp. 67-73.

11. Brereton, M.G., "The Non-Linear Viscoelastic Properties of Molten Polymers and Concentrated Solutions," Polymer Engineering and Science, Vol. 18, 1978, pp. 1050-1056.

12. Yanovski, Y.G., in "Relaksatzionnye yavleniya v Polimerakh (Relaxation Phenomena in Polymers)," ed. by Bartenev, G., and Zelenev, Y.V., Khimiya, Leningrad, 1972, p. 113.

13. Johnson, K.L., and Tevaarwerk, J.L., "Shear Behaviour of Elastohydrodynamic Oil Films," Proceedings of the Royal Society of London, Series A, Vol. 356, 1977, pp. 215-236.

14. Cheng, H.S., and Sternlicht, B., "A Numerical Solution for the Pressure, Temperature, and Film Thickness Between Two Infinitely Long, Lubricated Rolling and Sliding Cylinders, Under Heavy Loads," ASME JOURNAL OF BASIC ENGINEERING, VOL. 87, 1965, pp. 695-707.

15. Hutton, J.F., and Phillips, M.C., "Shear Modulus of Liquids at Elastohydrodynamic Lubrication Pressures," Nature, Physical Science, Vol. 238, 1972, p. 141.

Table 1

A summary of the reduced units in terms of which all quantities are given. Boltzmann's constant is denoted by k_B.

Quantity	Reduced Unit	SI Unit for Ar
distance	a	0.3405 nm
mass	m	6.64×10^{-26} kg
energy	u	1.65×10^{-21} J
time	$a(m/u)^{1/2}$	2.16 ps
density	a^{-3}	42.1 kg mol/m^3
temperature	u/k_B	119.8 K
pressure, stress	u/a^3	41.8 MPa
modulus	u/a^3	41.8 MPa
viscosity	$(mu)^{1/2}/a^2$.	9.03×10^{-5} Pa s
thermal conductivity	$k_B(m/u)^{-1/2}\sigma^{-2}$	1.88×10^{-2} J m^{-1} K^{-1} s^{-1}

Captions to the Figures

Fig. 1 A pictorial representation of the relationship between the FW MD technique and an EHD contact. The encounter of of molecules with the reflection boundaries in the z direction and periodic boundaries in the x and y directions are illustrated.

Fig. 2 The z dependence of the average x velocity for the ρ = 0.8442 and $\dot{\epsilon}$ = 0.3373 state using the FW model. The z coordinate system is measured from the center of the film.

Fig. 3 The non-linear behavior of: Δ BP L63/1271 [8] (P = 0.8 GPa, T = 27°C, U = 1.12 m/s), O 5P4E [7] (P = 0.45 GPa, T = 27°C, U = 0.6 m/s) and ∇ Oxilube 85/140 [9] (P = 1.2 GPa, T = 30°C, U = 2.2 m/s) from twin-disk experiments. The MHS model: Δ ρ = 0.8442, ∇ ρ = 0.92862, O ρ = 1.01304 and open square ρ = 1.2663.

Fig. 4 The non-linear behavior of: 5P4E [2] $\tau = 9 \times 10^{-3}$ s from experiment. The filled in: Δ ρ = 0.8442, ∇ ρ = 0.92862, O ρ = 1.01304 and square ρ = 1.2663 from MHS MD. The relaxation times, τ, are: 0.12, 0.30, 0.43, and 1.62, respectively.

Fig. 5 The density profile from the ρ = 1.01304 and $\dot{\epsilon}$ = 0.3584 FW calculation.

Fig. 6 A pictorial representation of the structural changes that take place on going from an unsheared (a) to a sheared (b) state. The arrows denote the line and plane of shear.

Fig. 7 The variation in the zz normal pressure conponent for the MHS systems. Δ ρ = 0.8442, ∇ ρ = 0.92862, O ρ = 1.01304 and square ρ = 1.2663.

Fig. 8 The time dependence of the reduced stress, $\sigma(t)/\dot{\epsilon}$: ---- ρ = 0.8442, $\dot{\epsilon}_0$ = 0.6745; ···· (a) actual ···· (b) predicted using equation (4) ρ = 0.92862, $\dot{\epsilon}_0$ = 0.6963; — — — ρ = 1.01304, $\dot{\epsilon}_0$ = 0.7168; —— ρ = 1.2663, $\dot{\epsilon}_0$ = 0.7721. The associated strain rate variations are indicated above the figure.

Fig. 9 The time dependence of the reduced stress, $\sigma(t)/\dot{\epsilon}_0$, for the ρ = 1.01304 state: —— $\dot{\epsilon}_0$ = 0.0896, ---- $\dot{\epsilon}_0$ = 0.3584, ···· $\dot{\epsilon}_0$ = 0.7168.

Fig. 10 The pressure dependence of G_∞: Δ Santotrac 40 [9]; O di(2-ethylhexyl) phthalate [9] from a twin-disk apparatus. Solid line G_∞ = (0.293 + 1.70P) GPa di(2-e)phthalate [15]. The filled in O are obtained from MHS MD.

Fig. 11 The time dependence of the normal pressure components for the ρ = 0.92862 and $\dot{\epsilon}_0$ = 0.6963 state: ····. $P_{zz}(t)$, —— $P_{xx}(t)$, and ---- $P_{yy}(t)$.

Fig. 12 The shear stress relaxation functions for the ρ = 0.8442 —— $\dot{\epsilon}$ = 0 and ---- $\dot{\epsilon}$ = 0.6745. The step in strain (ϵ = 3.6×10^{-3}) at t = 0 is illustrated above this figure.

Fig. 13 The variation in temperature in the z direction for the ρ = 1.01304 and $\dot{\epsilon}$ = 0.3584 state where T_0 = 0.722.

Fig. 14 The effect of non-linearity on thermal conductivity (λ). The symbols refer to the same calculations as for Fig. 7.

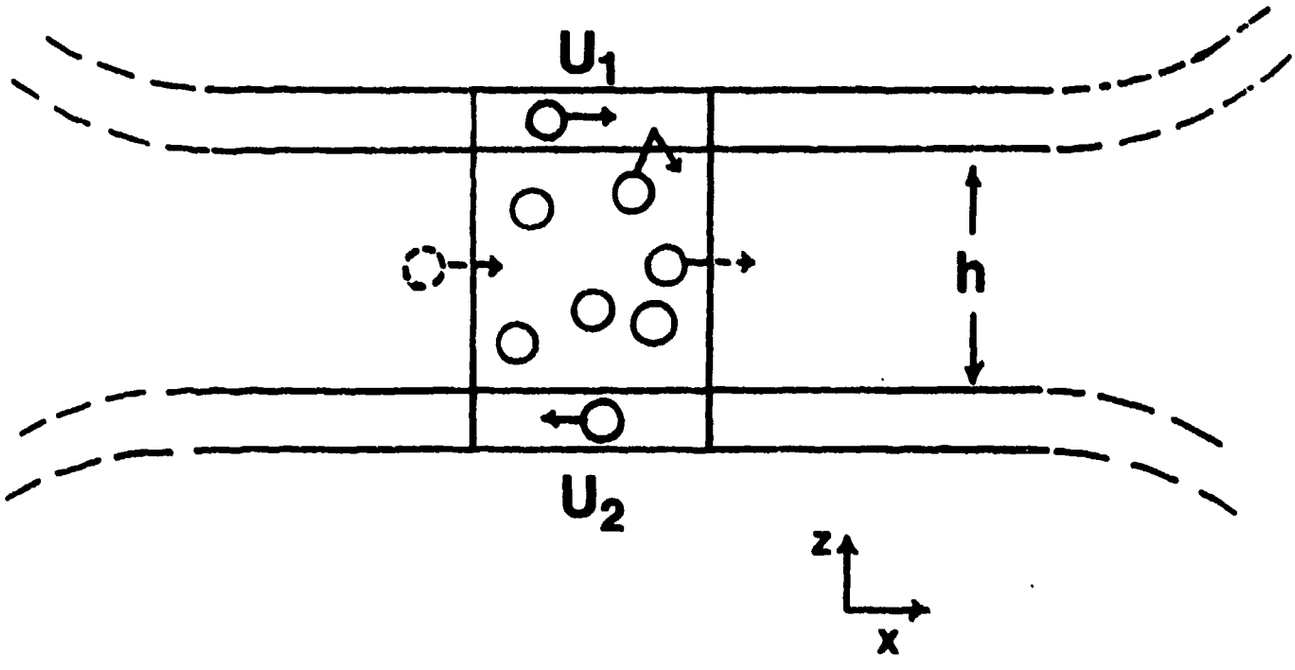

FIGURE 1

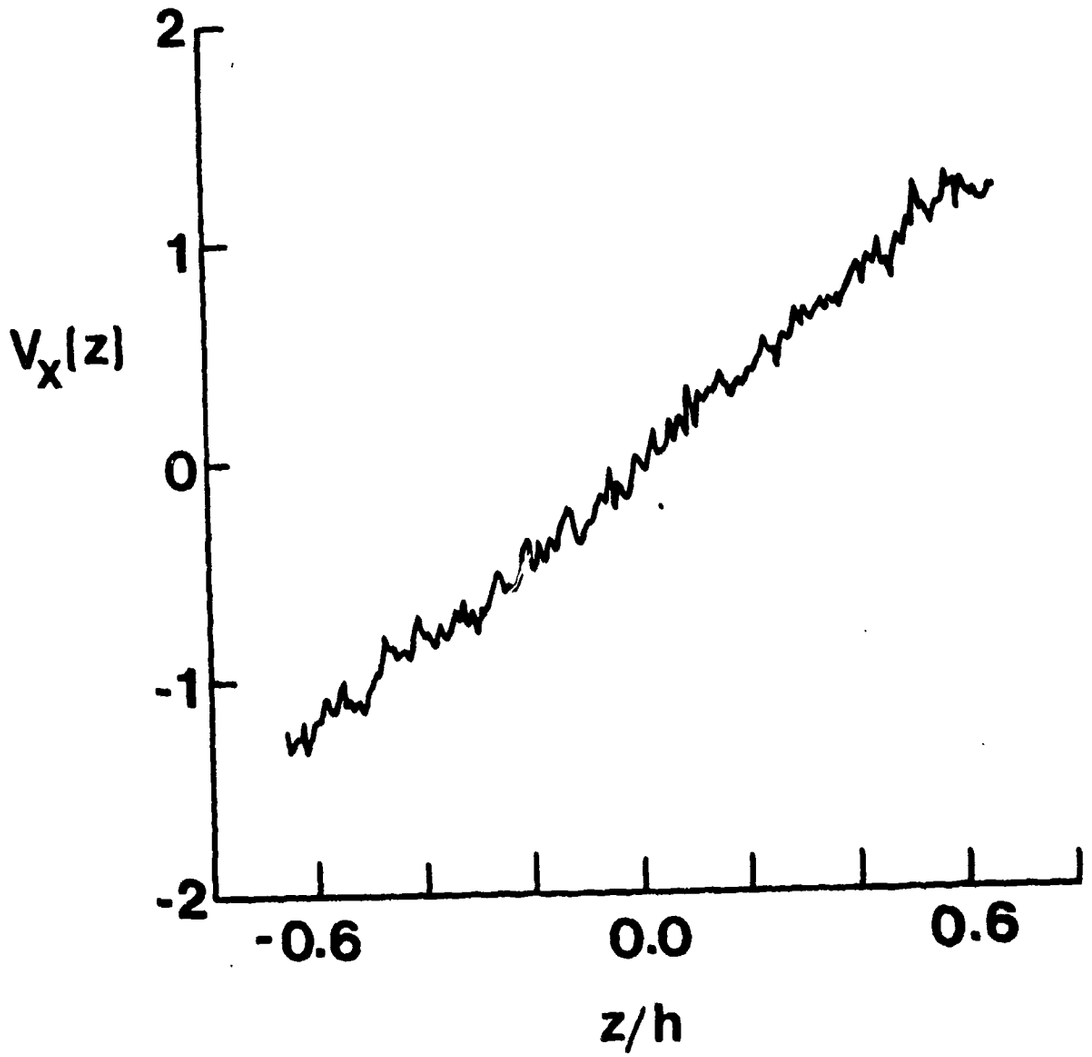

FIGURE 2

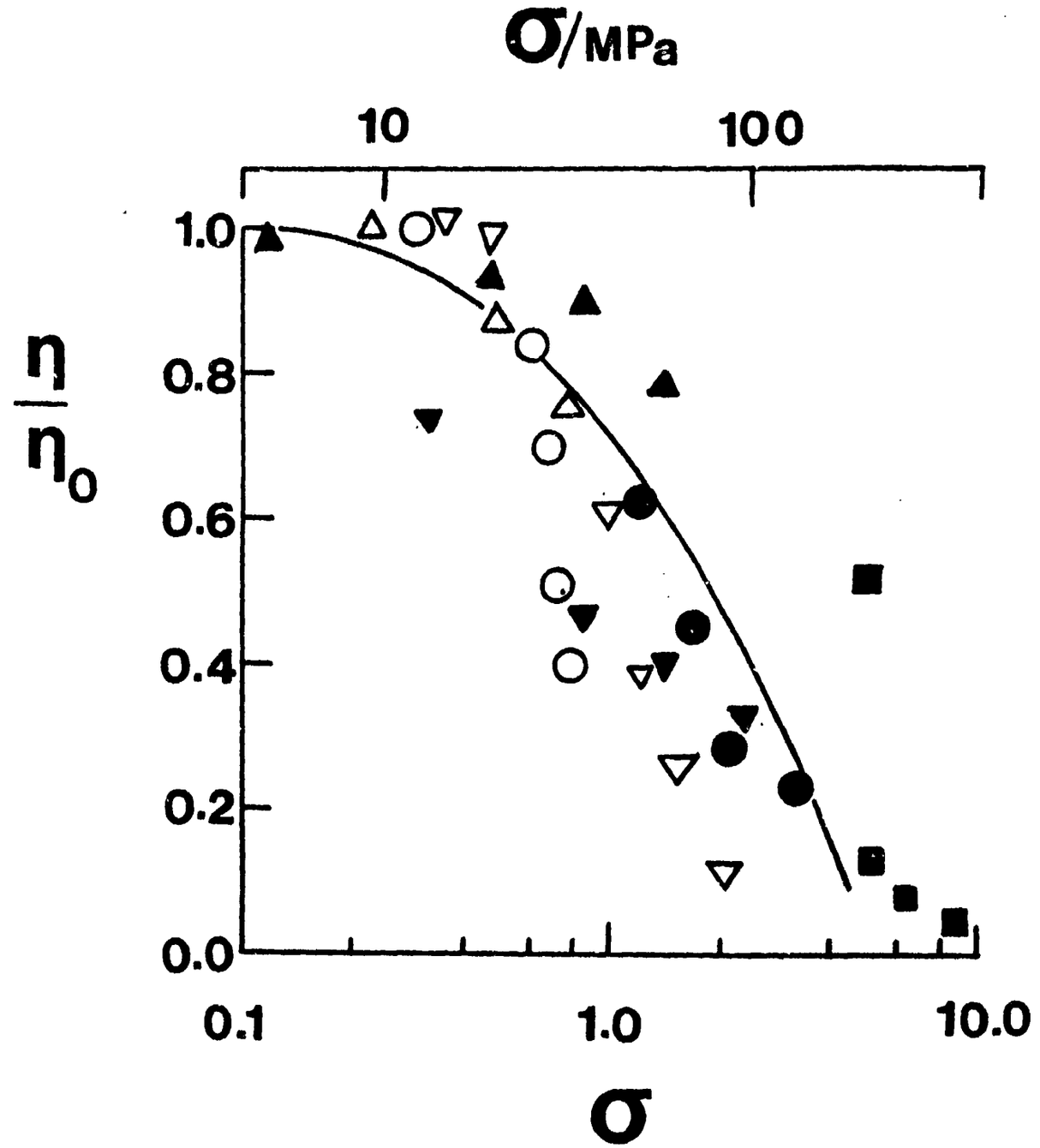

FIGURE 3

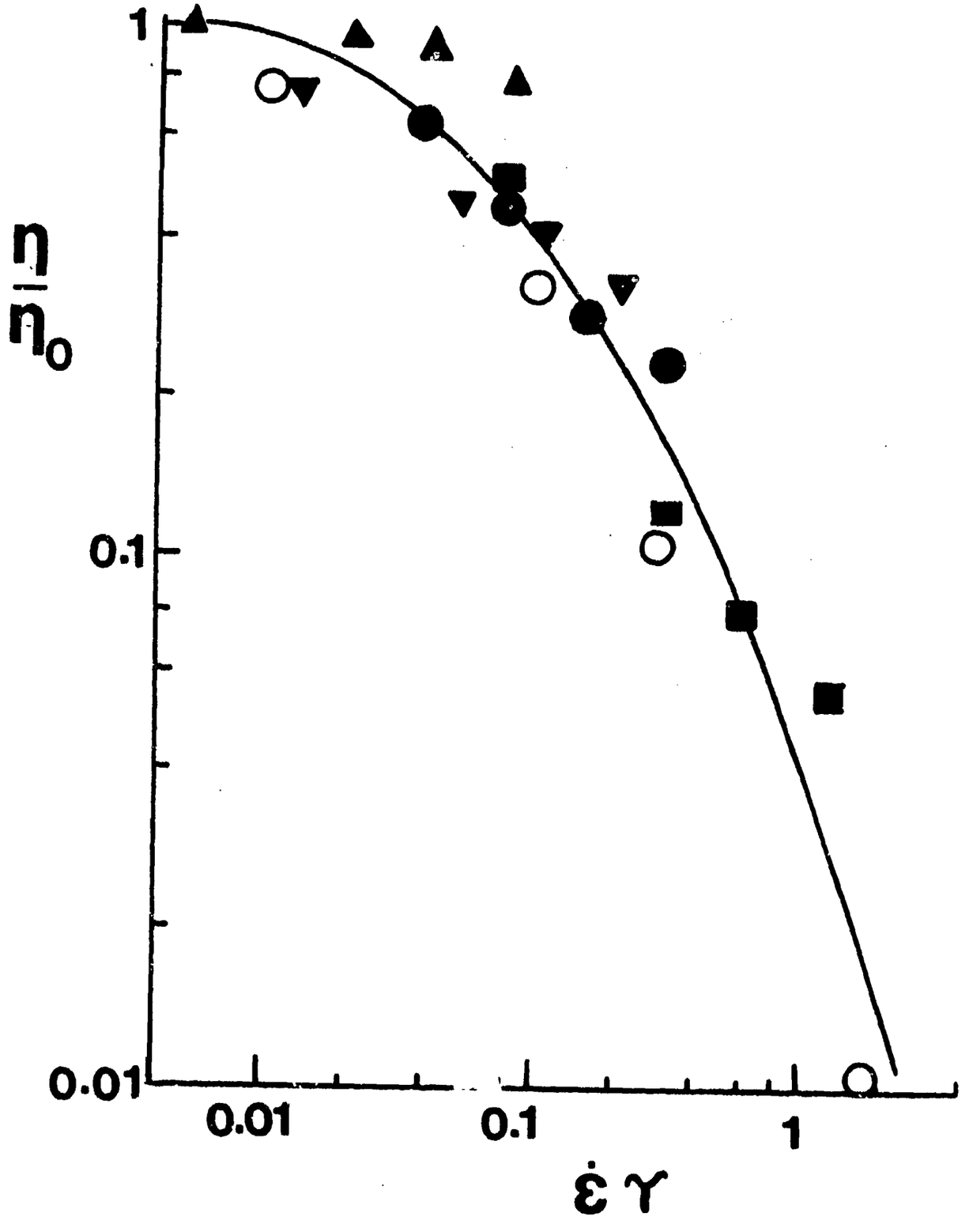

FIGURE 4

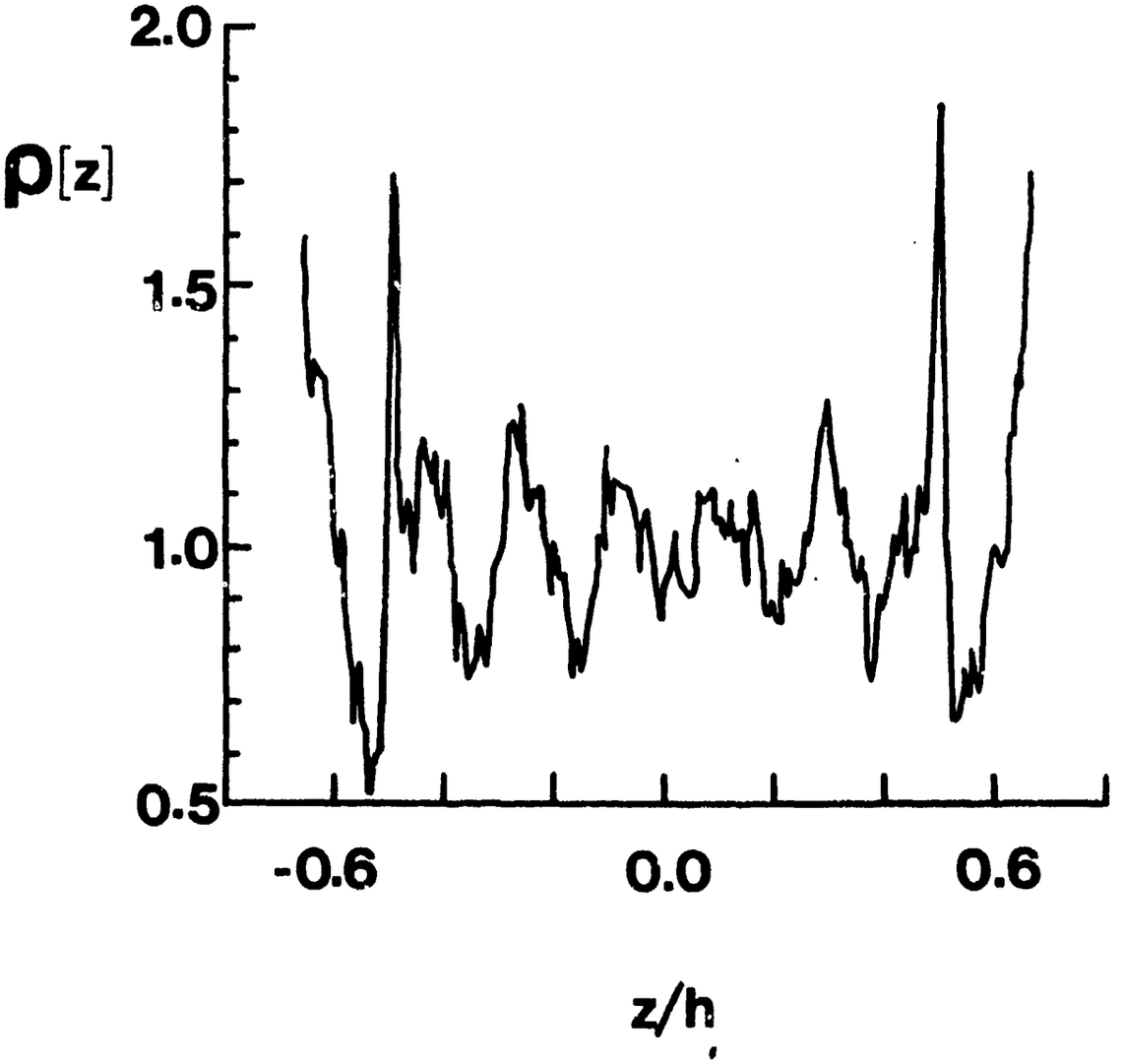

FIGURE 5

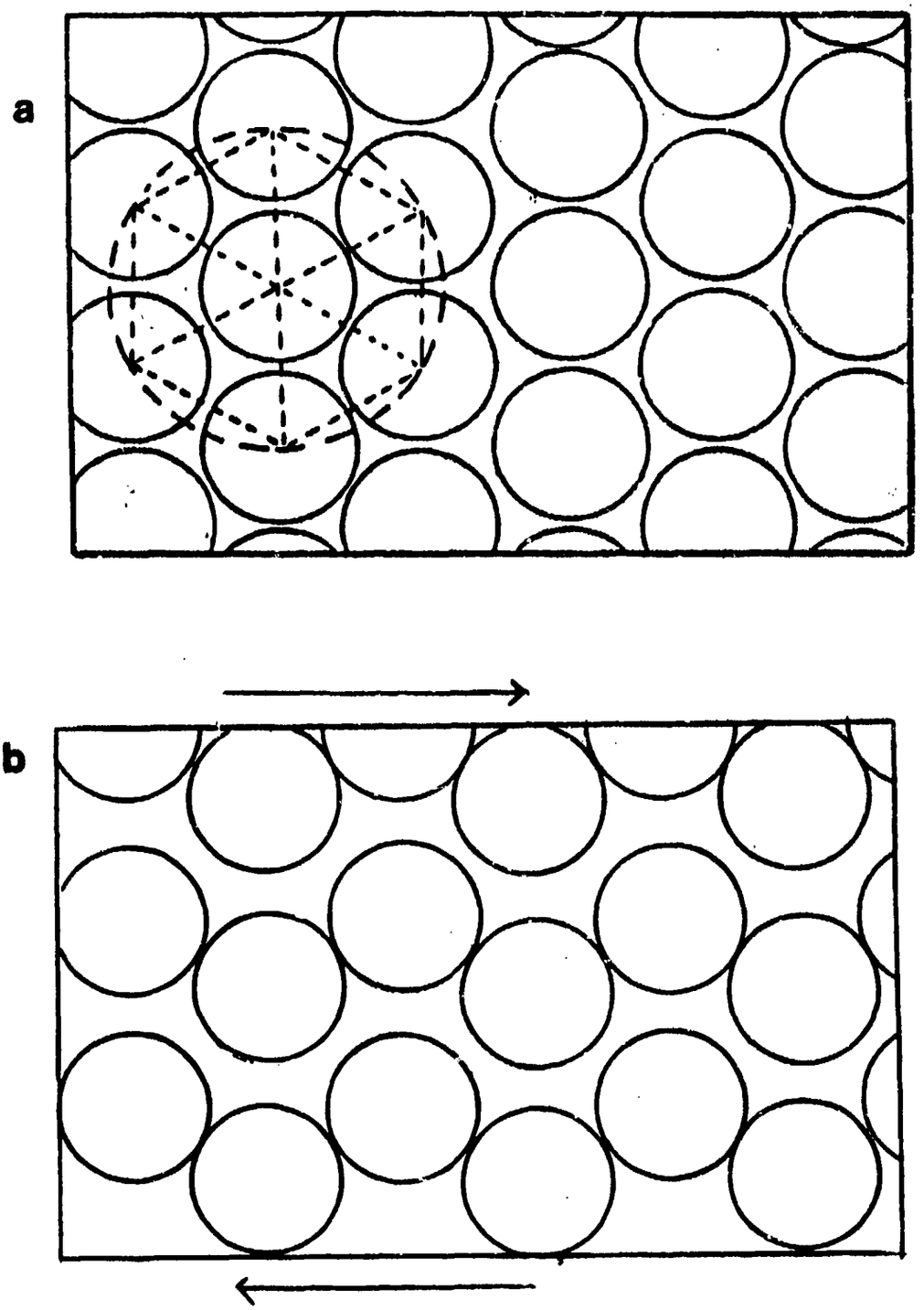

FIGURE 6

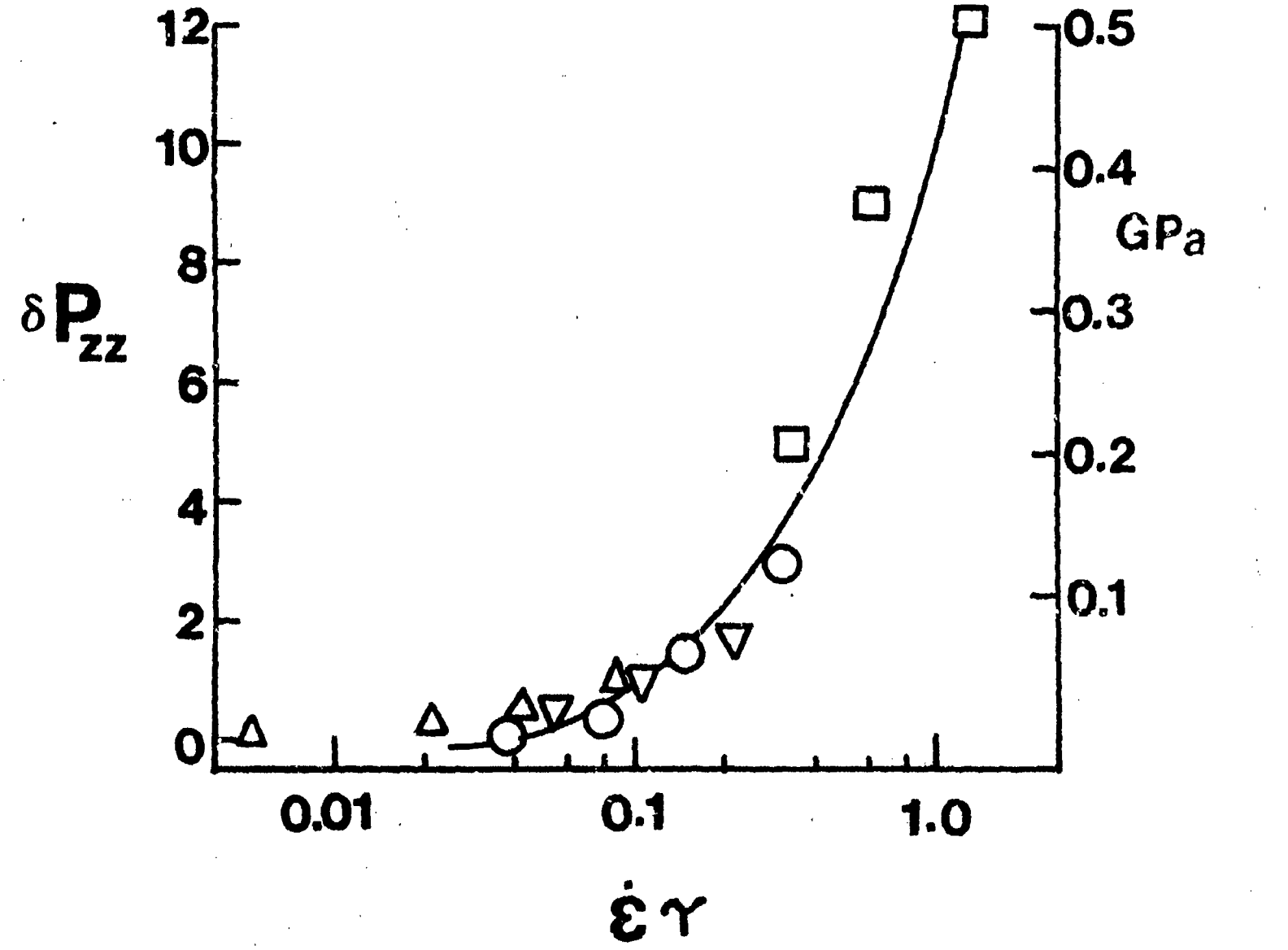
12
10
8
6
4
2
0
δP_{zz}
0.5
0.4
0.3
0.2
0.1
GPa
0.01
0.1
1.0
$\dot{\varepsilon}\gamma$

FIGURE 7

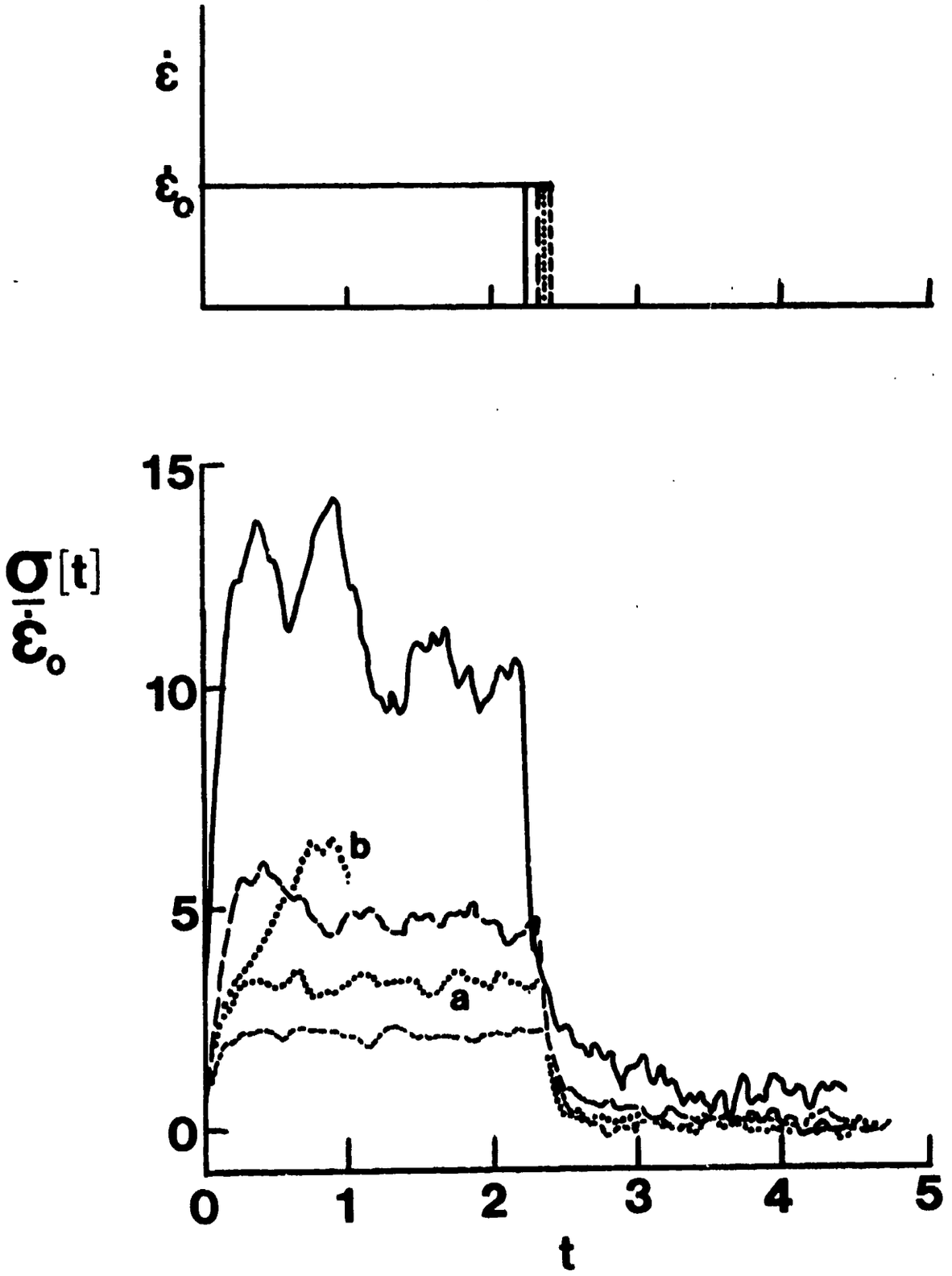
$\dot{\varepsilon}$
$\dot{\varepsilon}_o$
$\frac{\sigma[t]}{\dot{\varepsilon}_o}$
15
10
5
0
b
a
0
1
2
3
4
5
t

FIGURE 8

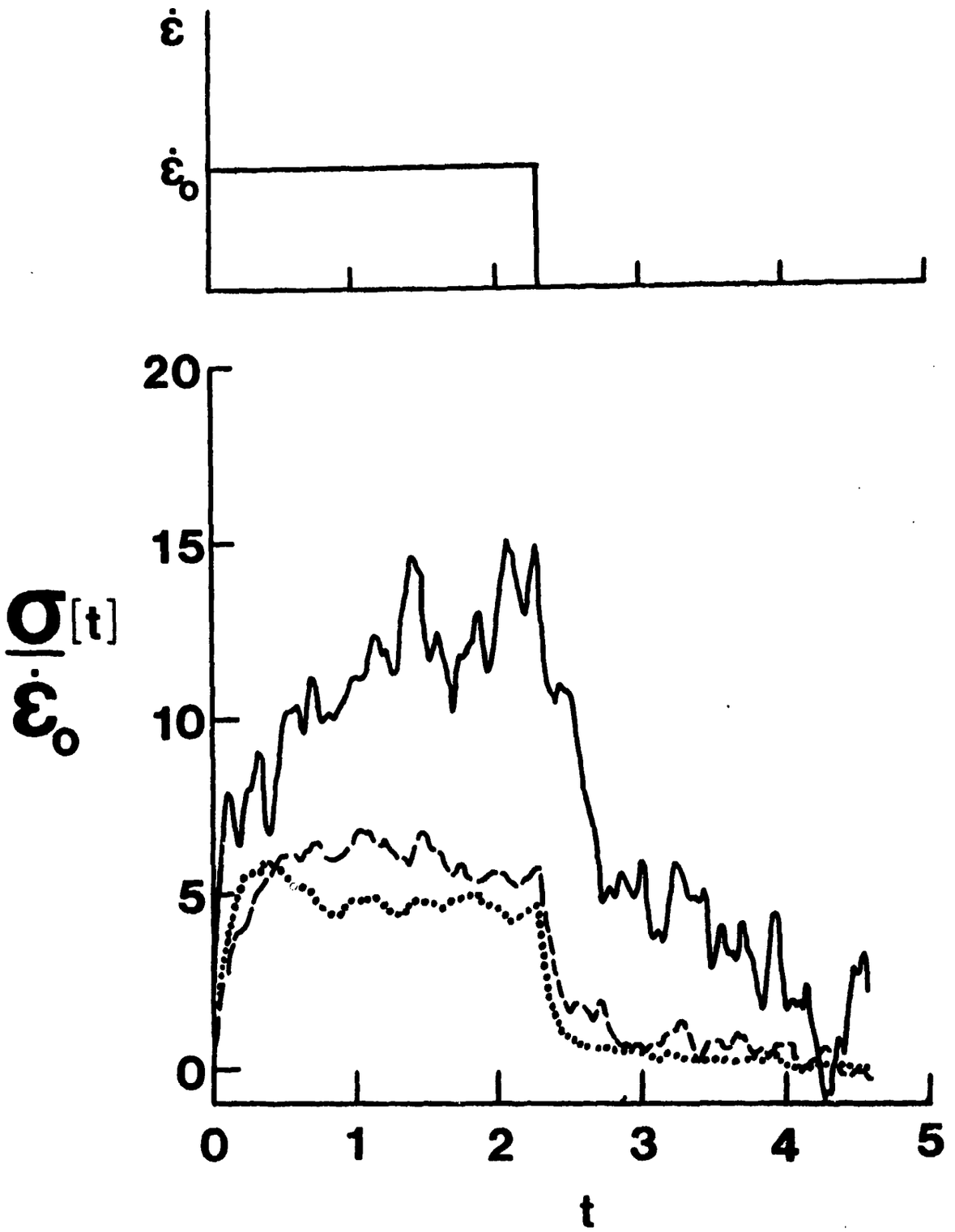
$\dot{\varepsilon}$
$\dot{\varepsilon}_o$
$\frac{\sigma[t]}{\dot{\varepsilon}_o}$
20
15
10
5
0
0
1
2
3
4
5
t

FIGURE 9

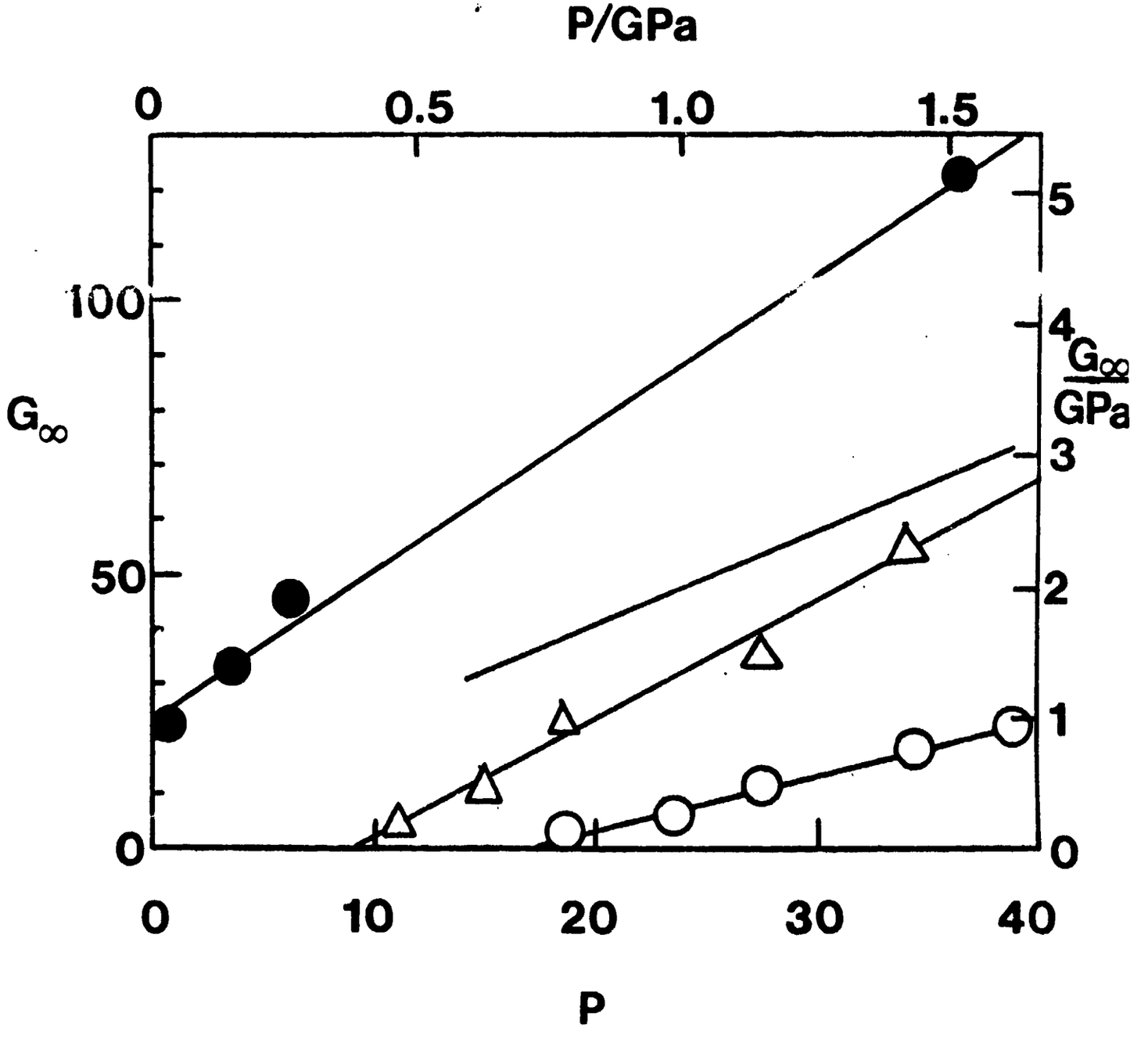
P/GPa
0
0.5
1.0
1.5
100
50
0
G_∞
5
4
3
2
1
0
$\frac{G_\infty}{GPa}$
0
10
20
30
40
P

FIGURE 10

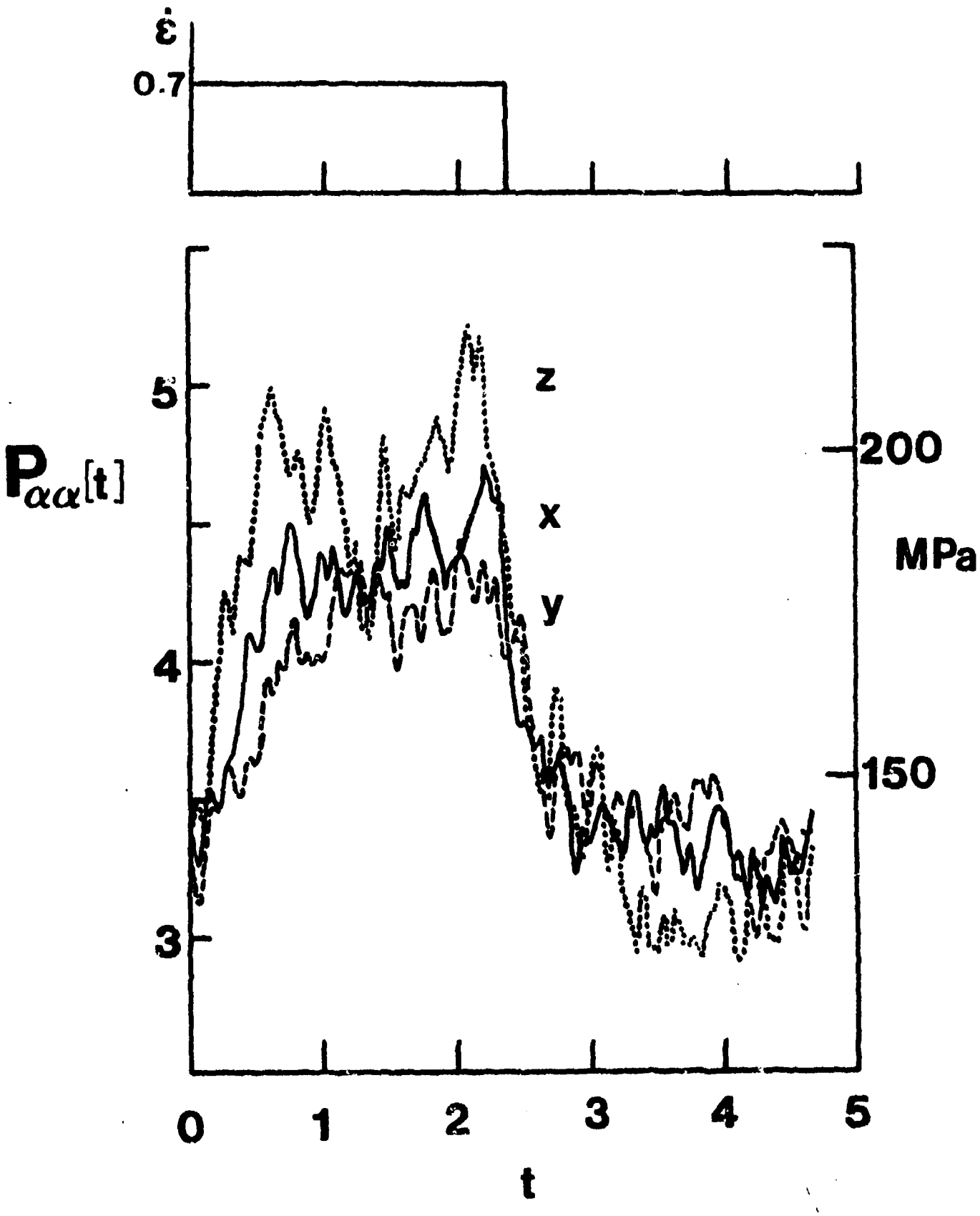

FIGURE 11

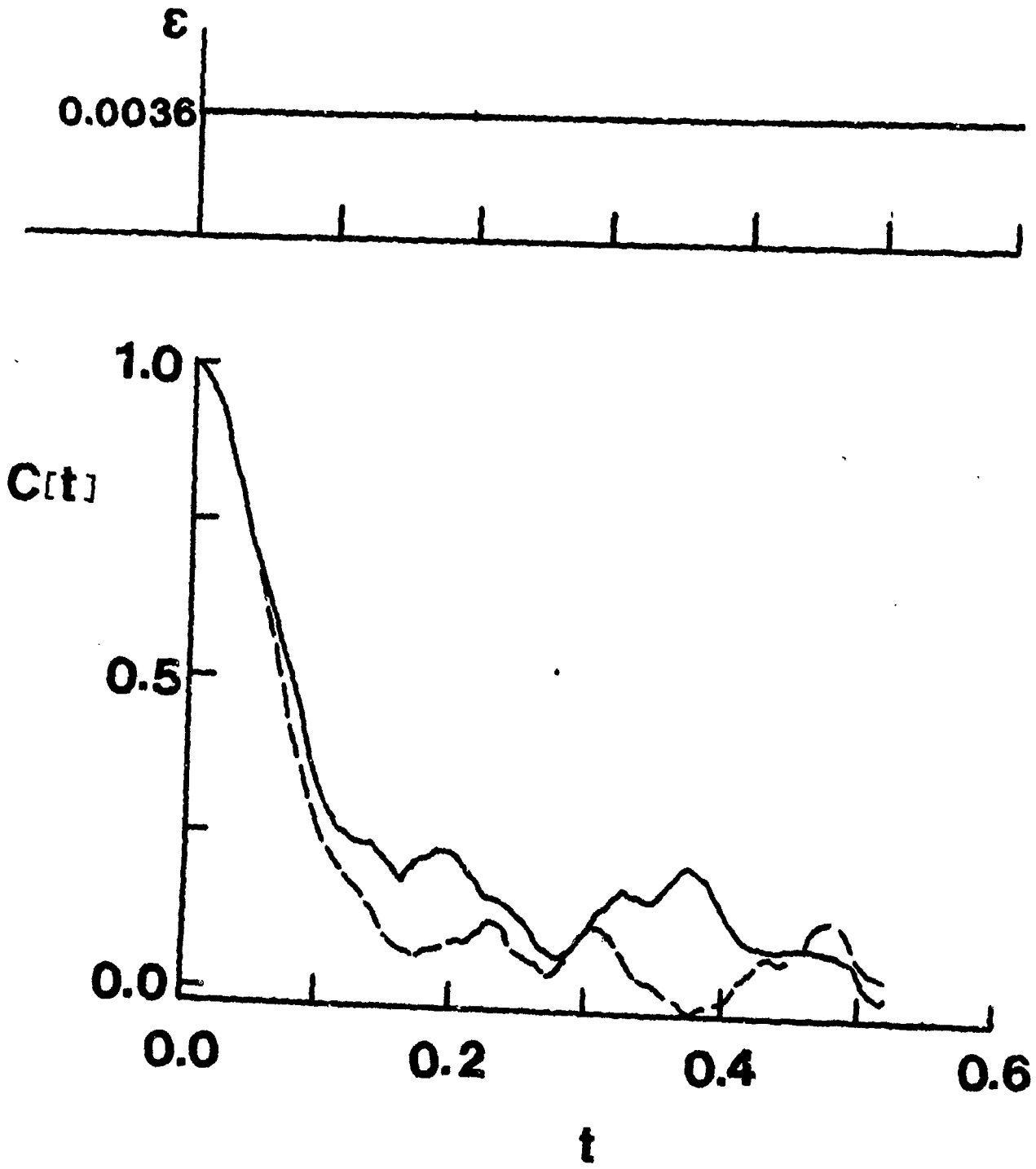

FIGURE 12

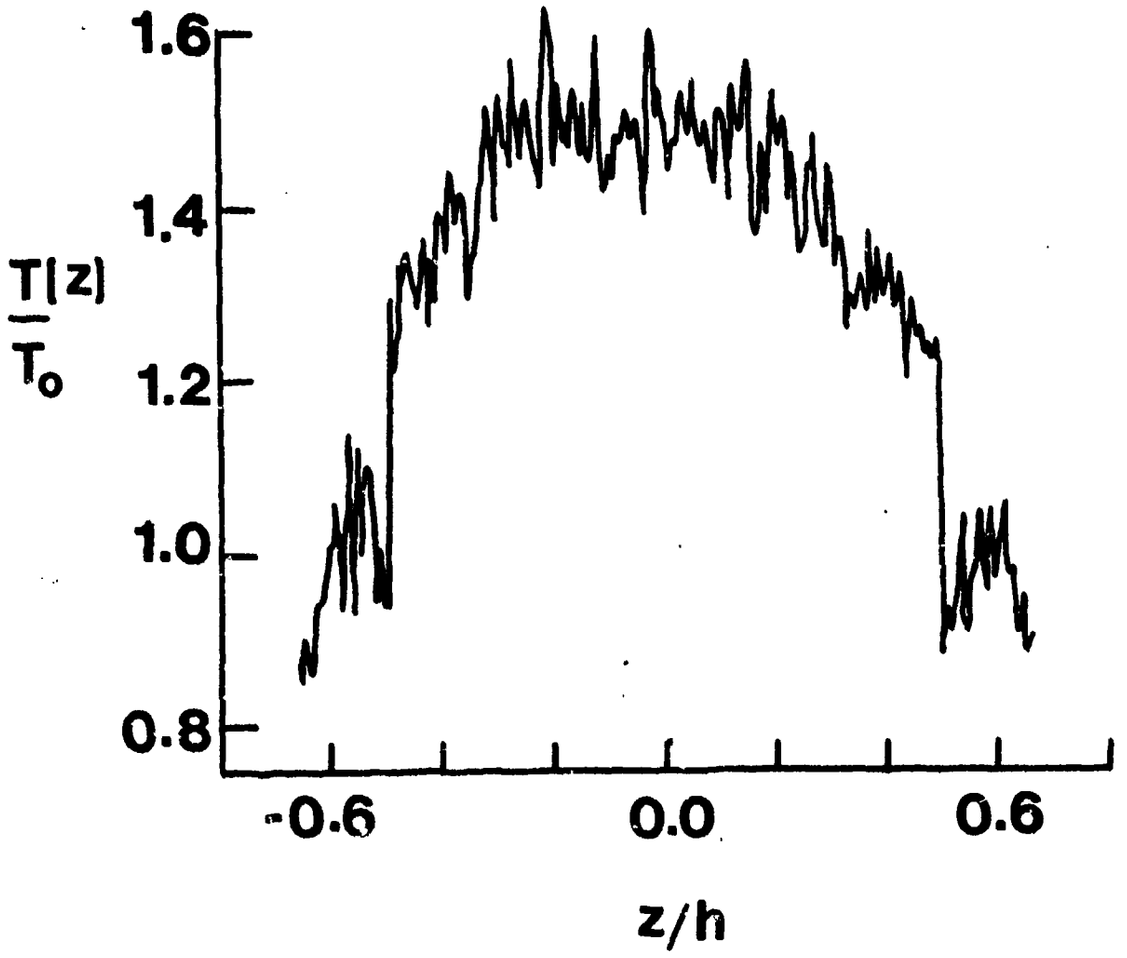

FIGURE 13

Section IV. A theory of non-linear response in liquids and amorphous solids.

by C. J. Montrose

A THEORY OF NONLINEAR RESPONSE IN LIQUIDS AND AMORPHOUS SOLIDS *

by

C.J. Montrose
Vitreous State Laboratory
The Catholic University of Ameri
Washington, D.C. 20064

ABSTRACT

A mathematical model of nonlinear viscoelastic stress relaxation is derived using heuristic arguments relating shear response to dynamical strain induced structural changes in the material. A parameter characterizing the limiting steady-state shear stress appears as a central feature of the model. General formulae are presented and some representative specific cases are considered. The predicted behavior is in qualitative agreement with both MD and "real" experimental observations.

---

* This work was supported by the Office of Naval Research (Contract No. N00014-81-K-0296).

INTRODUCTION

The shear stress response at time t to a shear strain rate history imposed over the time interval 0 to t is given for small stresses by the linear convolution integral form

$$\sigma(t) = \int_0^t dt' \; G_0(t-t')\dot{\epsilon}(t'). \tag{1}$$

In this $\sigma(t)$ is the shear stress at time t, $\dot{\epsilon}(t') = d\epsilon/dt'$ is the shear strain rate, and $G_0(t-t')$ is the shear stress relaxation function. In terms of this last, one can obtain the usual shear viscoelastic parameters of the material:

(1) The instantaneous shear rigidity modulus is just the value of G_0 at the zero-value of its argument, i.e.

$$G_0(0) = G_\infty \; . \tag{2}$$

We make use of this to define a normalized shear stress relaxation function $g_0(s)$ - -

$$G_0(s) \equiv G_\infty g_0(s) \; . \tag{3}$$

(2) The shear viscosity is the integral of the relaxation function G_0:

$$\eta_0 = \int_0^\infty ds \; G_0(s) \tag{4}$$

(3) The shear relaxation time is the integral of the normalized relaxation function:

$$\tau_0 = \int_0^\infty ds \; g_0(s) = \eta_0/G_\infty \; , \tag{5}$$

the second equality following from the use of Eq. (3) in the first. That the relations expressed in Eqs. (2) - (5) are appropriate can be seen by considering a few special strain-rate histories.

Consider first a step of strain $\Delta\epsilon_0$ switched on at the instant of time = 0^+. The shear strain rate is $\dot{\epsilon}(t') = \Delta\epsilon_0\delta(t')$ and from (1) the stress respons is

$$\sigma(t) = \Delta\epsilon_0 G_0(t). \tag{6}$$

At the instant t=0, this gives the instantaneous elastic response. Thus, $G_0(0)$ is indeed the instantaneous shear rigidity, G_∞.

In a similar fashion, we may examine the response to a steady strain rate $\dot{\epsilon}_0$ switched on at time = 0^+; here the stress is given by

$$\sigma(t) = \dot{\epsilon}_0 \int_0^t dt' \; G_0(t-t') = \dot{\epsilon}_0 \int_0^t ds \; G_0(s), \tag{7}$$

the second equality following from substituting $t'=t-s$ in the first. The steady-state viscous behavior is found by taking the $t \to \infty$ limit:

$$\sigma(t \to \infty) = \dot{\epsilon}_0 \int_0^\infty ds \; G_0(s) \tag{8}$$

The ratio $\sigma(t \to \infty)/\dot{\epsilon}_0$ is the usual definition of the viscosity in agreement with Eq. (4).

The results and formulae just given are the usual viscoelastic equations for the linear response of a system when the stresses and strains (and strain-rates) are small. The purpose of this paper is to develop formulae analogous to these which can be used in situations of large stresses and strains, and which will of course reduce to these in the appropriate limits. The paper consists of two main parts: in the first a heuristic approach is used to derive a generalized stress response formula analagous to (1) and to use this to define effective, i.e. strain-rate dependent, moduli, viscosities, and relaxation times. The behavior for some particularly simple impressed strain rate histories is examined. In the second part, specific forms (based roughly on the MD results obtained in this laboratory[1]) of the relevant shear and structural response functions in the theory are assumed. The consequences of these are worked out and the resulting behavior is compared with some existing experimental work.

THE NON-LINEAR RESPONSE EQUATIONS

In generalizing Eq. (1) for the case of finite amplitude shear rates, we assume that the same form can be used if explicit allowance for the dependence of (and dynamic response of) the stress relaxation function on strain rate is made.

Specifically, it is assumed that the stress relaxation function depends upon the structural configuration of the material, which, in turn, responds to the impressed shearing rate. The shear stress is thus expressed as

$$\sigma(t) = \int_0^t dt_0 G[t-t_0|t,\dot{\epsilon}]\dot{\epsilon}(t_0). \tag{9}$$

The form of G for a given shear rate is taken to be

$$G[t-t_0|t,\dot{\epsilon}] = G_0(t-t_0)\{1 - \lambda\int_0 dt_1\dot{\epsilon}(t_1)F[t-t_1|t,\dot{\epsilon}]\}. \tag{10}$$

where F is the structural relaxation function (explicitly time shear rate dependent) and λ is a "strength of coupling" parameter, for which a more physical interpretation will be given below. The structural relaxation function is assumed to depend on the material configuration in the same manner as G, that is, we take

$$F[t-t_1|t,\dot{\epsilon}] = f_0(t-t_1)\{1 - \lambda\int_0^t dt_2\dot{\epsilon}(t_2)F[t-t_2|t,\dot{\epsilon}]\}. \tag{11}$$

Combining (9)-(11) gives for the shear stress

$$\sigma(t) = \int_0^t dt_0\dot{\epsilon}(t_0)G_0(t-t_0) - \lambda\int_0^t dt_0\dot{\epsilon}(t_0)G_0(t-t_0)\int_0^t dt_1\dot{\epsilon}(t_1)f_0(t-t_1)$$
$$+ \lambda^2\int_0^t dt_0\dot{\epsilon}(t_0)G_0(t-t_0)\int_0^t dt_1\dot{\epsilon}(t_1)f_0(t-t_1)\int_0^t dt_2\dot{\epsilon}(t_2)F(t-t_2|t,\dot{\epsilon}) \tag{12}$$

Repeated use of Eq. (11) in (12) leads to an infinite series form for the stress:

$$\sigma(t) = \int_0^t dt_0\dot{\epsilon}(t_0)G_0(t-t_0)\sum_{n=0}^{\infty}(-\lambda)^n\left|\int_0^t dt'\dot{\epsilon}(t')f_0(t-t')\right|^n \tag{13}$$

It should be appreciated that the form in (13) can be obtained more formally from the general Green-Rivlin integral equation,[2]

$$\sigma(t) = \int_0^t dt_0\dot{\epsilon}(t_0)G_0(t-t_0) + \int_0^t dt_0\dot{\epsilon}(t_0)\int_0^t dt_1\dot{\epsilon}(t_1)G_1(t-t_0,\ t-t_1)$$
$$+ \int_0^t dt_0\dot{\epsilon}(t_0)\int_0^t dt_1\dot{\epsilon}(t_1)\int_0^t dt_2\dot{\epsilon}(t_2)G_2(t-t_0,\ t-t_1,\ t-t_2) + \ldots\ldots \tag{14}$$

by assuming that the n^{th} order response function is factorizable as

$$G_n(t-t_0, \ldots t-t_n) = G_0(t-t_0)(-\lambda)^n f_0(t-t_1)f_0(t-t_2) \ldots f_0(t-t_n). \qquad (15)$$

With the usual restrictions on the summand, the series in (13) can be summed in closed form; the result is

$$\sigma(t) = \frac{\int_0^t dt_0 \dot{\varepsilon}(t_0) G_0(t-t')}{1 + \lambda \int_0^t dt' \dot{\varepsilon}(t') f_0(t-t')} . \qquad (16)$$

Eq. (16) is the fundamental dynamical result of this paper. Note that without any loss of generality we may assume that f_0 is normalized as

$$f_0(0) = 1, \qquad (17)$$

absorbing any other factors into the coupling parameter λ. This also implies a definition of the structural relaxation time τ_s as

$$\tau_s = \int_0^\infty dt' f_0(t') . \qquad (18)$$

Eq. (16) can now be written in terms of somewhat more physical quantities by examining the steady-state ($t \to \infty$) form predicted by this equation when a steady shear rate

$$\dot{\varepsilon} = \begin{cases} 0 & (t<0) \\ \dot{\varepsilon} & (t>0) \end{cases} \qquad (19)$$

is applied. The result is

$$\sigma(\infty) = \dot{\varepsilon}_0 \tau_0 G_\infty / (1 + \dot{\varepsilon}_0 \lambda \tau_s) \qquad (20)$$

For large shear rates this becomes

$$\sigma(\infty) \xrightarrow[\dot{\varepsilon} \to \infty]{} G_\infty \tau_0 / \lambda \tau_s \equiv \sigma^* ; \qquad (21)$$

σ^* is seen to be the maximum steady state shear stress that can be sustained by

the system. Eq. (16) can now be cast as

$$\sigma(t) = \frac{G_\infty \int_0^t dt_0 \dot{\epsilon}(t_0) g_0(t-t_0)}{1 + \tau_0 (G_\infty/\sigma^*) \frac{1}{\tau_s} \int_0^t dt' \dot{\epsilon}(t') f_0(t-t')} \tag{22}$$

By considering the strain rate history given in (19) it is possible to define an effective shear-rate-dependent viscosity

$$\eta(\dot{\epsilon}_0) \equiv \sigma(\infty)/\dot{\epsilon}_0 \; ; \tag{23}$$

the form of this is easily found by substituting the second equality in (21) into (20):

$$\eta(\dot{\epsilon}_0) = \frac{G_\infty \tau_0}{1 + \dot{\epsilon}\tau_0 \, (G_\infty/\sigma^*)} \tag{24}$$

This is sketched in Figure 1. An effective rigidity modulus can also be defined by considering the instantaneous stress developed upon application of a step in strain $\Delta\epsilon_0$. Here we obtain

$$G(\Delta\epsilon_0) \equiv \frac{\sigma(0^+)}{\Delta\epsilon_0} = \frac{G_\infty}{1 + \Delta\epsilon_0 (G_\infty \tau_0/\sigma^* \tau_s)} \; . \tag{25}$$

SPECIAL CASES

In the sample computations presented in this section we have used the following typical functional forms and parameter values:

A. $g_0(t) = a \exp(-t/\tau_1) + (1-a)\exp(-t/\tau_2)$

$a = 0.9$

$\tau_2/\tau_1 = 9$

$\tau_0 = \tau_2/5$

B. $f_0(t) = \exp(-t/\tau_2)$

$\tau_s = \tau_2$

C. $G_\infty/\sigma^* = 10$

Figure 2 presents computations using these functions and parameters in Eq. (22) for the strain rate history given in (19). Observe that both the stress overshoot and shear thinning effects observed by Heyes et al[1] (section I of this report) are reproduced. As expected, these effects become more pronounced for large values of the reduced strain rate.

We have also examined the behavior when a step of strain $\Delta\varepsilon_0$ is switched on at time = 0. For this case the strain dependent shear rigidity is given by Eq. (25) and is plotted in Figure 3. The time evolution of the stress is easily computed to be

$$\sigma(t) = G_\infty \Delta\varepsilon_0 \frac{g_0(t)}{1 + \Delta\varepsilon_0 (G_\infty \tau_0/\sigma^* \tau_s) f_0(t)} \quad . \tag{26}$$

This is plotted in Figure 4.

As a last case we consider the application of a steady shear rate [see Eq.(19)] at time = 0, followed by the application of a small (infinitesimal) step of strain $\delta\varepsilon$ imposed at a time $t^* >> \tau_0$, i.e. after the stress has reached its steady state value. The incremental stress $\delta\sigma$ is calculated to be

$$\delta\sigma(t) = \frac{G_\infty \delta\varepsilon}{1 + \dot{\varepsilon}_0 \tau_0 (G_\infty/\sigma^*)} \left\{ g_0(t) - \frac{\dot{\varepsilon}_0 \tau_0 (G_\infty/\sigma^*)}{1 + \dot{\varepsilon}_0 \tau_0 (G_\infty/\sigma^*)} (\tau_0/\tau_s) f_0(t) \right\}; \tag{27}$$

in this equation, the time variable t represents the time following the application of the strain increment. From this equation we can define an effective shear-rate dependent rigidity

$$G(\dot{\varepsilon}_0) \equiv \frac{\delta\sigma(0)}{\delta\varepsilon} = G_\infty \frac{1 + \dot{\varepsilon}_0 \tau_0 (G_\infty/\sigma^*)(1 - \tau_0/\tau_s)}{[1 + \varepsilon_0 \tau_0 (G_\infty/\sigma^*)]^2} \quad , \tag{28}$$

and a shear-rate dependent stress relaxation function

$$g(t;\dot{\epsilon}_0) = \frac{g_0(t) - \dot{\epsilon}_0\tau_0(G_\infty/\sigma^*)[g_0(t) - (\tau_0/\tau_s)f_0(t)]}{1 + \epsilon_0\tau_0(G_\infty/\sigma^*)(1-\tau_0/\tau_s)} \tag{29}$$

This last is plotted in Figure 5. Again there is qualitative agreement with the observations of Heyes et al.[1]

REFERENCES

1. D.M. Heyes, J.J. Kim, C.J. Montrose, and T.A. Litovitz, J. Chem. Phys. 73, 3987 (1980).

2. See, for example, D.W. Hadley and I.M. Ward, Rep. Prog. Phys. 38, 1143 (1975).

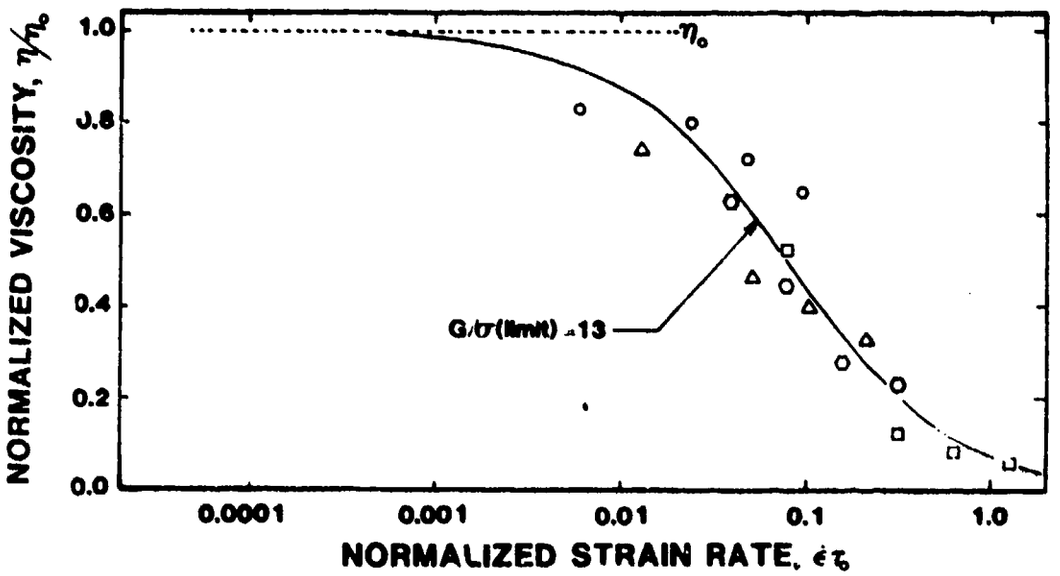

FIGURE 1. The shear-rate dependent viscosity plotted versus reduced strain rate. The data points are MD results (Section I, this report) and the value $G/\sigma(\text{limit})$, i.e. G_∞/σ^*, of 13 was chosen to best fit these data.

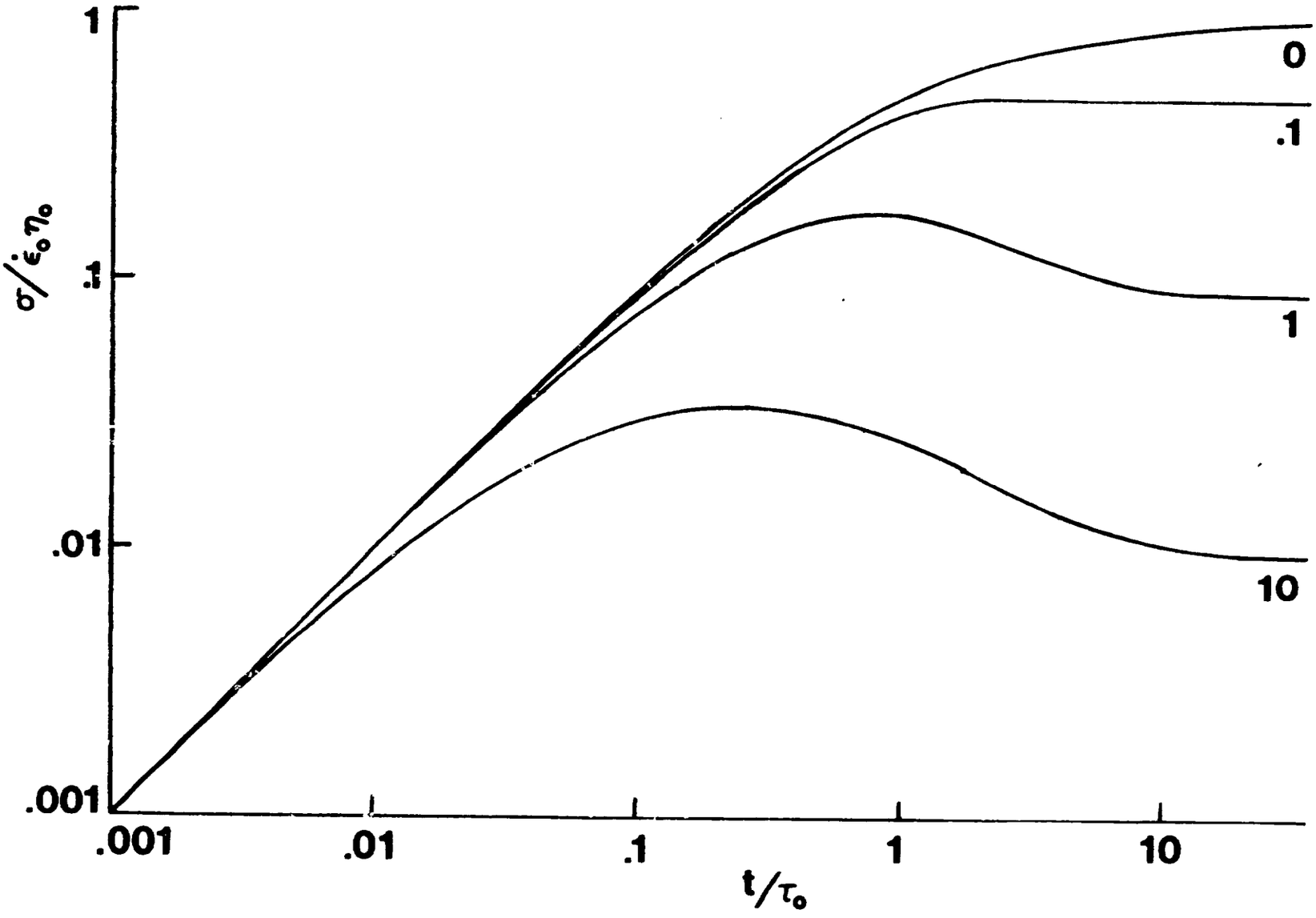

FIGURE 2. Normalized shear stress versus reduced time for various values of the reduced strain rate $\dot{\epsilon}\tau_o$ shown at the right.

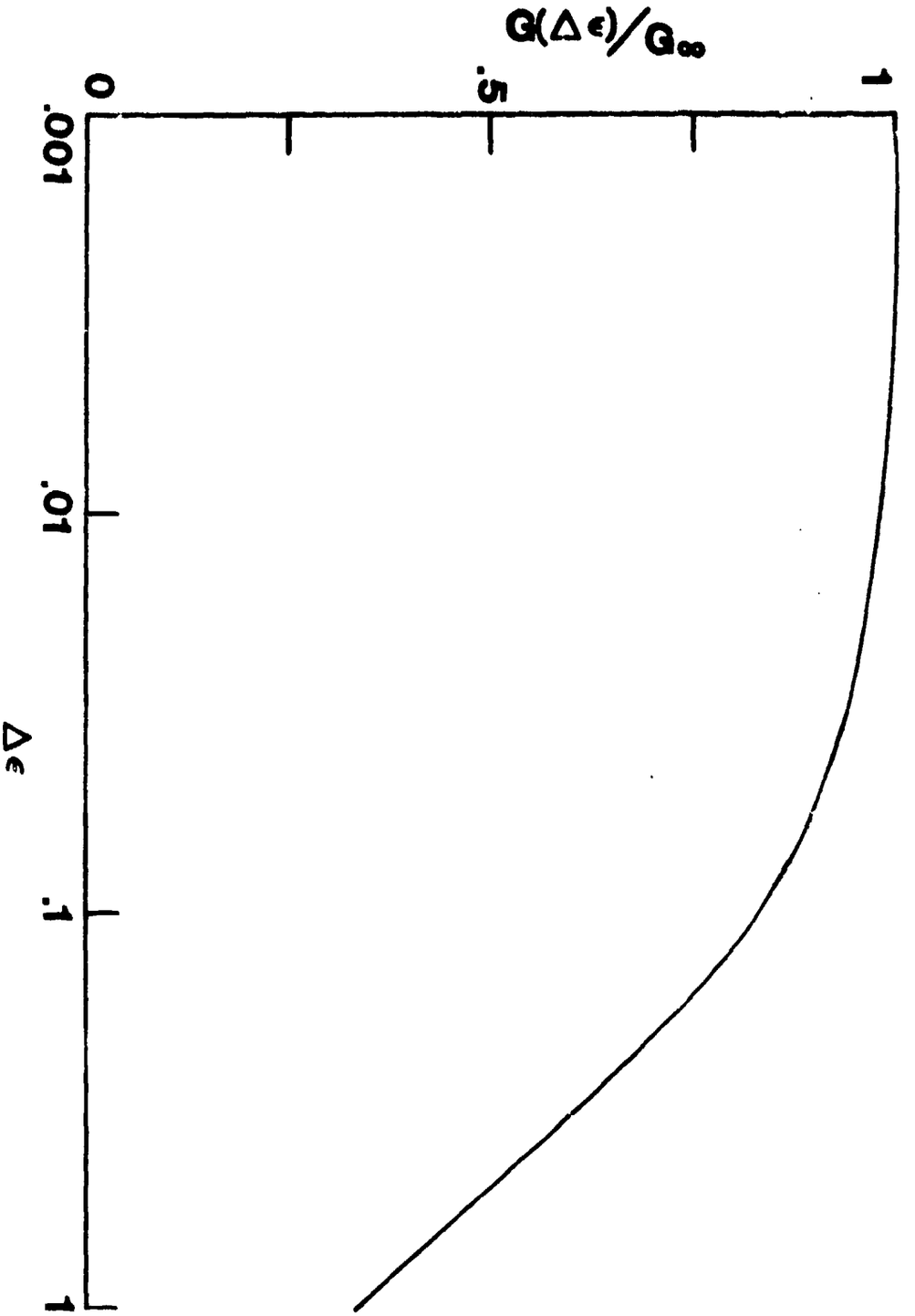

FIGURE 3. Effective strain dependent instantaneous rigidity versus strain.

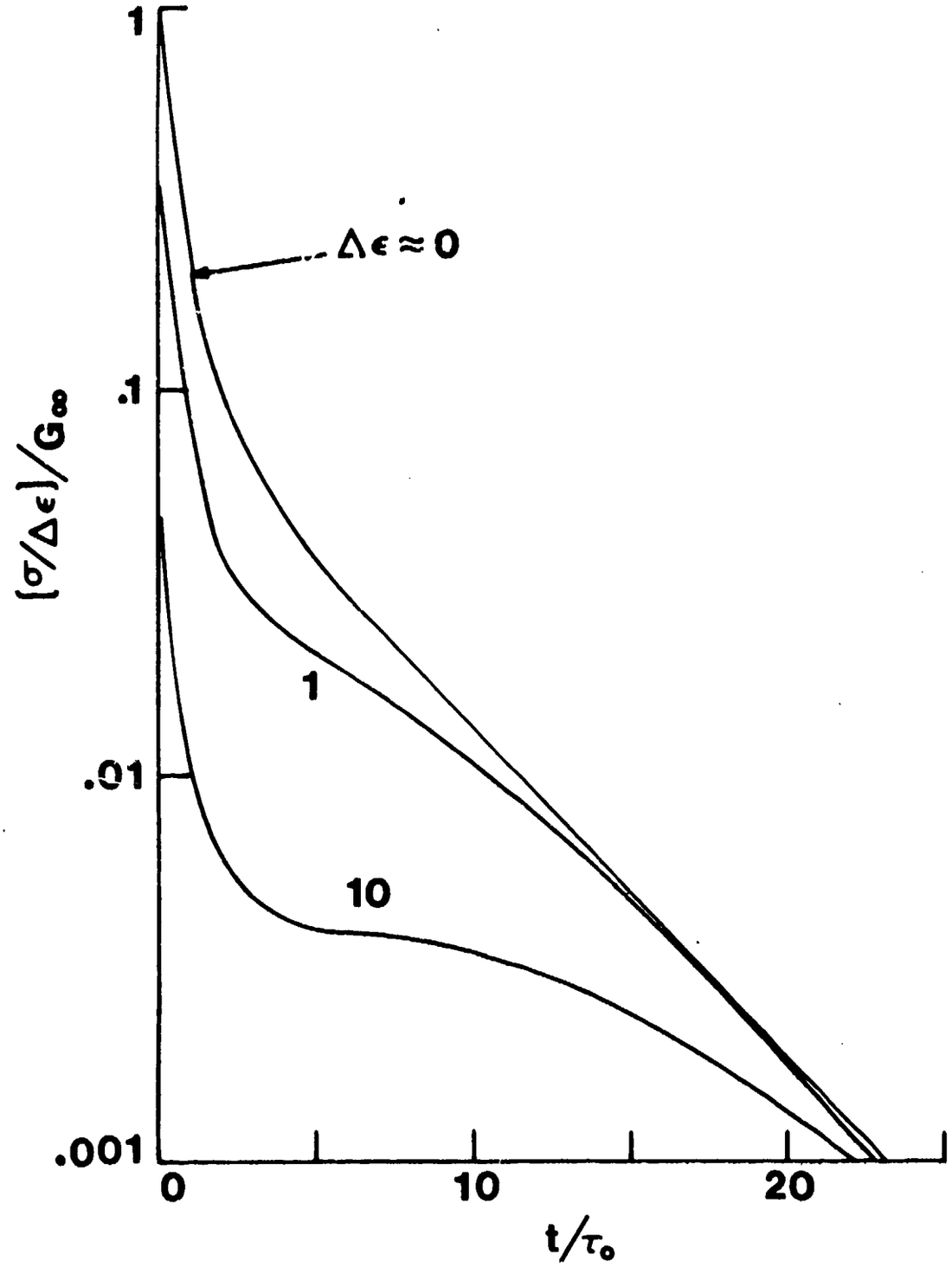

FIGURE 4. Normalized stress response to an applied step of strain $\Delta\epsilon$ switched on at t = 0.

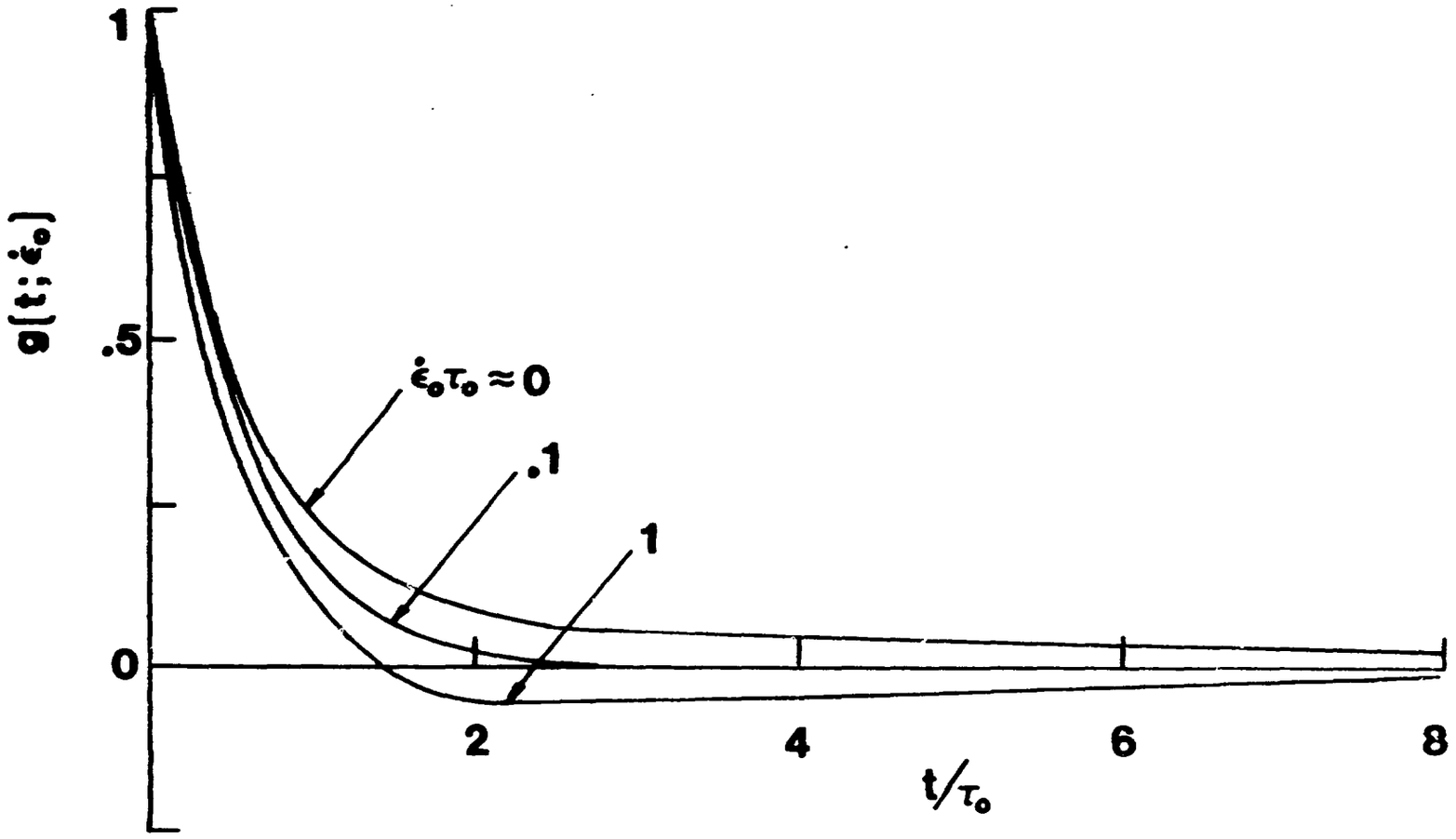

FIGURE 5. The shear-rate-dependent stress relaxation function versus time for reduced strain rate values of 0, 0.1, and 1.

Section V. A molecular dynamics study of structural changes accompanying material failure: Preliminary results.

by C. J. Montrose and S. D. Grant

A MOLECULAR DYNAMIC STUDY OF STRUCTURAL CHANGES ACCCMPANYING MATERIAL FAILURE: PRELIMINARY RESULTS

by

S. D. Grant and C. J. Montrose

Vitreous State Laboratory
The Catholic University of America
Washington, D.C. 20064

INTRODUCTION

In a recent paper[1] we reported a molecular dynamics (MD) study of the nonlinear shear response of stable and metastable (undercooled) liquid systems. Among the principal results of this work was the observation that accompanying, and indeed responsible for, the reduction in the effective viscosity (shear thinning) at elevated shear rates is a reorganization of the liquid structure into laminae approximately aligned with the shear force. The effect of this is to facilitate flow and hence reduce the shearing stress that is required to maintain the shear rate. At the time it was hypothesized that this structural reorganization could be viewed as the precursor of a material failure process, the actual fracture of the system being prevented by rapid molecular diffusion that acts as a local "healing" mechanism. To investigate this hypothesis we have undertaken a set of MD experiments on systems that have been rapidly quenched to low temperatures -- glasses--so that, on the time scale of the experiments, molecular diffusion is arrested. In this note, we report some preliminary results of those experiments.

COMPUTATIONS AND RESULTS

The system under investigation is an assembly of 108 particles (a few runs have been carried out on larger systems) interacting pairwise via a Lennard-Jones 6-12 potential

$$\phi(r) = 4\varepsilon[(\sigma/r)^{12} - (\sigma/r)^{6}].$$

The equations of motion were integrated using the Verlet algorithm with a time step of about 0.01.[2] The results that we present here were obtained at a temperature of 0.10 and a density of 1.013. This state was reached by rapidly (in one time step) "crushing" a triple-point liquid system (T = .722 and ρ = .8442) to achieve a 20% densification, then allowing this state to equilibrate, and finally "quenching" the system (again in one time step) to the desired temperature. The rapid densification and cooling steps inhibit those structural rearrangements that are required for crystallization to occur.

The experiment consists on switching on a shear strain rate $\dot{\epsilon}_{xy}$ at time = 0[3] and examining the subsequent time evolution of the system. The temperature was held constant by scaling the particle velocities after each time step. Among the system properties "measured" were the shear and normal stress components and distribution functions characterizing the local structure.

Typical of the results obtained is the plot of shear (xy) stress versus time shown in Fig. 1. As is evident the stress rises until approximately t = 12 at which time (when the strain is about 6%) it drops precipitously to zero. This stress release

is interpreted as a failure mode of the material; fracture in the normal sense cannot occur because of the confinement condition imposed by the density constraint on the system. This effect was quite reproducible occuring in three separate runs with $\dot{\epsilon}_{xy} = .005$ and in one with $\dot{\epsilon}_{xy} = .001$. In all cases the stress release occurs at stresses $\simeq 0.6$ and at strains of 5% to 6%.

One of the runs with $\dot{\epsilon}_{xy} = .005$ was continued out to $t \simeq 75$ (Fig. 2). Observe that following the failure at $t \simeq 12$, the stress, after hovering near zero for a short time begins to rise at $t \simeq 20$ before dropping at $t \simeq 42$. Note that at this point the stress has risen to a value more than twice as large as the level initially required to initiate failure. This growth and sudden fall of the stress is repeated again between $t \simeq 50$ and $t \simeq 72$.

The time dependence of the other stress components are shown for the same run in Figs. 3 through 8.

Accompanying each of the major stress changes are significant structural rearrangements. These are pictured in Figs 9(a) and (b). It is evident that the initial stress buildup causes a stratification of the amorphous structure; the failure of the system coincides with a reorientation of these strata. Continued shearing of the system leads to a "reconstruction" of the material in which it is reconfigured as a crystalline solid.

This is illustrated in Figs. 10 - 12 where the radial distribution function is given at various time instants. At the later

time instants the crystalline character of the material is clear; the positions of the first four peaks in the RDF's are in the ratios 1, $\sqrt{2}$, $\sqrt{3}$, and $\sqrt{4}$ indicating an FCC crystal structure.

ACKNOWLEDGEMENT

This work was supported by the Office of Naval Research (Contract No. N0OO14-81-K-0296).

REFERENCES AND FOOTNOTES

1. D.M. Heyes, J.J. Kim, C.J. Montrose and T.A. Litovitz, J. Chem. Phys. 73, 3987 (1980).

2. Natural Lennard-Jones units are used for all quantities in this note. The basic units are energy--ε, length--σ, and time--$\sqrt{m\sigma^2/\varepsilon}$ where m is the mass of one particle. All other quantities are expressed in terms of these units.

3. The shear was introduced using the "homogeneous shear method." See, for example, T. Naitoh and S. Ono, J. Chem. Phys. 70, 4515 (1979) and D.J. Evans, Mol. Phys. 37, 1745 (1979).

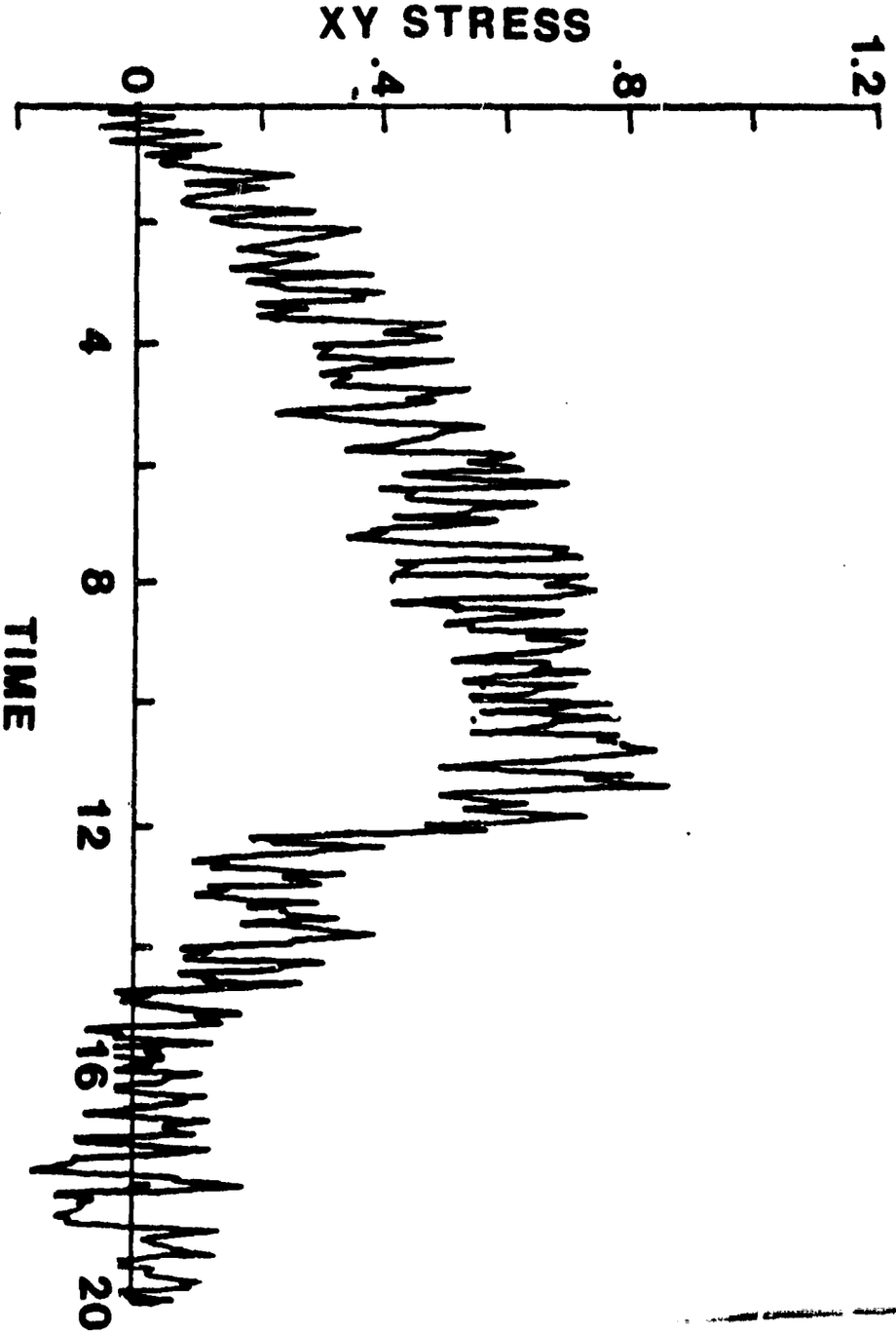

FIGURE 1. Shear stress versus time following the application of a steady shear strain rate = 0.005 switched on at time = 0.

PRECEDING PAGE BLANK-NOT FILMED

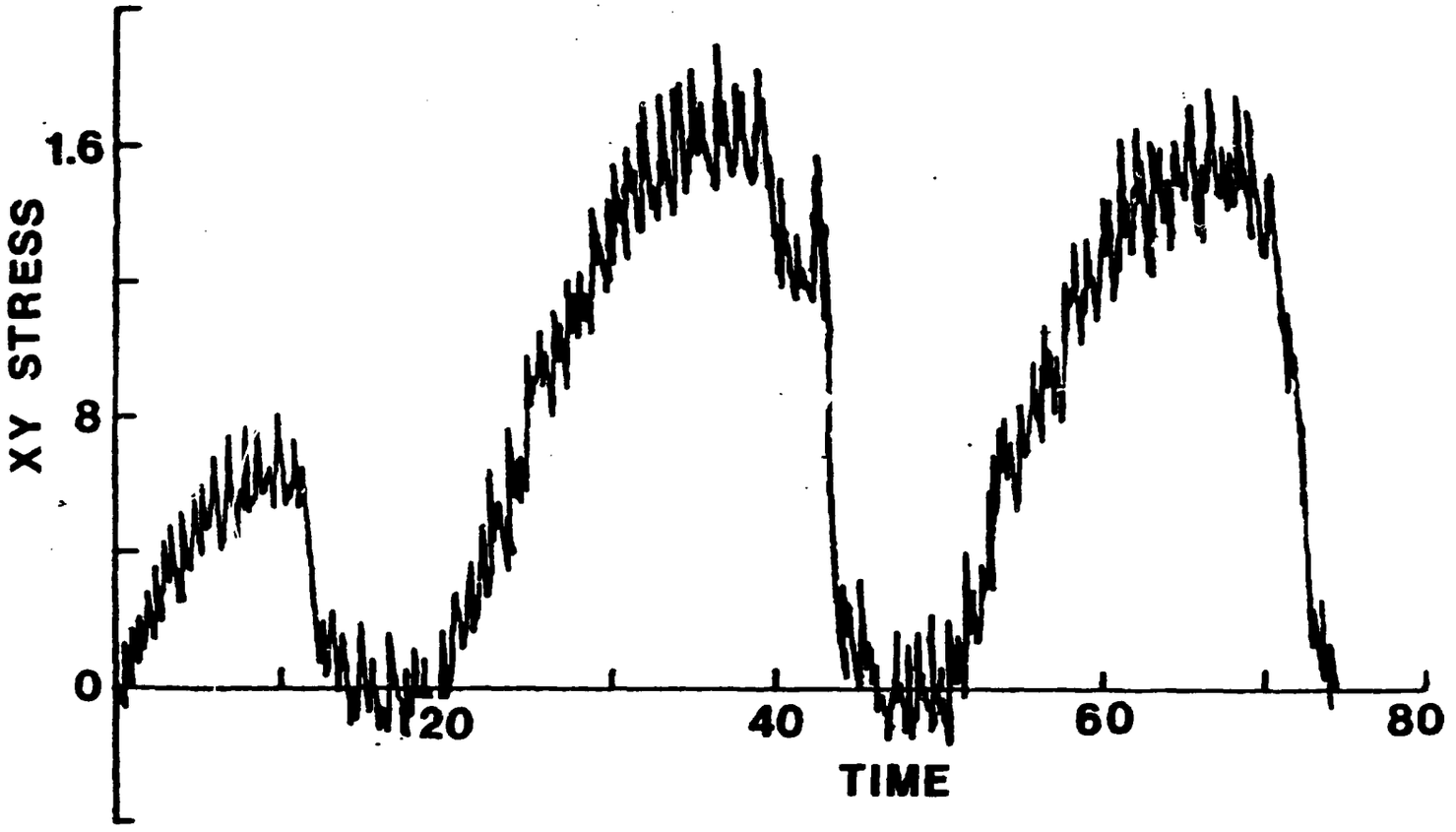

FIGURE 2. Shear stress versus time following the application of a steady shear strain rate = 0.005 switched on at time = 0.

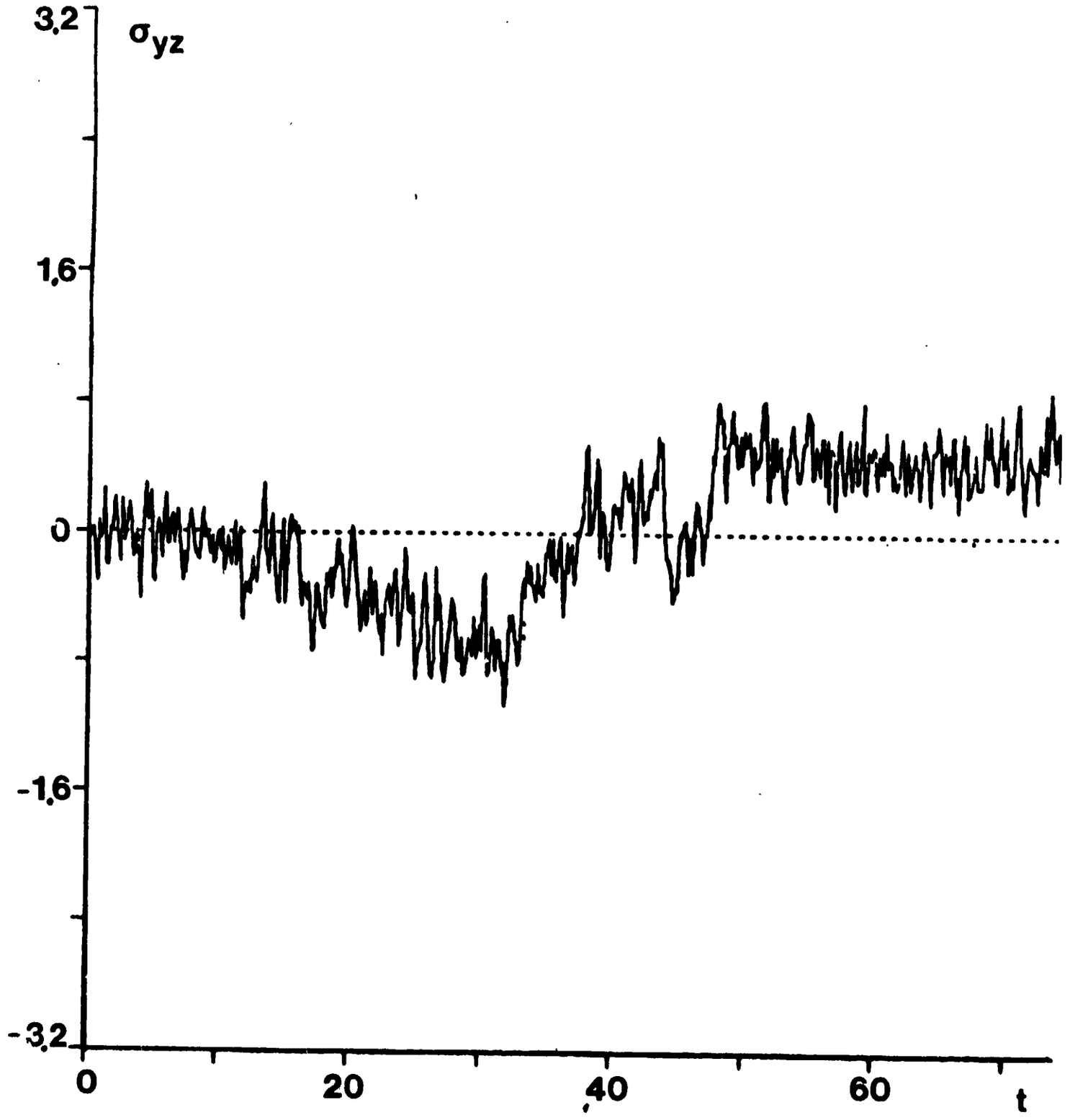

FIGURE 3. The yz-component of stress versus time following the application of a steady xy shear rate = .005 at t = 0.

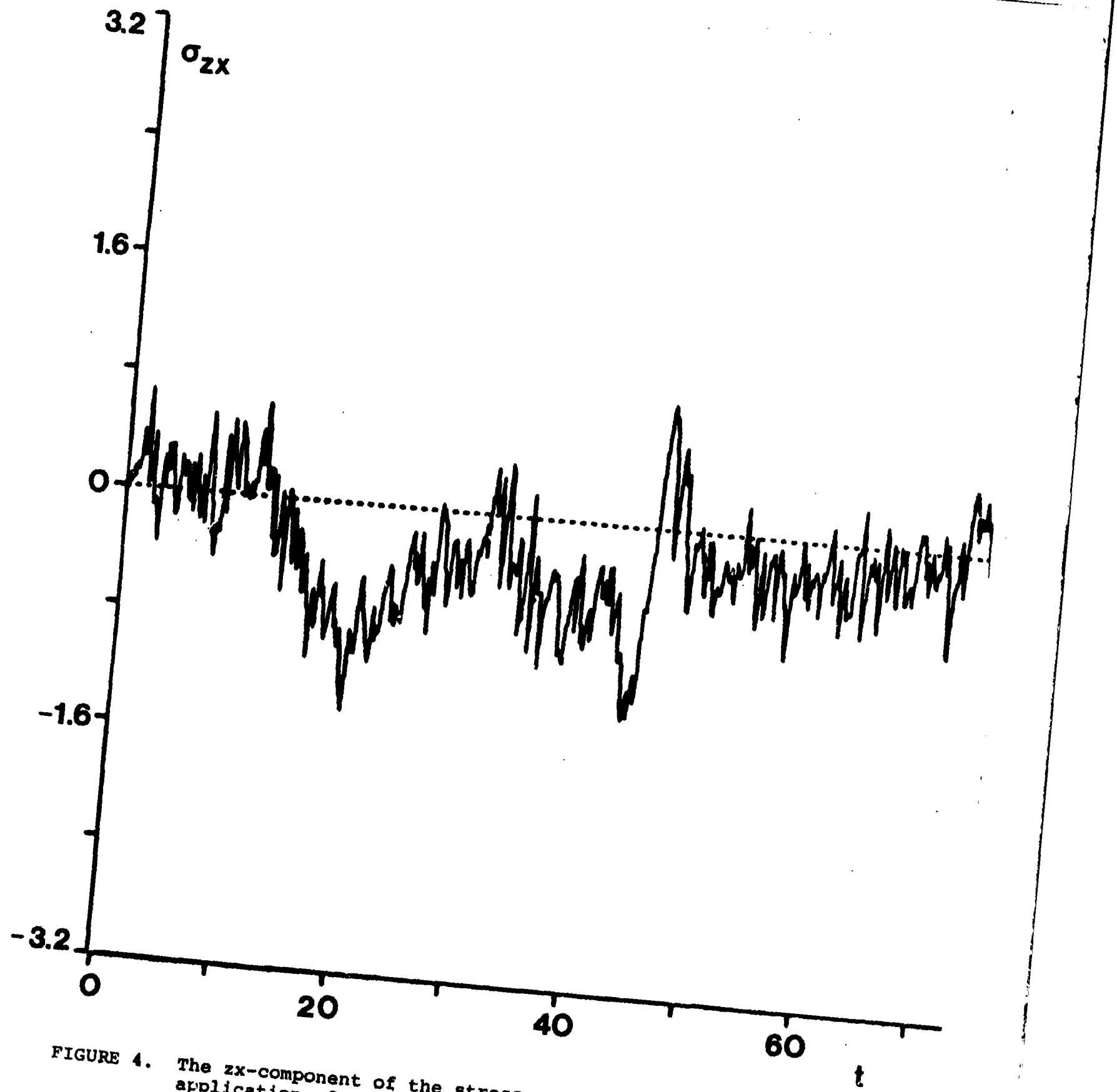

FIGURE 4. The zx-component of the stress versus time following the application of a steady xy shear rate = .005 at t = 0.

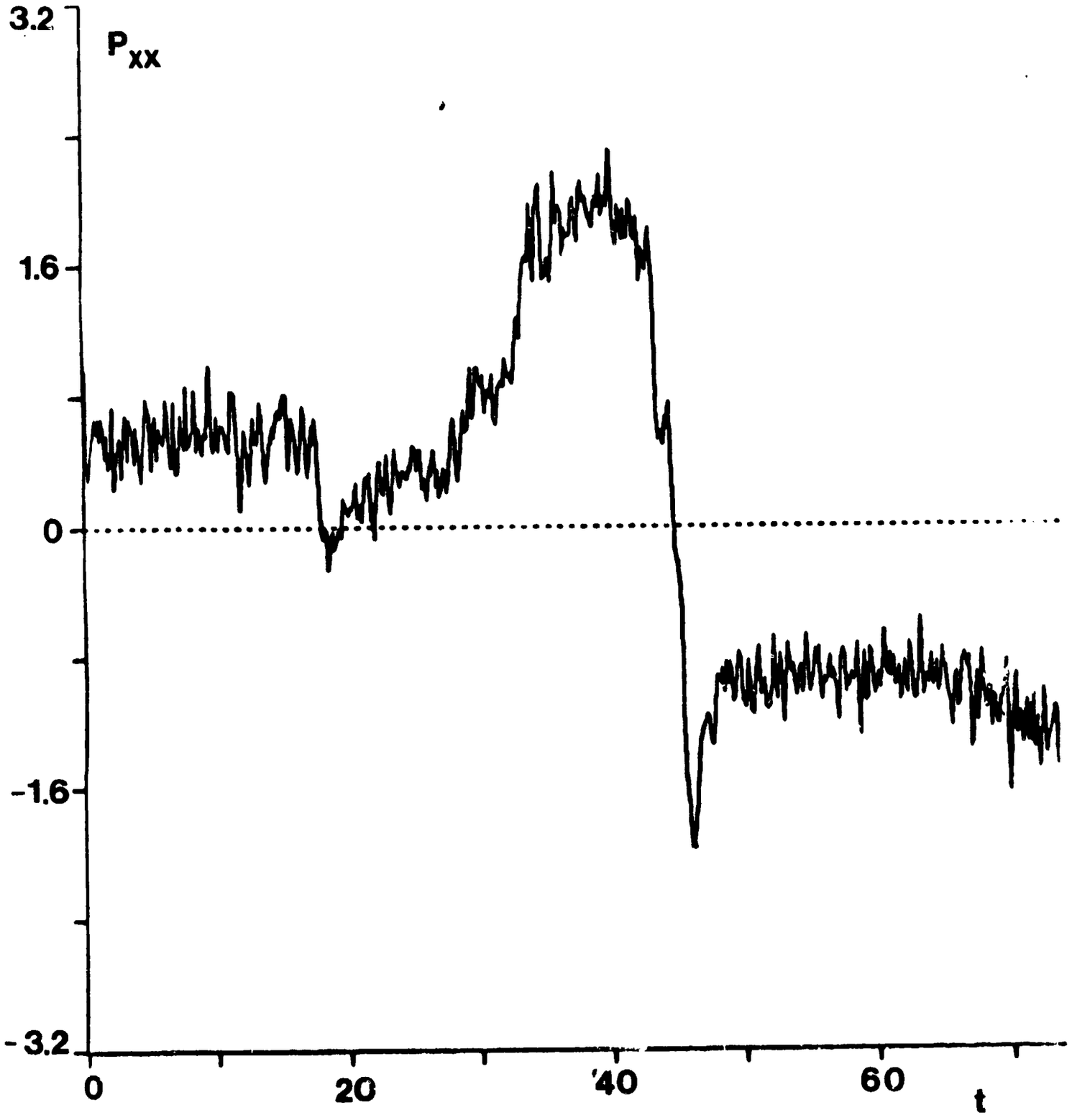

FIGURE 5. The xx-component of the pressure tensor (the negative of the stress tensor) versus time following the application of a steady xy shear rate at t = 0.

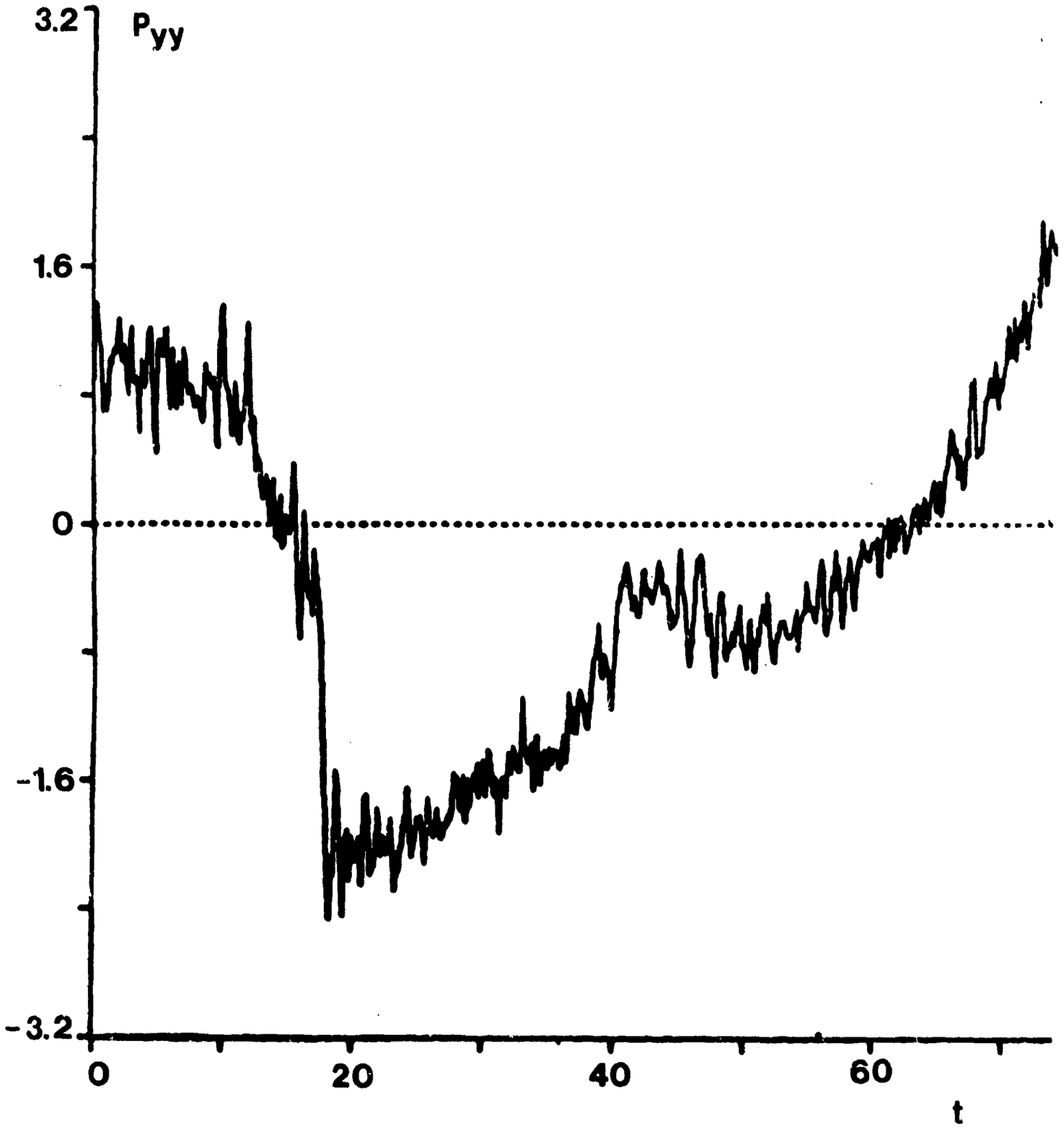

FIGURE 6. The yy-component of the pressure tensor versus time following the application of a steady xy shear rate switched on at t = 0.

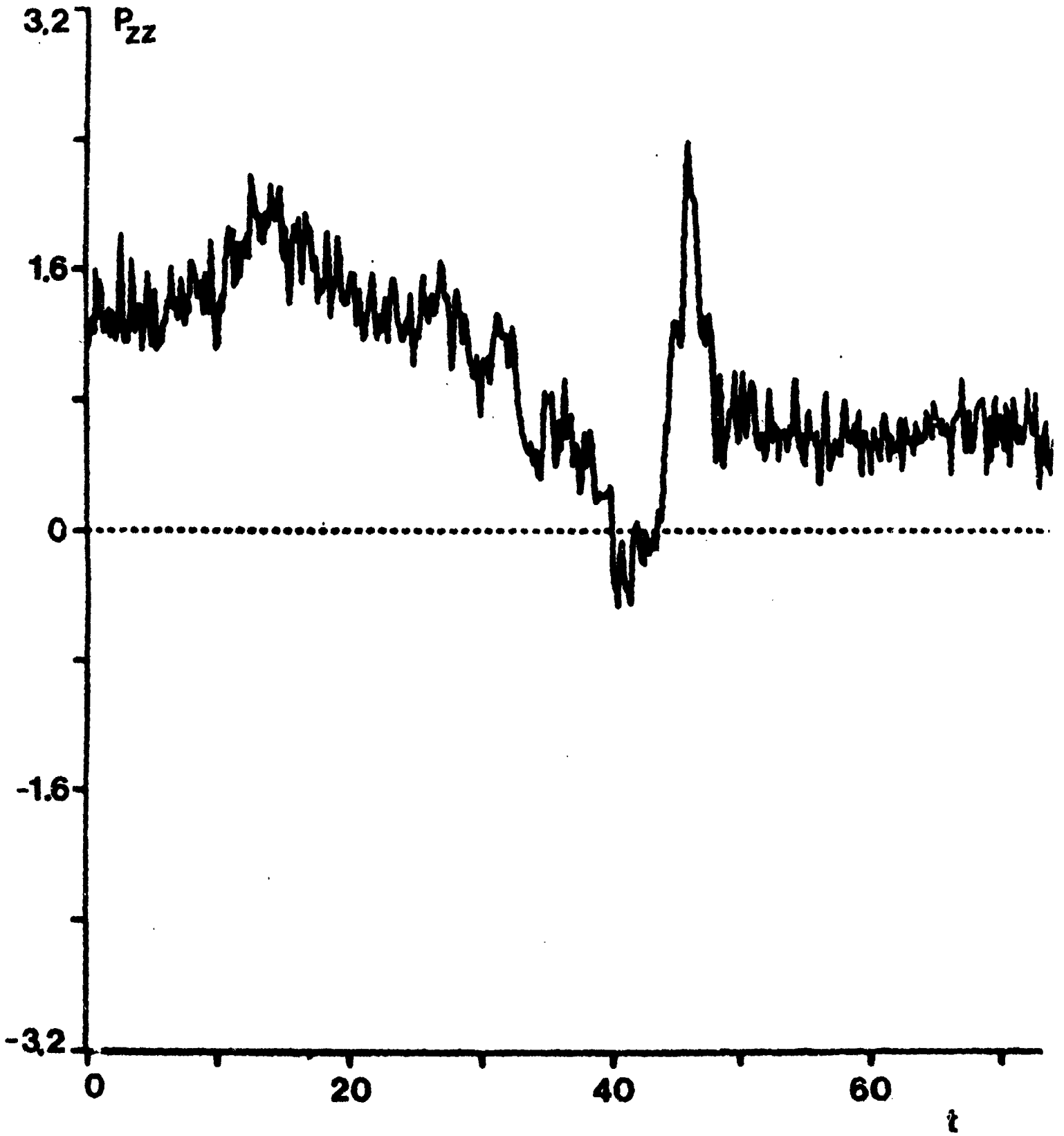

FIGURE 7. The zz-component of the pressure tensor versus time following the application of a steady xy shear rate switched on at t = 0.

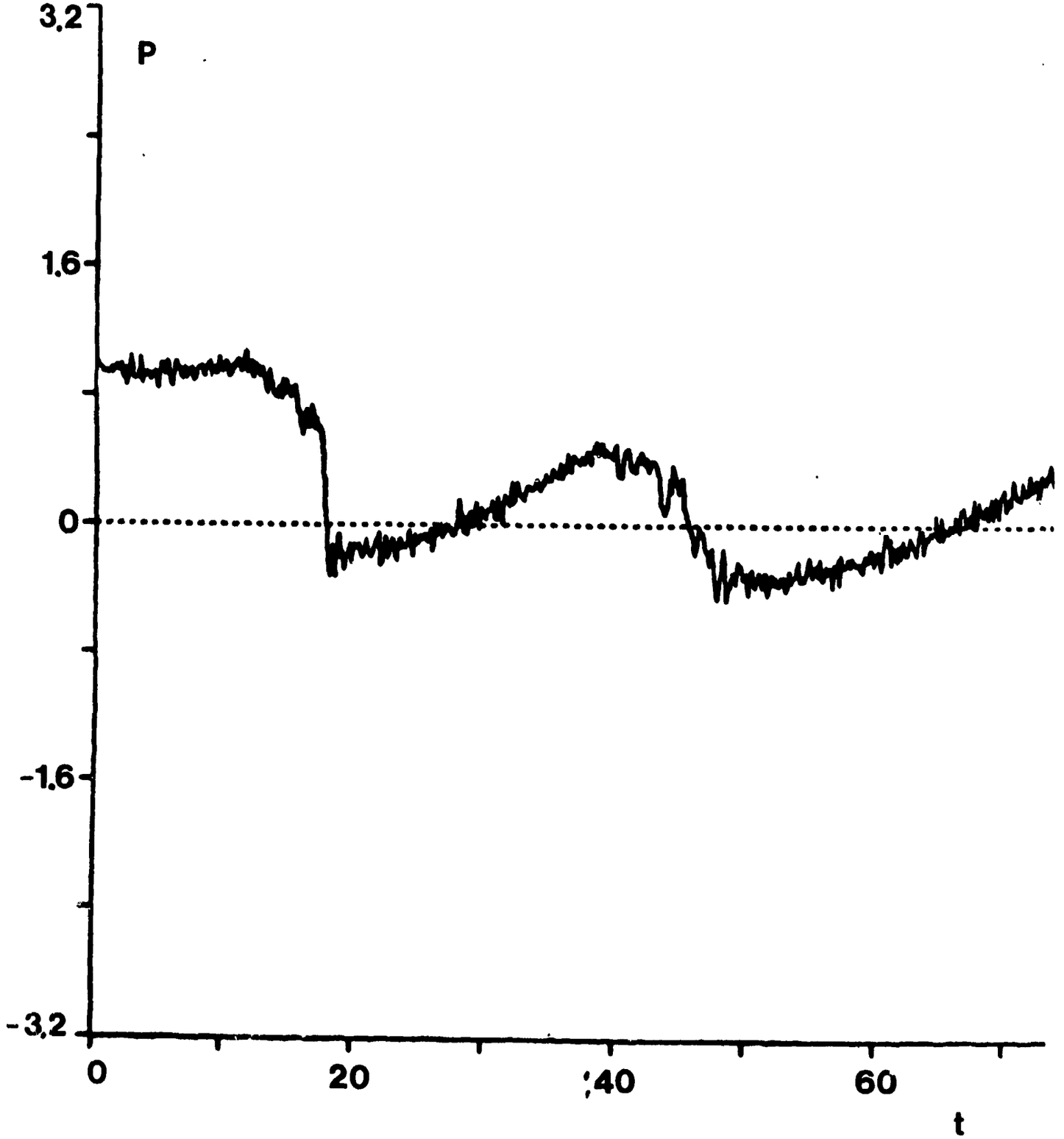

FIGURE 8. The pressure $P = (P_{xx} + P_{yy} + P_{zz})/3$ versus time following the application of a steady xz shear rate at $t = 0$.

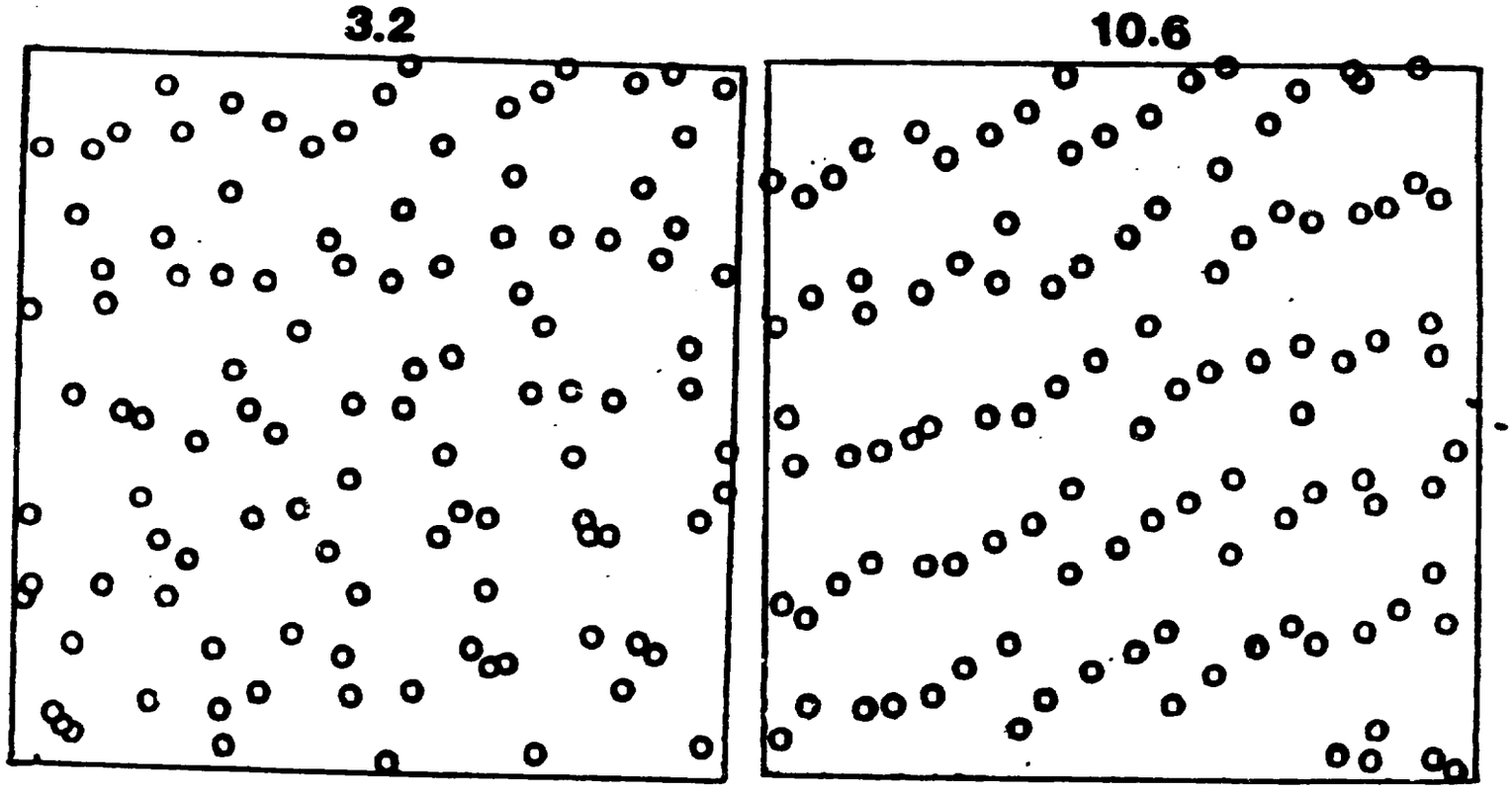

FIGURE 9(a). The positions of the particles' centers-of-mass projected on the xy-plane at two time instants following the application of a steady xy shear rate = .005 at t = 0.

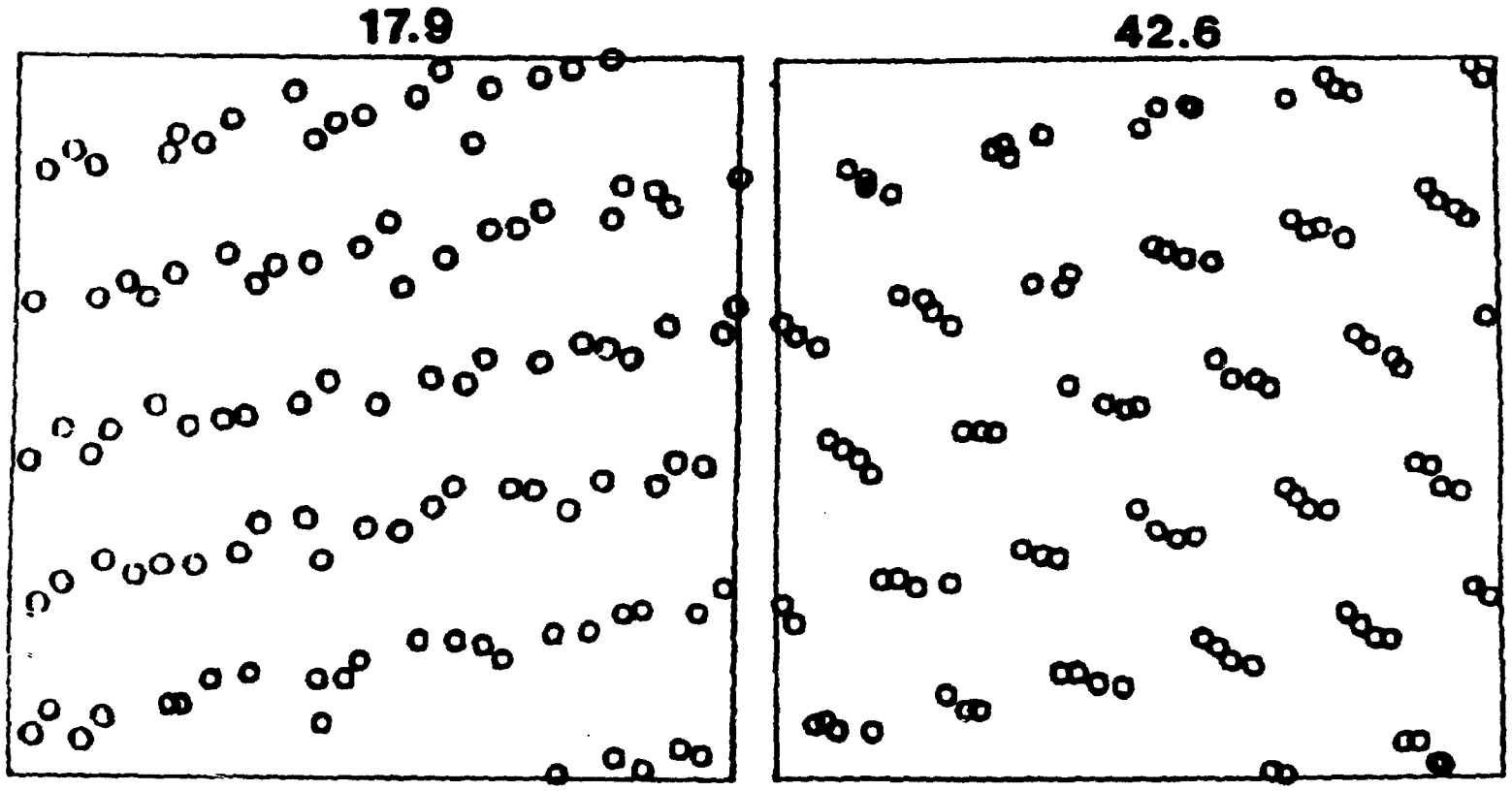

FIGURE 9(b). The same as Fig. 9(a) except at the time instants 17.9 and 42.6.

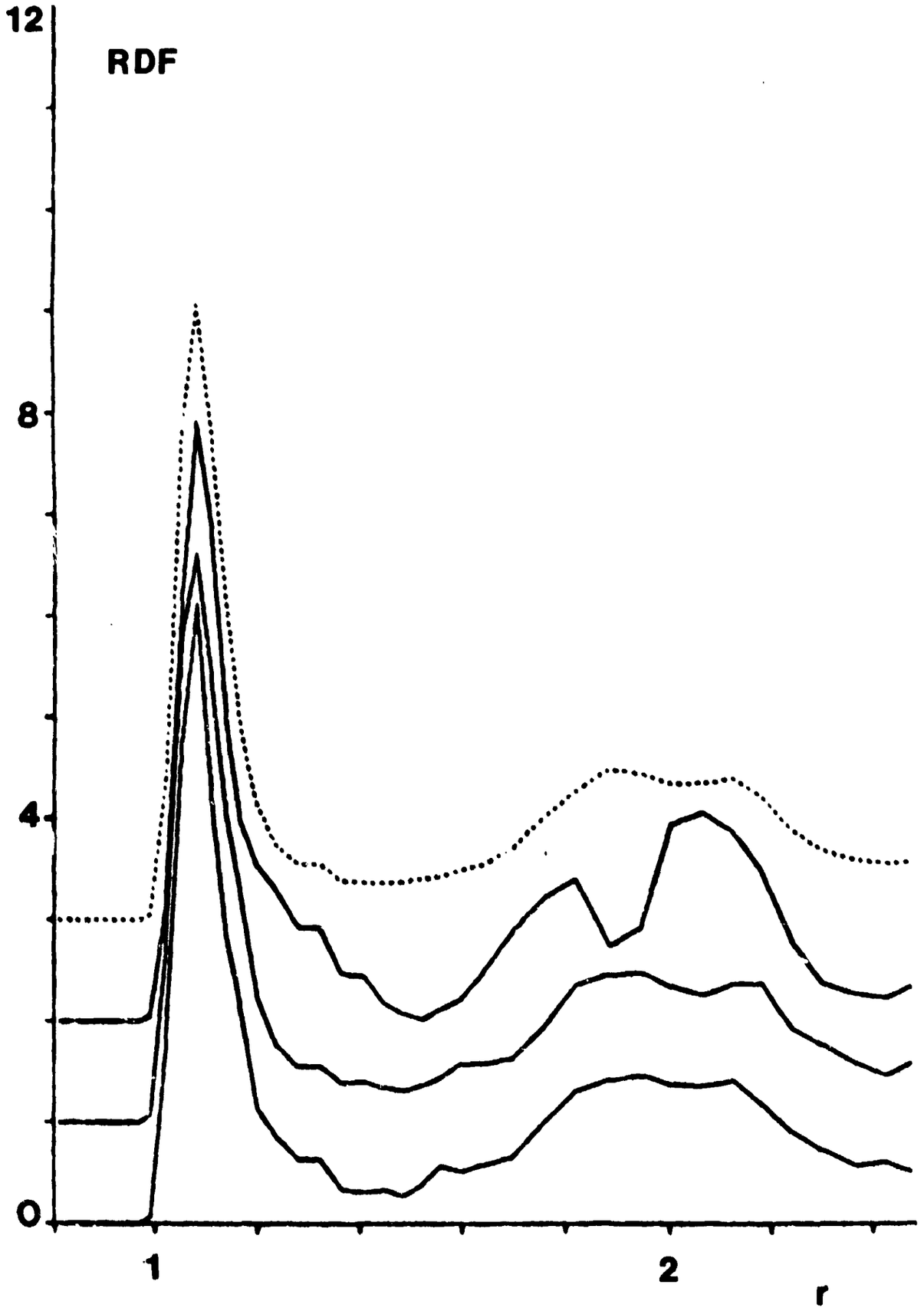

FIGURE 10. The radial distribution of the system at the time instants 6.9, 15.2 and 23.4 (reading up). The curves are displaced by one unit; the dotted curve is the equilibrium distribution function.

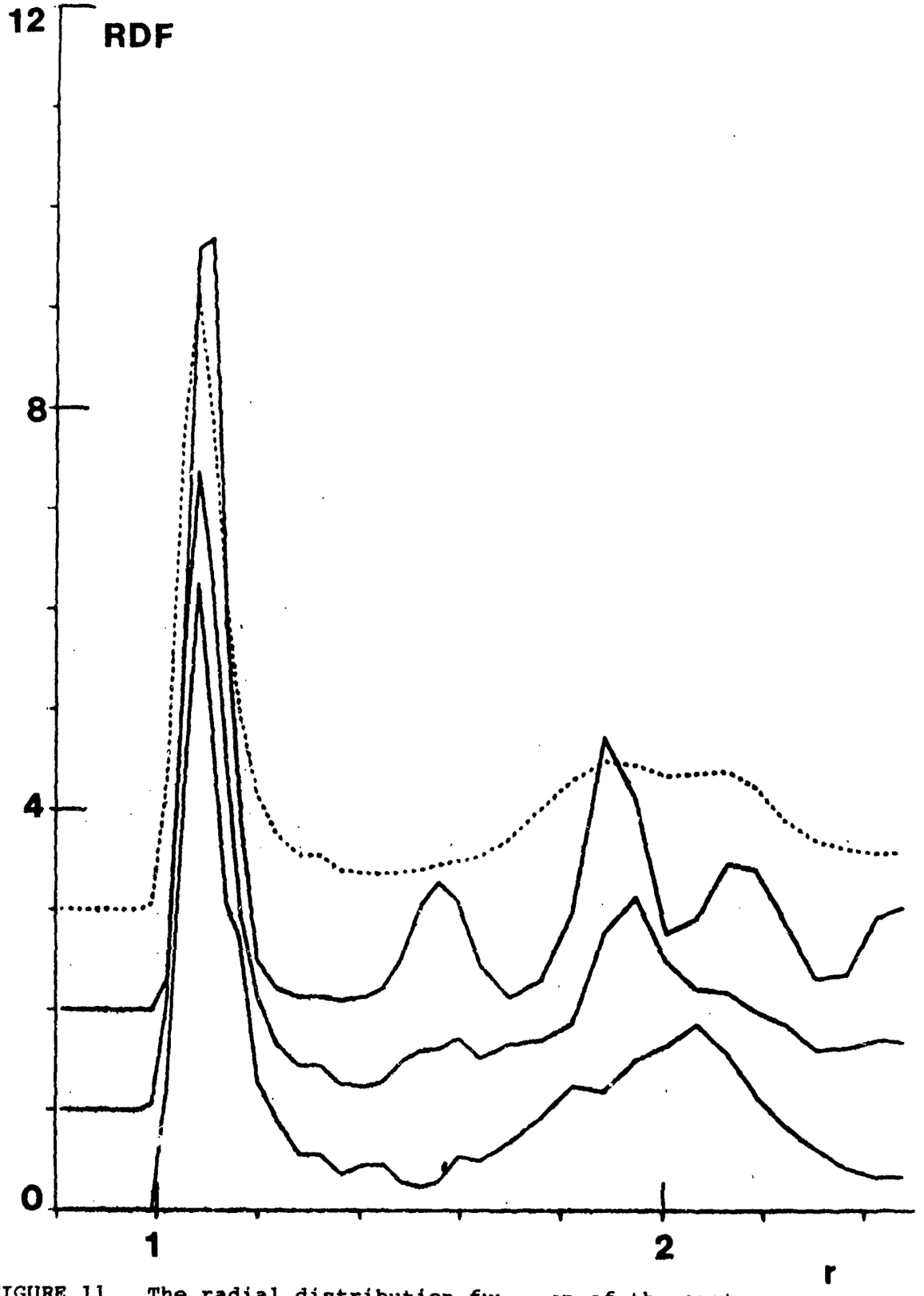

FIGURE 11. The radial distribution fu· ɔn of the system at the time instants 31 · 9 and 48.2 (reading up).

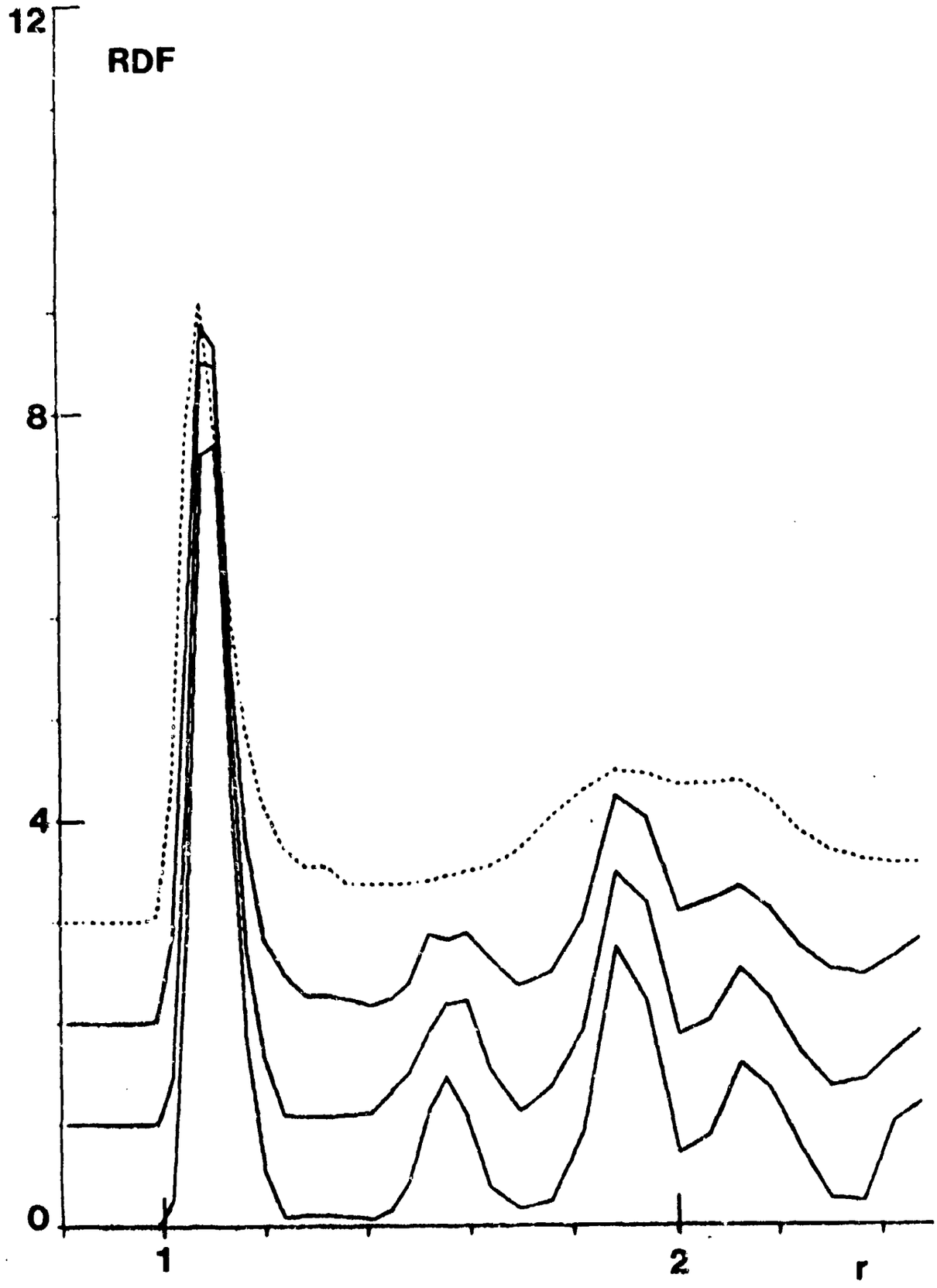

FIGURE 12. The radial distribution function of the system at the time instants 56.5, 64.7 and 73.0 (reading up).

Section VI. Non-newtonian viscous flow in glass.

by J. H. Simmons, R. K. Mohr
and C. J. Montrose

Non-Newtonian Viscous Flow in Glass

by

Joseph H. Simmons, Robert K. Mohr, and C. J. Montrose

Department of Physics
Catholic University of America
Washington, D.C. 20064

ABSTRACT

The viscosity of a soda-lime silica glass was measured at high strain rates. The data show non-Newtonian viscous flow in this inorganic oxide glass with the viscosity values below the expected Newtonian value. Following the imposition of large, steady strain rates, the observed stress increases with time to a maximum and then decreases to a time-independent value. A comparison of the viscosity behavior of this glass with the molecular dynamics results in a "Lennard-Jones" glass shows a number of points of correspondence and suggests the interpretation of the non-Newtonian behavior as resulting from structural rearrangements in the material. The combined data show that the sustained, steady-state stress asymptotically approaches a maximum at very high strain rates. This limiting stress is interpreted as the actual cohesive strength of the material and is calculated to be $1.4 \times 10^8 N/m^2$ (20,000 psi) for the glass under study.

INTRODUCTION

The strain rate response of non-crystalline materials under an applied stress has generally been observed to be linear (Newtonian) for low stress or strain rates. Organic materials have exhibited large deviations from Newtonian behavior both in the pseudoplastic direction (below Newtonian viscosity) and the dilatant direction (above Newtonian viscosity).[1] Since a correspondence between specific structural changes and the non-Newtonian response has not been determined for these materials, it has been generally surmised that the non-Newtonian behavior is a result of complex molecular chain kinetics such as unfolding, stretching, cross-linking, etc.

Recent "experiments" with Lennard-Jones spheres in a glassy state using molecular dynamics (MD) calculations have also shown the onset of non-Newtonian behavior under increasing strain rates or applied stresses.[2,3] The calculations show that when an applied shear strain rate is imposed on a box containing Lennard-Jones spheres, the resulting stress is proportional to the applied strain rate, $\dot{\varepsilon}$, only for low strain rate values ($\dot{\varepsilon}\tau_0 << 1$, where τ_0 is the shear isothermal relaxation time in the Newtonian region). At higher strain rates, the measured stresses and the corresponding viscosity do not reach their expected Newtonian value, with the deviation growing for increasing strain rates. The resulting behavior is shown in Figure 1. Since in Lennard-Jones glasses the atoms interact only via central forces, it seems clear that the observed non-linear behavior in MD calculations is a fundamental property of the liquid or glassy state.

Oxide glasses consist of ions which bind with both an ionic and a covalent character. Silicate glasses have not demonstrated any chain characteristics, and therefore, they offer a set of materials whose behavior can be compared to MD Lennard-Jones glasses. Some differences are expected since silicate glasses exhibit some covalent (directional) bonding. But much similarity is also expected since a large portion of their molecular make-up is ionic.

Measurements by Li and Uhlmann on rubidium silicate glasses[4] have shown the existence of a non-Newtonian region in the viscoelastic response of the glass to an applied constant load. As is the case for MD glasses, the deviation from Newtonian behavior was in the pseudoplastic direction. However, the dynamics of the non-Newtonian behavior of the glass were not studied in detail. We have analyzed their data, and a comparison of their results to MD experiments and to our results is presented below.

In this paper, a stable silicate glass was selected for an investigation of non-Newtonian behavior. The glass is a standard reference material for viscosity issued by the National Bureau of Standards.[5] Its Newtonian viscosity has been measured at great length and its stability in air at high-temperatures has been established through numerous tests.[5,6,7]

The experiment which we present is conducted differently from that of Li and Uhlmann, and is designed to reproduce the conditions of the MD calculations. The experiment is conducted at constant strain rate rather than constant stress or applied

load. While these conditions are interchangeable when the material is exhibiting Newtonian behavior, they are not equivalent when the response is non-linear. Constant strain-rate experiments were performed because they allow a detailed study of the non-linear behavior before the onset of material failure.

Experiment

Measurements were conducted on an oxide glass fiber whose composition is shown in Table 1. Fibers were made by hand drawing from the molten glass at 1150°C, and had diameters of 0.1 to 1mm.

TABLE 1* - GLASS COMPOSITION

SiO_2	70.5%	Sb_2O_3	1.1%
K_2O	7.7%	SO_3	0.2%
Na_2O	8.7%	Al_2O_3, Fe_2O_3	0.2%
CaO	11.6%		

*This glass is known as NBS-710 Viscosity Standard.

Each tested fiber was inserted through a furnace 12cm long with a narrow central channel and was attached to a stationary fixture at the bottom end and to a moveable load cell at the top end. See Fig. 2 for a schematic of the fiber and furnace arrangement. The furnace was designed to yield a relatively constant temperature over most of its length (±3°C over 90mm) and to drop rapidly in temperature at each end (ΔT = -20°C in less than 6mm). This guaranteed a constant, well defined hot zone. At selected temperatures, the fiber was elongated at a

constant rate while the resulting force was measured. The measurements were conducted at all the different strain rates studied before the temperature was changed.

Since the length of hot fiber was fixed by the furnace, this resulted in a constant applied strain rate. The fiber diameter was reduced as its total length increased, therefore it was necessary to calculate a correction for the steady-state cross-sectional area reduction. Steady-state refers to the condition where the cross-sectional area decreases uniformly over the entire hot-length of the fiber. This is selected to differentiate it from localized necking which we shall discuss later. An exact solution to the steady-state correction is:

$$A(t) = A_0 e^{-\dot{\epsilon}(t-t_0)}, \qquad (1)$$

where A_0 is the area at t_0 and $\dot{\epsilon}$ is the strain rate. The validity of this correction was verified by the measurement of the expected Newtonian viscosity at low strain rates before and after substantial elongation at high strain rates. Using this area correction, plots of the variation of developed stress with time were obtained for different applied constant strain rates. A typical dependence of stress on strain rate is shown in Fig. 3. Note the linear region at low strain rates, and the pseudo-plastic deviation at higher strain rates. The apparent viscosity n was calculated as follows:

$$\eta = \frac{1}{3}\frac{\sigma}{\dot{\epsilon}} \qquad (2)$$

where σ is the developed stress.* Figure 4 shows the temperature dependence of the Newtonian viscosity measured at low strain rates.

*This is a commonly used definition of viscosity in the Newtonian region. The definition of viscosity in non-Newtonian regions becomes somewhat ambiguous and others[4] have suggested that $\eta=1/3(\partial\sigma/\partial\dot{\epsilon})$ is a more appropriate definition (the two definitions are equal in the Newtonian region). The use of Eq. 2, however allows us to plot viscosity as a function of time at fixed $\dot{\epsilon}$ and this is more useful for our fixed strain rate experiments. The use of the differential form requires data with very low scatter to calculate the viscosity with any accuracy and therefore is not used here.

Discussion

A. Experimental Results

A study of the non-linear behavior of this glass and a comparison with the Lennard-Jones, molecular dynamics experiments are best effected by looking at the time dependence of the apparent viscosity for a given applied constant strain rate. Figures 5 and 6 show the non-Newtonian behavior for two different temperatures. The onset of non-linear behavior occurs at higher strain rates for higher temperatures and lower viscosities. The slow increase in viscosity to its Newtonian value, η_0, at the low strain rates corresponds to shear relaxation effects in the glass, and the time to reach the steady-state, Newtonian behavior is proportional to the average shear relaxation time, $\tau_0 = \eta_0/G$ where G is the instantaneous shear modulus.

As the strain rate is increased, three significant effects can be observed. First, the apparent viscosity approaches a steady-state value for long times. This steady-state, apparent viscosity decreases with increasing strain rate. Second, there is a short-time overshoot of this steady-state value during the shear relaxation period. Third, the slower shear relaxation processes appear to be short-circuited by a faster process which leads to the lowered viscosity. These results are qualitatively identical to the behavior of Lennard-Jones spheres in the MD experiment (Fig. 1). This process appears to be a structural breakdown mechanism and occurs at earlier times for increased strain rates (i.e. compare the curves with $\dot{\varepsilon} = 72\times 10^{-4}$/sec. and 18×10^{-4}/sec. in Fig. 5). It appears that the high strain rates

cause a breakdown of the glass structure which in turn allows stress relaxation to occur by the faster available mechanisms rather than the sum of all relaxation mechanisms. Because, the Newtonian shear relaxation processes and the structural breakdown processes have different relaxation times and amplitudes, there is an overshoot in the apparent viscosity.

Each set of tests shown on Figs. 5 and 6 was conducted on a single fiber. The measurements gave the same steady-state viscosity values at each given $\dot{\varepsilon}$ whether the measurements were made following a higher or a lower $\dot{\varepsilon}$. Therefore, the steady-state viscosity values appear to be independent of past history. In each figure, the highest $\dot{\varepsilon}$ value corresponds to a failure of the fiber. In Fig. 5, the viscosity appears to be approaching steady-state when failure occurs.

B. Heating Effects

It is apparent that the observed non-linear behavior of the silicate glass fibers is similar to the behavior of the Lennard-Jones glass. Before a discussion of similarities and differences between these two results, it is necessary to establish that test conditions were similar. For example, in the MD experiments, the temperature was maintained constant. Therefore it is necessary to determine whether the silicate glass fibers were heated above the furnace temperature at the higher strain rates, and whether the heating, if present, would be sufficient to cause the decrease that was observed in the viscosity. For example, the drop in observed viscosity at 563°C from the Newtonian value of 3.2×10^{12}P to the pseudo-plastic value of $1.1 \times$

$10^{12}P$ (at the strain rate of $7.2 \times 10^{-4} sec^{-1}$) corresponds to a temperature increase of 10°C.

A lower limit to the rate of heat loss from a fiber can be calculated using the radiative heat transfer coefficient, H, defined for small temperature differences between the fiber and the furnace as:

$$H = 4eST^3 \qquad (3)$$

where e is the glass emissivity, S is the Stefan-Boltzmann constant and T is the absolute temperature. The rate of heat loss dQ/dt is then given by

$$\frac{dQ}{dt} = HA_s\Delta T \qquad (4)$$

where A_s is the surface area of the fiber in the furnace and ΔT is the temperature difference between the fiber and the furnace. Using $S = 5.67 \times 10^{-8} J/sec \cdot m^2 \cdot K^4$, $T = 836K$, and $e = 0.9$ we calculated a value for $H = 1.2 \times 10^2 J/K \cdot m^2 \cdot sec$. This value is an underestimate of the total heat transfer coefficient since only radiative mechanisms have been considered. Paek and Kurkjian[8] have estimated H from cooling rate measurements made on glass fibers with similar dimensions as those tested here. Their estimate yielded $H = 2.9 \times 10^2 J/K \cdot m^2 \cdot sec$ which is consistent with our calculation.

A calculation of the rate of doing work on the fiber was made to determine an upper limit on any resulting temperature rise. The rate of doing work is

$$\frac{dW}{dt} = \sigma\dot{\varepsilon}V \qquad (5)$$

where V is the volume of the fiber given by $\ell \cdot A(t)$. Under steady-state conditions the maximum rate of heat input due to conversion of all the work to heat was calculated to be 3.37×10^{-4}J/sec. Since the surface area of the fiber in the furnace was approximately $1cm^2$ the largest temperature rise that could be supported considering only radiative heat loss is less than 0.03°C. This is far below the value of 10°C necessary to cause the observed non-linear behavior. Therefore, we can reasonably conclude that the non-linear behavior of the glass during these experiments was not a result of localized heating of the fiber, and the test does duplicate the isothermal conditions of the MD experiments.

C. Mechanism

During the MD experiments, it is possible to arrest the system and examine its structure. The examinations of systems having undergone extensive non-linear behavior showed definite structural changes indicative of a layering effect for planar shear. The layers appear to form almost parallel to the shear planes with a small angular deviation from the shear direction. The angles decrease with increasing shear rates.[2] Real glasses may also be suddenly frozen by rapid cooling to temperatures below the glass transition temperature. However, structural examinations of real glasses on the molecular level are difficult and cannot be made directly. Therefore, we have not yet attempted to gather structural correspondence for the non-linear behavior.

It is possible however, to discuss the non-linear behavior of real, inorganic glasses by comparison with MD results. The reduced steady-state viscosity (apparent viscosity divided by Newtonian viscosity, η/η_0) can be plotted versus stress or versus reduced strain rate (strain rate times the Newtonian average relaxation time, $\dot{\varepsilon}\tau_0$) for each temperature. In both instances, the data reduces to the same general shape, although it appears to us that the reduction with reduced strain rate is better. Both inorganic glass experiments and the MD data follow the same general behavior.

The decrease in viscosity with increasing strain rate results from an asymptotic approach of the sustained steady-state stress to a maximum value (σ_{limit}) at very high strain rates. The existence of a limit in the sustainable steady-state stress indicates that if the system is placed under a stress greater than the limit, steady-state conditions cannot be maintained and catastrophic failure ensues. This stress limit, therefore, can be interpreted as the actual cohesive strength of the material. This result shows a unique and valuable feature of the non-Newtonian viscosity studies since the actual cohesive strength of the material is obtained here without a need to fracture the material.

A calculation of the limiting stress requires some extrapolation of the data to very high shear rates. In this task, we rely on the similarity between the measurements conducted on the soda-lime silica glass and the MD calculations on the Lennard-Jones glass. The normalized viscosity of both systems reduces

to the same curve when the shear rate is normalized through the function $\dot{\varepsilon}\tau_0/\alpha$ where α is an adjustable parameter. The value of α is found to be 0.0063 for the soda-lime silica glass, 0.0053 for the rubidium silicate glass and 0.077 for the Lennard-Jones glass. Reduced in this fashion, all data follow the same behavior, independent of temperature and composition as shown in Fig. 7.

The fall-off in reduced viscosity at increasing strain rates, thus appears to result from dynamic changes in the structure of the material which accompany the large applied strain rates. Reduction of this data from different temperatures on the same glass by use of the average Newtonian shear relaxation time indicates that the structural rearrangement is controlled by the shear flow processes in the glass.

The functional dependence of the decrease in normalized viscosity can be obtained from an equation based on the concept of a limiting stress used by Bair and Winer to discuss similar behavior for highly viscous organic lubricants.[9] The equation was derived by Montrose using semi-empirical arguments.[10] The equation yields a simple relationship between reduced viscosity and the normalized strain rate function, $\dot{\varepsilon}\tau_0/\alpha$:

$$\frac{\eta}{\eta_0} = \frac{1}{1 + \dot{\varepsilon}\tau_0/\alpha} \qquad (6)$$

where the factor α is found to be the ratio of the maximum stress sustained by the system and the instantaneous shear modulus of the glass, σ_{limit}/G. The fit of this equation to the data is also shown in Fig. 7.

σ_{limit} is the maximum stress developed in the system under steady-state conditions as the strain rate goes to infinity without material failure. Therefore, σ_{limit} represents the actual cohesive strength of the material. This actual cohesive strength is interpreted as the maximum stress sustainable by the material when the stress is applied at a rate slower than the effective relaxation time of the glass. Its existence suggests that when viscous or plastic flow occurs under an increasing tensile or shear stress, there is a stress value where steady-state flow cannot be sustained and the material fractures at the point where the stress is applied. In the case of loaded fibers, this result suggests that as the diameter of the fiber undergoes localized necking, a point is reached when $\sigma_{applied} > \sigma_{limit}$ and fracture occurs, rather than continued necking of the fiber.

In the MD experiments, an independent measurement of σ_{limit}/G was conducted and agrees very well with the value of α obtained by fitting the non-linear viscosity to Eq. 6.

This generalized behavior of inorganic glasses at different temperatures and composition is an encouraging basis for the development of molecular models to interpret non-linear behavior in inorganic glasses. The strong similarities to the MD glasses indicate that the effect is indeed a result of structural rearrangements in the glasses. The parameter, α appears to be linked to the strength of some average structural bond of the material at the temperature of measurement. Therefore, this experiment offers a direct measurement of the cohesive strength

of different glasses and a possibility for measuring its temperature dependence. The values obtained here show that both oxide glasses can only sustain stresses about 1/160 of their shear modulus while the Lennard-Jones glasses can go up to about 1/10 of the shear modulus. This result is reasonable from structural considerations since the bonding forces in the LJ glass are spherically symmetric, while a significant portion of the bonding of the oxide glasses is covalent and therefore highly directional. It is expected that these covalent bonds are much less resistant to shear stresses since they can break by bond rotation than are the non-directional ionic bonds which break by bond extension alone. Estimating a shear modulus for the soda-lime silica glass of 2.2×10^{10}Pa, based on high temperature ultrasonic sound velocity measurements, our interpretation of the reported measurements yield an actual cohesive strength of 1.4×10^{8}Pa (20 Kpsi) for this glass at temperatures near 560°C, and Newtonian viscosities of 10^{10}-10^{11}Pa·s (10^{11}-10^{12}Poise).

SUMMARY AND CONCLUSIONS

The viscosity of a stable, soda-lime silica glass was measured at high shear rates. The results showed a non-Newtonian viscosity behavior of the pseudo-plastic type. As a function of time, the viscosity at high, constant strain rates first increased to a maximum, then decreased to a constant time-independent value, lower than the expected Newtonian viscosity. The time independent behavior at long times yields a steady-state viscosity which is a function of the applied strain rate.

The measurements when compared to molecular dynamic calculations on a Lennard-Jones material show unexpected similarity in the time and temperature dependence of the non-Newtonian viscosity. The observed behavior also agrees with earlier work on a rubidium silicate glass. Comparison of these data indicates that the time evolution of the viscosity of the silicate glasses corresponds to that calculated for the Lennard-Jones glasses which is known to result from a structural rearrangement in the material under high deformation rates.

An examination of the combined data of the inorganic glasses and the MD glass showed that the steady-state, sustained stress under applied constant strain rates approaches a limiting stress value, σ_{limit}, for infinite strain rates. This limiting sustained stress is interpreted as the actual cohesive strength of the glass since any applied stress greater than σ_{limit} cannot be sustained under steady-state conditions and leads to catastrophic failure. The extrapolation of data using a semi-empirical model showed that σ_{limit} for the two inorganic glasses

analyzed is near 1/160 times the rigid shear modulus, or approximately 20Kpsi for the soda lime silica glass. These results suggest a mechanism for material failure at high temperatures (under conditions of plastic flow). By this mechanism, an applied shear stress greater than σ_{limit} induces initially a plastic flow reaction which changes to fracture when the structure attempts to adjust to the stressed condition. An applied shear stress lower than σ_{limit} induces a plastic flow reaction which reaches a steady state strain rate as the structure rearranges itself to accomodate the stress.

ACKNOWLEDGMENT

The molecular dynamics experiments described in this paper were supported by the Office of Naval Research (Contract No. N00014-75-C-0856).

FIGURE CAPTIONS

Fig. 1 -- Results from molecular dynamics calculations. Shear stress versus time for the shear strain rates shown at the right, switched on at time zero. Note the stress overshoot at the upper strain rate. (See Ref. 2 for details).

Fig. 2 -- Details of the furnace and load cell assemblies. The end heaters, 1 and 3 were adjusted to obtain a uniform temperature in the furnace.

Fig. 3 -- Variation of stress versus strain rate for the soda-lime-silica glass. The deviation from Newtonian behavior is clearly seen for strain rates above $1.5 \times 10^{-4} sec^{-1}$.

Fig. 4 -- Newtonian Viscosity of the measured soda-lime-silica glass.

Fig. 5 -- Measured viscosity versus time for the strain rates shown, switched on at time zero. The dashed line is the Newtonian value.

Fig. 6 -- Measured viscosity versus time for the strain rates shown, switched on at time zero. The dashed line is the Newtonian value.

Fig. 7 -- Plots of viscosity reduced by the Newtonian value versus normalized strain rates, $\dot{\varepsilon}\tau_0$ for various temperatures. The solid line represents equation (6) and shows how a reduction of the strain rate by the single parameter of: G/σ(limit) can fit the data from three totally different materials:

a) Rubidium-silicate data from Li and Uhlmann[4] analyzed by the method presented in this paper. The temperatures are as follows: open circles = 528°C, solid trianges = 555°C, open triangles = 536°C, squares = 501°C, solid circles = 480°C.

b) Soda-lime-silica glass whose measurement is described here. The temperatures are as follows: circles = 563°C, diamonds = 574°C, triangles = 593°C, and squares = 596°C. The two solid points are estimates of viscosity before failure.

c) Molecular dynamics calculations on a Lennard-Jones glass.[2] Here different densities are used to represent different thermodynamic states. The densities are in terms of the triple point density, ρ_T: circles = $1\rho_T$, triangles = $1.1\rho_T$, diamonds = $1.2\rho_T$, and squares = $1.5\rho_T$.

REFERENCES

1. D. W. Hadley and I. M. Ward, Rep. Prog. Phys. 38, 1143-1215 (1975).

2. D. M. Heyes, J. J. Kim, C. J. Montrose, and T. A. Litovitz, J. Chem. Phys. 73, 3987-3996 (1980).

3. W. T. Ashurst and W. G. Hoover, Phys. Rev. A. 11, 658 (1975).

4. J. H. Li and D. R. Uhlmann, J. Non-Crystalline Solids, 3, 127 (1970).

5. National Bureau of Standards, Standard Reference Material No. 710, Soda-Lime-Silica Glass.

6. A. Napolitano and E. G. Hawkins. J. Res. NBS 68A, 439 (1964).

7. A. Napolitano, J. H. Simmons, D. H. Blackburn, and R. E. Chidester, J. Res. NBS 78A, 323 (1974).

8. U. C. Paek and C. R. Kurkjian, J. Amer. Ceram. Soc., 58 #7-8, 330 (1975).

9. S. Bair and W. O. Winer, A.S.M.E. J. Lub. Tech., (1979); (1979).

10. C. J. Montrose, ONR Technical Report, Contract No. N00014-75-C-0856, Jan. 1981.

EXPERIMENTAL SETUP

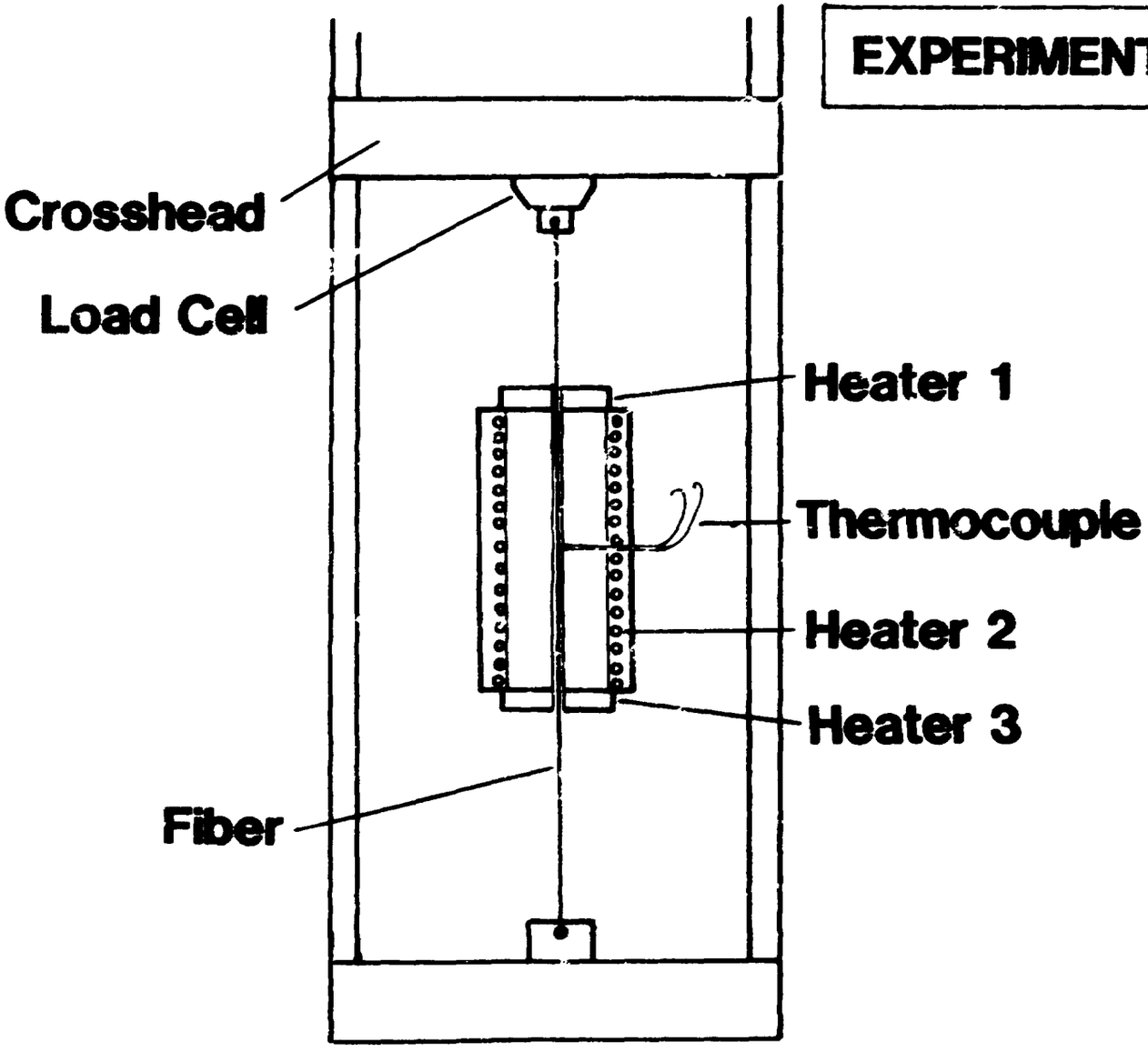

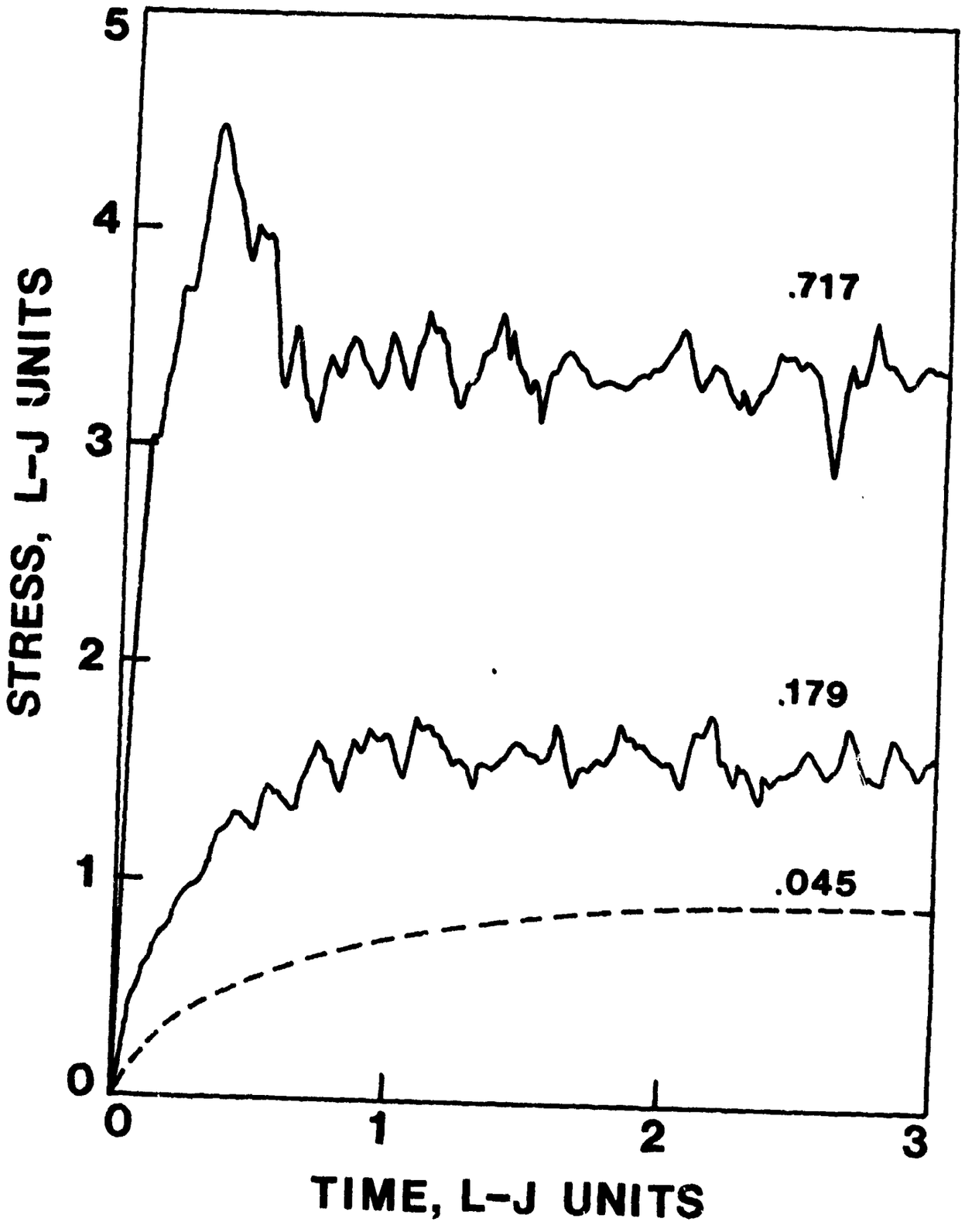
5
4
3
2
1
0
STRESS, L-J UNITS
.717
.179
.045
0
1
2
3
TIME, L-J UNITS

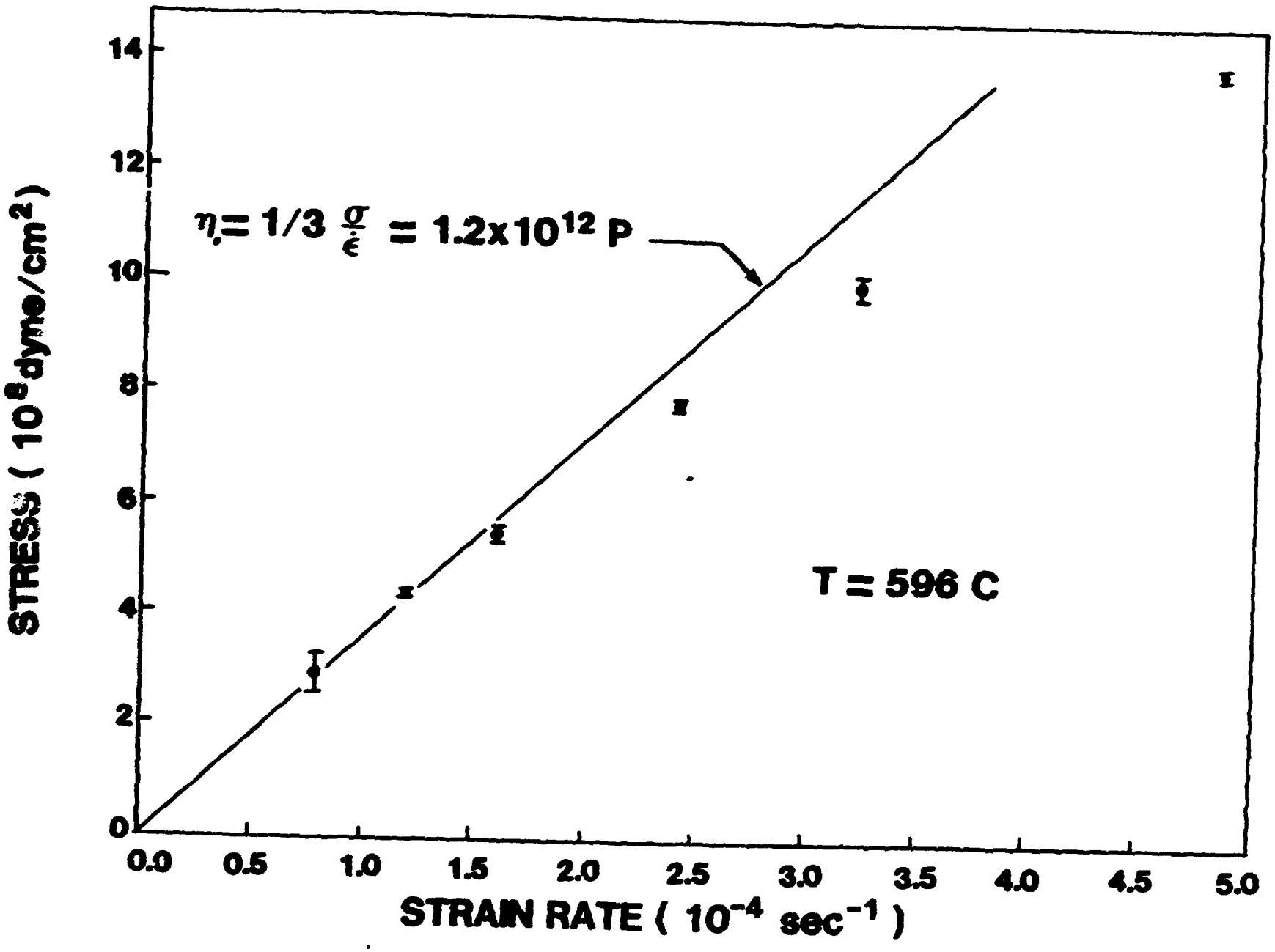
$\eta = 1/3 \frac{\sigma}{\dot{\epsilon}} = 1.2 \times 10^{12}$ P
T = 596 C
STRESS (10^8 dyne/cm^2)
STRAIN RATE (10^{-4} sec^{-1})
0
2
4
6
8
10
12
14
0.0
0.5
1.0
1.5
2.0
2.5
3.0
3.5
4.0
4.5
5.0

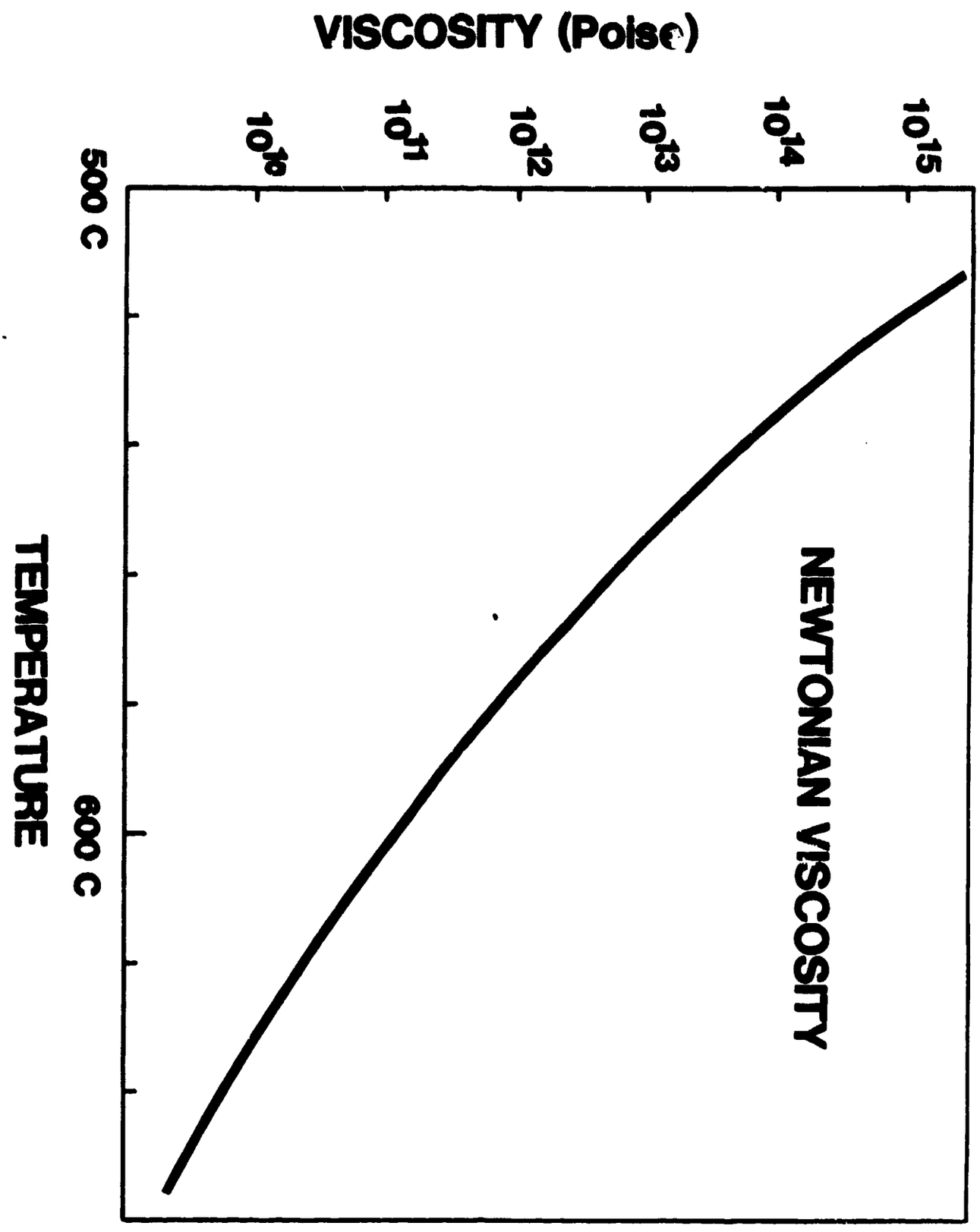
VISCOSITY (Poise)
10^{10}
10^{11}
10^{12}
10^{13}
10^{14}
10^{15}
500 C
600 C
TEMPERATURE
NEWTONIAN VISCOSITY

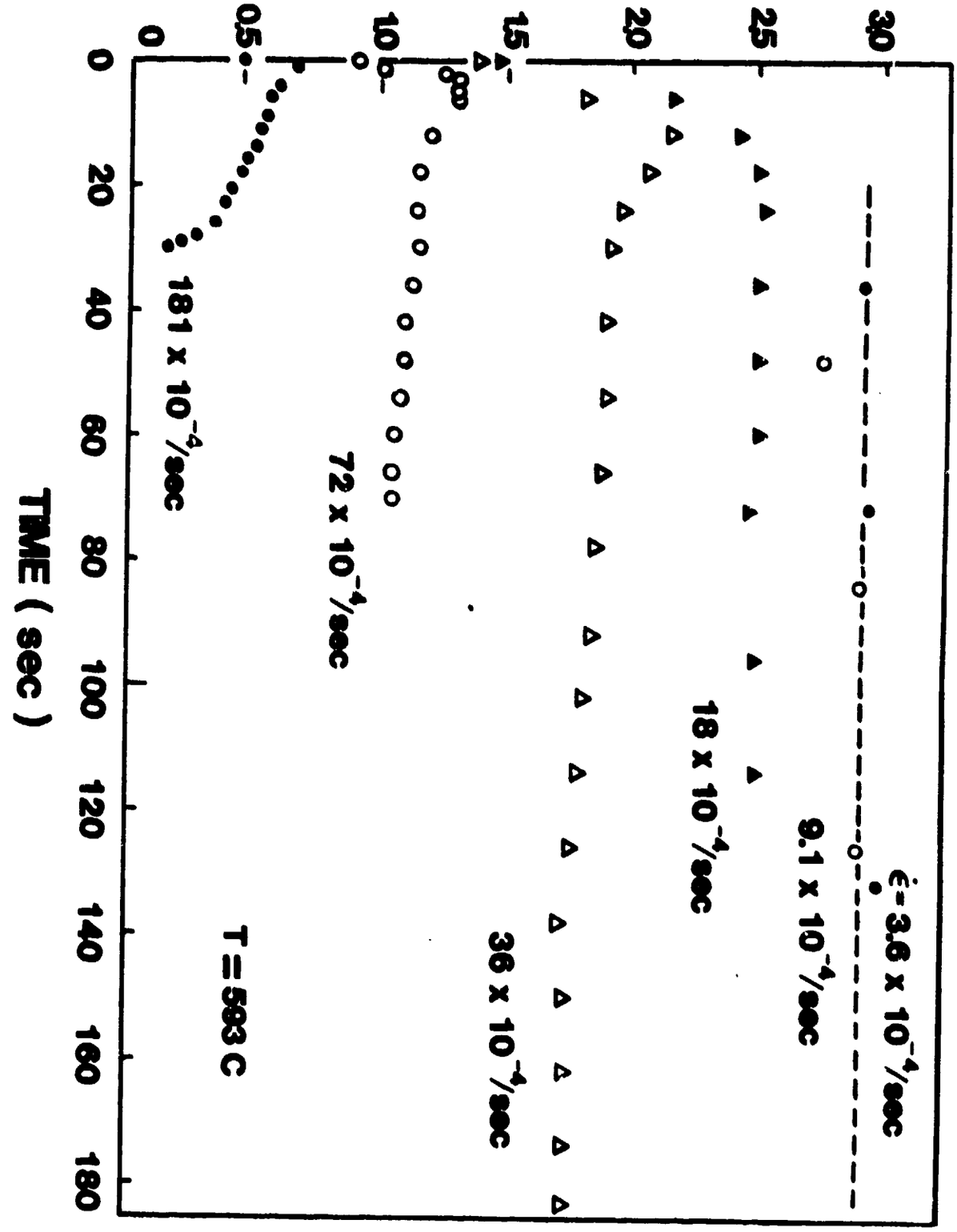
APPARENT VISCOSITY (10^{11}Poise)
30
25
20
15
10
5
0
0
20
40
60
80
100
120
140
160
180
TIME (sec)
$\dot{\epsilon}$= 3.6 x 10^{-4}/sec
9.1 x 10^{-4}/sec
18 x 10^{-4}/sec
36 x 10^{-4}/sec
72 x 10^{-4}/sec
181 x 10^{-4}/sec
T = 503 C

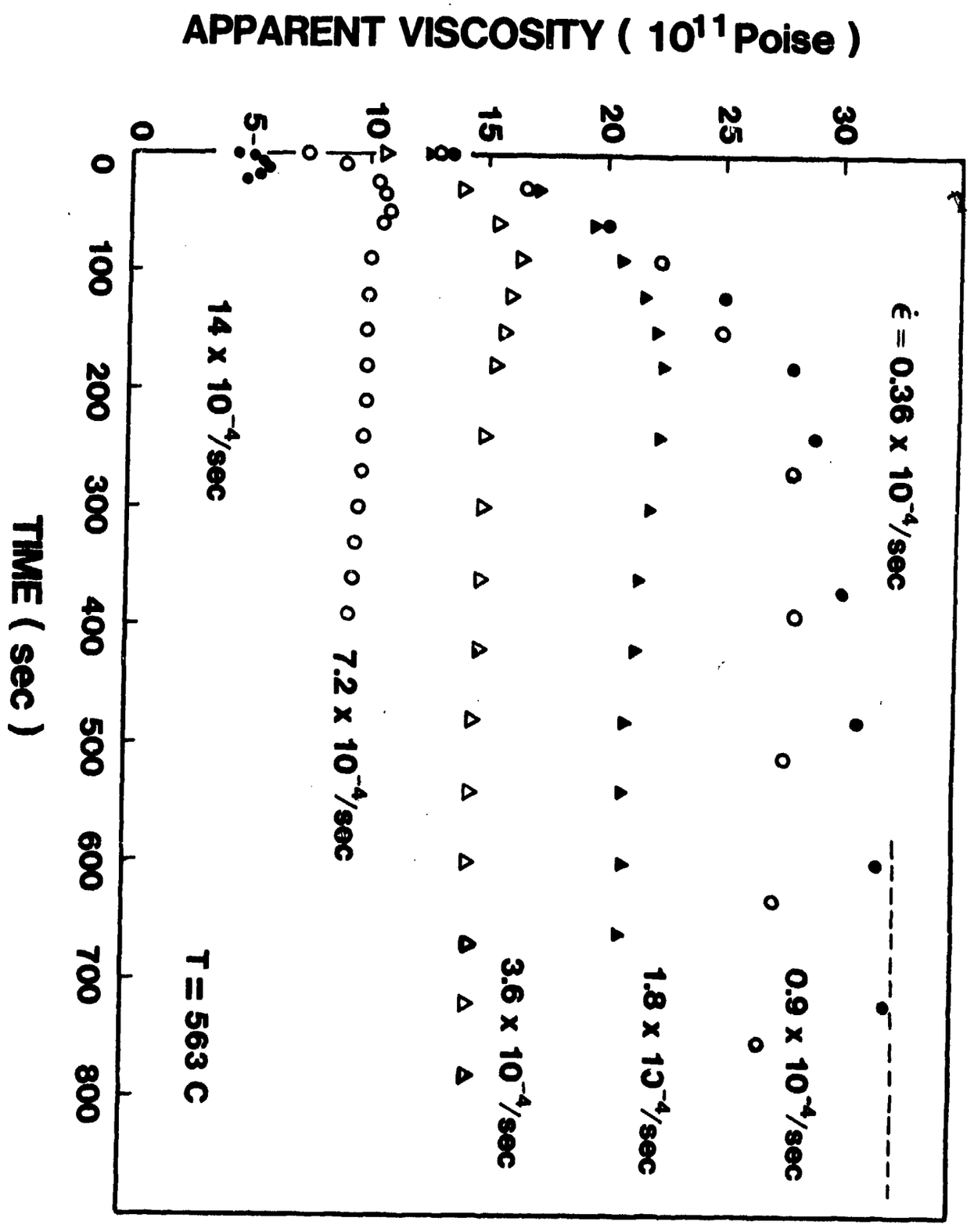
APPARENT VISCOSITY (10^{11} Poise)
30
25
20
15
10
5
0
0
100
200
300
400
500
600
700
800
TIME (sec)
$\dot{\epsilon}$ = 0.36 x 10^{-4}/sec
0.9 x 10^{-4}/sec
1.8 x 10^{-4}/sec
3.6 x 10^{-4}/sec
7.2 x 10^{-4}/sec
14 x 10^{-4}/sec
T = 563 C

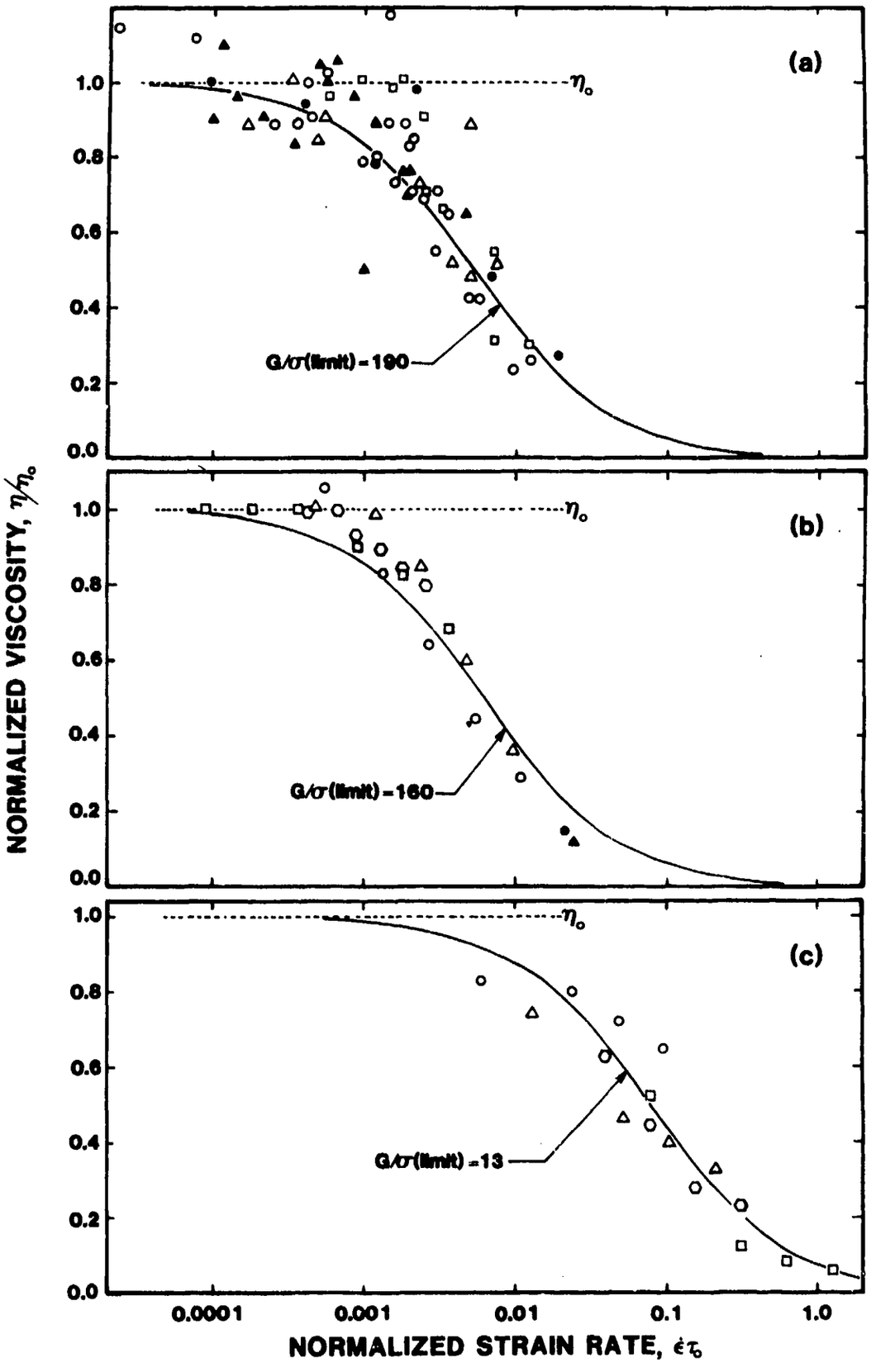
(a)
(b)
(c)
η_o
G/σ(limit) = 190
G/σ(limit) = 160
G/σ(limit) = 13
NORMALIZED VISCOSITY, η/η_o
NORMALIZED STRAIN RATE, $\dot{\epsilon}\tau_o$
0.0
0.2
0.4
0.6
0.8
1.0
0.0001
0.001
0.01
0.1
1.0

DISTRIBUTION LIST

	No. Copies
Dr. R.G. Rhoades Commander Army Missile Command DRSMI-R Redstone Arsenal, AL 35898	1
Dr. W.D. Stephens Atlantic Research Corp. Pine Ridge Plant 7511 Wellington Rd. Gainesville, VA 22065	1
Dr. A.W. Barrows Ballistic Research Laboratory USA ARRADCOM DRDAR-BLP Aberdeen Proving Ground, MD 21005	1
Dr. C.M. Frey Chemical Systems Division P.O. Box 358 Sunnyvale, CA 94086	1
Professor F. Rodriguez Cornell University School of Chemical Engineering Olin Hall, Ithaca, N.Y. 14853	1
Defense Technical Information Center DTIC-DDA-2 Cameron Station Alexandria, VA 22314	12
Dr. Rocco C. Musso Hercules Aerospace Division Hercules Incorporated Alleghany Ballistic Lab P.O. Box 210 Washington, D.C. 21502	1
Dr. Ronald L. Simmons Hercules Inc. Eglin AFATL/DLDL Eglin AFB, FL 32542	12

	No. Copies
Dr. E.H. Debutts Hercules Inc. Baccus Works P.O. Box 98 Magna, UT 84044	1
Dr. James H. Thacher Hercules Inc. Magna Baccus Works P.O. Box 98 Magna, UT 84044	1
Mr. Theordore M. Gilliland Johns Hopkins University APL Chemical Propulsion Info. Agency Johns Hopkins Road Laurel, MD 20810	1
Dr. R. McGuire Lawrence Livermore Laboratory University of California Code L-324 Livermore, CA 94550	1
Dr. Jack Linsk Lockheed Missiles & Space Co. P.O. Box 504 Code Org. 83-10, Bldg. 154 Sunnyvale, CA 94088	1
Dr. B.G. Craig Los Alamos National Lab P.O. Box 1663 NSP/DOD, MS-245 Los Alamos, NM 87545	1
Dr. R.L. Rabie WX-2, MS-952 Los Alamos National Lab. P.O. Box 1663 Los Alamos NM 87545	1
Dr. P. Rogers, WX-2 Los Alamos Scientific Lab. P.O. Box 1663 Los Alamos, NM 87545	1

PRECEDING PAGE BLANK-NOT FILMED

DISTRIBUTION LIST

	No. Copies
Mr. R. Brown Naval Air Systems Command Code 330 Washington, D.C. 20361	1
Dr. H. Rosenwasser Naval Air Systems Command AIR-310C Washington, D.C. 20360	1
Mr. B. Sobers Naval Air Systems Command Code 03P25 Washington, D.C. 20360	1
Dr. L.R. Rothstein Assistant Director Naval Explosives Dev. Engineering Dept. Naval Weapons Station Yorktown, VA 23691	1
Lionel Dickinson Naval Explosive Ordnance Disposal Tech. Center Code D Indian Head, MD 20640	1
Mr. C.L. Adams Naval Ordnance Station Code PM4 Indian Head, MD 20640	1
Mr. S. Mitchell Naval Ordnance Station Code 5253 Indian Head, MD 20640	1
Dr. William Tolles Dean of Research Naval Postgraduate School Monterey, CA 93940	1
Naval Research Lab. Code 6100 Washington, D.C. 20375	1
Dr. J. Schnur Naval Research Lab. Code 6510 Washington, D.C. 20375	1
Mr. R. Beauregard Naval Sea Systems Command SEA 64E Washington, D.C. 20362	1
Mr. G. Edwards Naval Sea Systems Command Code 62R3 Washington, D.C. 20362	1
Mr. John Boyle Materials Branch Naval Ship Engineering Center Philadelphia, PA 19112	1
Dr. H.G. Adolph Naval Surface Weapons Center Code R11 White Oak Silver Spring, MD 20910	1
Dr. T.D. Austin Naval Surface Weapons Center Code R16 Indian Head, MD 20640	1
Dr. T. Hall Code R-11 Naval Surface Weapons Center White Oak Laboratory Silver Spring, MD 20910	1
Mr. G.L. Mackenzie Naval Surface Weapons Center Code R101 Indian Head, MD 20640	1
Dr. K.F. Mueller Naval Surface Weapons Center Code R11 White Oak Silver Spring, MD 20910	1

DISTRIBUTION LIST

	No. Copies
Mr. J. Murrin Naval Sea Systems Command Code 62R2 Washington, D.C. 20362	1
Dr. D.J. Pastine Naval Surface Weapons Cneter Code R04 White Oak Silver Spring, MD 20910	1
Mr. L. Roslund Naval Surface Weapons Center Code R122 White Oak, Silver Spring MD 20910	1
Mr. M. Stosz Naval Surface Weapons Center Code R121 White Oak Silver Spring, MD 20910	1
Dr. E. Zimmet Naval Surface Weapons Center Code R13 White Oak Silver Spring, MD 20910	1
D.R. Derr Naval Weapons Center Code 388 China Lake, CA 93555	1
Mr. Lee N. Gilbert Naval Weapons Center Code 3205 China Lake, CA 93555	1
Dr. E. Martin Naval Weapons Center Code 3858 China Lake, CA 93555	1
Mr. R. McCarten Naval Weapons Center Code 3272 China Lake, CA 93555	

	No. Copies
Dr. A. Nielsen Naval Weapons Center Code 385 China Lake, CA 93555	1
Dr. R. Reed, Jr. Naval Weapons Center Code 388 China Lake, CA 93555	1
Dr. L. Smith Naval Weapons Center Code 3205 China Lake, CA 93555	1
Dr. B. Douda Naval Weapons Support Center Code 5042 Crane, Indiana 47522	1
Dr. A. Faulstich Chief of Naval Technology MAT Code 0716 Washington, D.C. 20360	1
LCDR J. Walker Chief of Naval Material Office of Naval Technology MAT, Code 0712 Washington, D.C. 20360	1
Mr. Joe McCartney Naval Ocean Systems Center San Diego, CA 92152	1
Dr. S. Yamamoto Marine Sciences Division Naval Ocean Systems Center San Diego, CA 91232	1
Dr. G. Bosmajian Applied Chemistry Division Naval Ship Research & Development Center Annapolis, MD 21401	1
Dr. H. Shuey Rohn and Haas Company Huntsville, Alabama 35801	1

DISTRIBUTION LIST

	No. Copies
Dr. J.F. Kincaid Strategic Systems Project Office Department of the Navy Room 901 Washington, D.C. 20376	1
Strategic Systems Project Office Propulsion Unit Code SP2731 Department of the Navy Washington, D.C. 20376	1
Mr. E.L. Throckmorton Strategic Systems Project Office Department of the Navy Room 1048 Washington, D.C. 20376	1
Dr. D.A. Flanigan Thiokol Huntsville Division Huntsville, Alabama 35807	1
Mr. G.F. Mangum Thiokol Corporation Huntsville Division Huntsville, Alabama 35807	1
Mr. E.S. Sutton Thiokol Corporation Elkton Division P.O. Box 241 Elkton, MD 21921	1
Dr. G. Thompson Thiokol Wasatch Division MS 240 P.O. Box 524 Brigham City, UT 84302	1
Dr. T.F. Davidson Technical Director Thiokol Corporation Government Systems Group P.O. Box 9258 Ogden, Utah 84409	1
Dr. C.W. Vriesen Thiokol Elkton Division P.O. Box 241 Elkton, MD 21921	1
Dr. J.C. Hinshaw Thiokol Wasatch Division P.O. Box 524 Brigham City, Utah 83402	1
U.S. Army Research Office Chemical & Biological Sciences Division P.O. Box 12211 Research Triangle Park NC 27709	1
Dr. R.F. Walker USA ARRADCOM DRDAR-LCE Dover, NJ 07801	1
Dr. T. Sinden Munitions Directorate Propellants and Explsoives Defence Equipment Staff British Embassy 3100 Massachusetts Ave. Washington, D.C. 20008	1
LTC B. Loving AFROL/LK Edwards AFB, CA 93523	1
Professor Alan N. Gent Institute of Polymer Science University of Akron Akron, OH 44325	1
Mr. J. M. Frankle Army Ballistic Research Labs ARRADCOM Code DRDAR-BLI Aberdeen Proving Ground, MD 21005	1

DISTRIBUTION LIST

	No. Copies
Dr. Ingo W. May Army Ballistic Research Labs ARRADCOM Code DRDAR-BLI Aberdeen Proving Ground, MD 21005	1
Professor N.W. Tschoegl California Institute of Tech Dept. of Chemical Engineering Pasadena, CA 91125	1
Professor M.D. Nicol University of California Dept. of Chemistry 405 Hilgard Avenue Los Angeles, CA 90024	1
Professor A. G. Evans University of California Berkeley, CA 94720	1
Professor T. Litovitz Catholic Univ. of America Physics Department 520 Michigan Ave., N.E. Washington, D.C. 20017	1
Professor W. G. Knauss Graduate Aeronautical Lab California Institute of Tech. Pasadena, CA 91125	1
Professor Edward Price Georgia Institute of Tech. School of Aerospace Engin. Atlanta, Georgia 30332	1
Dr. Kenneth O. Hartman Hercules Aerospace Division Hercules Incorporated P.O. Box 210 Cumberland, MD 21502	1
Dr. Thor L. Smith IBM Research Lab D42.282 San Jose, CA 95193	1
Dr. J. P. Marshall Dept. 52-35, Bldg. 204/2 Lockheed Missile & Space Co. 3251 Hanover Street Palo Alto, CA 94304	1
Joan L. Janney Los Alamos National Lab Mail Stop 920 Los Alamos, NM 87545	1
Dr. J. M. Walsh Los Alamos Scientific Lab Los Alamos, NM 87545	1
Professor R. W. Armstrong Univ. of Maryland Department of Mechanical Eng. College Park, MD 20742	1
Prof. Richard A. Reinhardt Naval Postgraduate School Physics & Chemistry Dept. Monterey, CA 93940	1
Dr. R. Bernecker Naval Surface Weapons Center Code R13 White Oak, Silver Spring, MD 20910	1
Dr. M. J. Kamlet Naval Surface Weapons Center Code R11 White Oak, Silver Spring, MD 20910	1
Professor J. D. Achenbach Northwestern University Dept. of Civil Engineering Evanston, IL 60201	1
Dr. N. L. Basdekas Office of Naval Research Mechanics Program, Code 432 Arlington, VA 22217	1
Professor Kenneth Kuo Pennsylvania State Univ. Dept. of Mechanical Engineering University Park, PA 16802	1

DISTRIBUTION LIST

	No. Copies	No. Copies
Dr. S. Sheffield Sandia Laboratories Division 2513 P.O. Box 5800 Albuquerque, NM 87185	1	
Dr. M. Farber Space Sciences, Inc. 135 Maple Avenue Monrovia, CA 91016	1	
Dr. y. M. Gupta SRI International 333 Ravenswood AVenue Menlo Park, CA 94025	1	
Mr. M. Hill SRI International 333 Ravenswood Avenue Menlo Park, CA 94025	1	
Profes. Richard A. Schapery Texas A& Univ. Dept of Civil Engineering College Station, TX 77843	1	
Dr. Stephen wanson Univ. of Utan Dept. of Mech. & Industrial Engineering MEB 3008 Salt Lake City, UT 84112	1	
Mr. J. D. Byrd Thiokol Corp. Huntsville Huntsville Div. Huntsville, AL 35807	1	
Professor G. D. Duvall Washington State University Dept. of Physics Pullman, WA 99163	1	
Prof. T. Dickinson Washington State University Dept. of Physics Pullman, WA 99163	1	